Title
Reliability-Based Integrity Management of Natural Gas Pipelines Subject to Spatio-Temporal Corrosive Environment

Author
Wu, Keo-Yuan

Publication Date
2020

Peer reviewed|Thesis/dissertation

UNIVERSITY OF CALIFORNIA
Los Angeles

Reliability-Based Integrity Management of Natural Gas Pipelines Subject to Spatio-Temporal Corrosive Environment

A dissertation submitted in partial satisfaction of the
requirements for the degree Doctor of Philosophy
in Materials Science and Engineering

by

Keo-Yuan Wu

2020

ABSTRACT OF THE DISSERTATION

Reliability-Based Integrity Management of Natural Gas Pipelines Subject to Spatio-Temporal Corrosive Environment

by

Keo-Yuan Wu
Doctor of Philosophy in Materials Science and Engineering
University of California, Los Angeles, 2020
Professor Ali Mosleh, Chair

Pipeline integrity management refers to an approach of understanding and operating pipelines in a safe and reliable manner. In this work, firstly, a probabilistic predictive model for internal corrosion of natural gas pipelines subject to aqueous CO_2/H_2S environment has been proposed. The model regards uniform and pitting corrosion as two main corrosion mechanisms and has been calibrated with the experimental data in a deterministic framework. Methodologies of simulating and accounting for temporal and spatial variabilities of operating parameters have been proposed and applied to the model for field applications. The model has been validated against field data from eight wet gas gathering pipelines in a probabilistic framework. Secondly, a reinforcement learning (RL)-based maintenance scheduler has been proposed for pipeline maintenance optimization problems by leveraging the proposed predictive corrosion model and the Q-learning and Sarsa algorithms. A case study has shown the superiority of the proposed maintenance scheduler over the periodic maintenance policy in reducing the maintenance costs. Finally, the

previous two parts of work have been integrated into a pipeline system integrity management software featuring pipeline health monitoring, corrosion prognosis, system-level failure analysis, sensor placement optimization, and inspection/maintenance optimization. A case study has been provided to demonstrate the capabilities of the software.

The dissertation of Keo-Yuan Wu is approved.

Jenn-Ming Yang

Qibing Pei

Henry Burton

Ali Mosleh, Committee Chair

University of California, Los Angeles

2020

Table of Contents

List of Figures

List of Tables

Acknowledgements

I would like to express my gratitude to many people who helped me during my PhD journey. Firstly, I would like to thank Professor Ali Mosleh, who brought me into the family of the B. John Garrick Institute for the Risk Sciences (GIRS) and gave me invaluable knowledge and foresight. His support and encouragement motivated me to move forward with a steady pace and finish this amazing journey. I owe you a lot of gratitude for being patient with my lack of contributions in the first two years as I was still trying to become familiar with a totally new domain knowledge. You helped me to shape myself into a better student, scholar, and to-be-father. Being your student is one of the best decisions I have made throughout my life.

I would also thank my colleagues Wadie Chalgham and Zahra Mahmoodzadeh at GIRS for their kind assistance and advices in important aspects of my work. I am also thankful to Dr. Yuan-Shang Chang for his support as a colleague and friend, sharing office, and life journey.

I would like to share my happiness and gratitude to my parents and beloved wife, Yi-Huan Tsai. Without their support, I wouldn't have gone this far. Yi-Huan; thank you for taking good care of me and sharing the burden with me. Your companionship gave me power and courage to overcome challenges and my academic goal.

I also express my deepest appreciation of the funding support by Pipeline System Integrity Management research project sponsored by the Petroleum Institute, Abu Dhabi, UAE through a subaward from the University of Maryland Department of Mechanical Engineering.

Vita

Education

2013	M.S. Materials Science & Engineering National Tsing Hua University Hsinchu, Taiwan
2011	B.S. Materials Science & Engineering National Chung Hsing University Taichung, Taiwan

Research/Work Experience

Graduate Research Assisant: The Garrick Institute for the Risk Sciences, UCLA

Modeling of pipeline corrosion and reliability analysis for gas pipelines for Pipeline System Integrity Management project from Petroleum Institute (PI) of Abu Dhabi, United Arab Emirate (UAE).

Start Date: 2016/02**; End Date**: 2020/06

Supervisor's Name: Ali Mosleh

Metallurgist Intern: Failure Analysis Lab, Intertek, Santa Clara, CA, USA

Metallurgical evaluations with a focus on boiler tubes; Root-cause failure analysis on components in power industry and delivered technical reports to customer; Data analysis on a Due Diligence project for wind turbines.

Start Date: 2019/06**; End Date**: 2019/09

Associate Engineer: Fundamental Laboratory (R&D group), SDI Corporation, Taiwan

PbSnAg solder joint wetting research with solder injection experiments to increase the bonding strength; Residual stress analysis of Cu lead frames and successfully pointed out a drawback of

the stamping process; Failure analysis (e.g. film delamination, oxidation) on the flawed electronic products.

Start Date: 2019/06**; End Date**: 2019/09

Graduate Research Assisant: High Entropy Alloys Lab, National Tsing Hua University, Taiwan

Fundamental reseach on Superconductivity in high-entropy alloys; Fabrication and characterization of Refractory Metal-Cemented Fused Carbides.

Start Date: 2011/09**; End Date**: 2013/07

Supervisor's Name: Swe-Kai Chen

Teaching Experience

2018/09	Teaching Assistant and Grader MSE-298 "Reliability Engineering Fundamentals" given by Prof. Ali Mosleh at UCLA Materials Science and Engineering
2019/01	Teaching Assistant and Grader mae-174 "Risk Analysis for Engineers and Scientists" given by Prof. Ali Mosleh at UCLA Mechanical and Aerospace Engineering

Publication

Wu, K.Y., Chen, S.K. and Wu, J.M., 2018. Superconducting in Equal Molar NbTaTiZr-Based High-Entropy Alloys. *Natural Science*, *10*(03), p.110.

Wu, K.Y. and Mosleh, A., 2019. Effect of temporal variability of operating parameters in corrosion modelling for natural gas pipelines subject to uniform corrosion. *Journal of Natural Gas Science and Engineering*, *69*, p.102930.

Wu, K.Y. and Mosleh, A., 2018. Probabilistic Model for Internal Uniform/Pitting Corrosion of Gas pipelines. *Probabilistic Safety Assessment and Management PSAM 14*, p.13.

Wu, K.Y., Diaconeasa, M.A. and Mosleh, A., 2018. The Impact of Time-Varying Operating Parameters on the Corrosion Rate and Depth of Gas Pipelines. *Probabilistic Safety Assessment and Management PSAM 14*, p.10.

1 Introduction

1.1 Background

Much of the world relies on hydrocarbons including oil and natural gas as one of the main energy sources. Before they are processed into fuels and sent to the customers, they have to be extracted from underground either onshore or offshore and undergo a series of treatment to get rid of the impurities. Natural gas, compared to oil, creates less carbon pollution and doesn't emit poisonous byproducts such as SO_x and NO_x during the combustion process for power generation; therefore, the demand for it has increased. A schematic diagram of a network of natural gas production in the oil and gas industry is shown Figure 1.

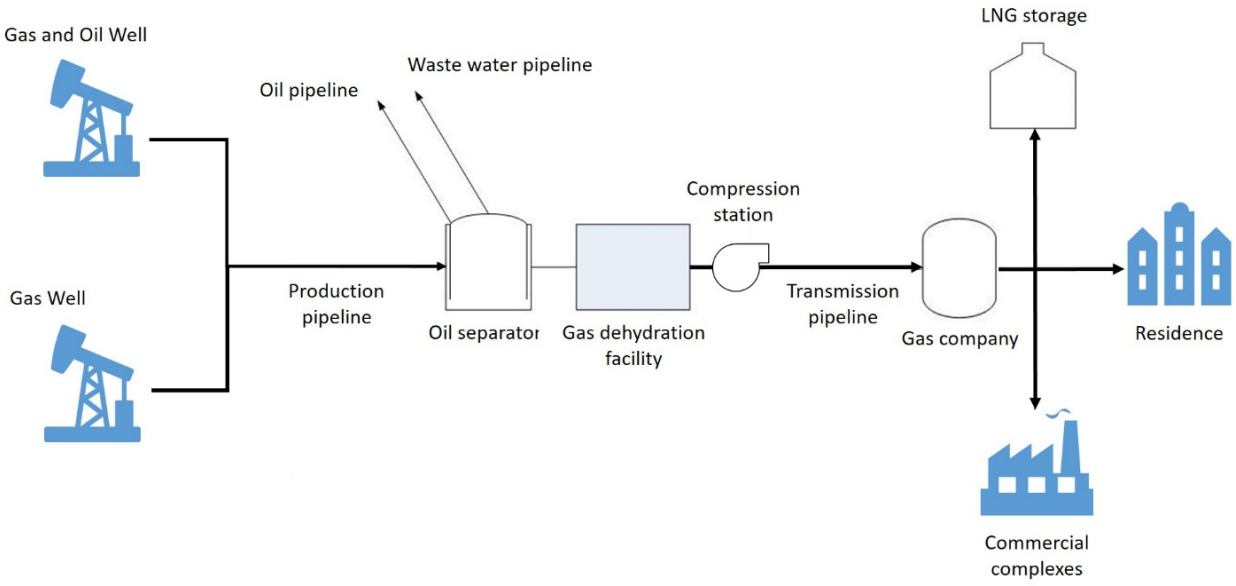

Figure 1. Flow of natural gas production in the oil and gas industry.

During the operation, different types of pipelines are used to transport hydrocarbons from the upstream to the downstream. For example, production pipelines transport oil, gas, and water from

the wellhead to the oil separator, which separates the gas from oil and water, and then to the gas dehydration facility to further dehydrate the remaining water and other impurities in the gas. In addition, transmission pipelines are built to transport natural gas to the production facility where they are processed to become fuel products and finally to the customers. According to Kiefner and Rosenfeld's report [1], the total lengths of interstate and intrastate natural gas transmission pipelines in the United States are already more than 305,000 miles by 2000 and the major locations of them are shown in Figure 2.

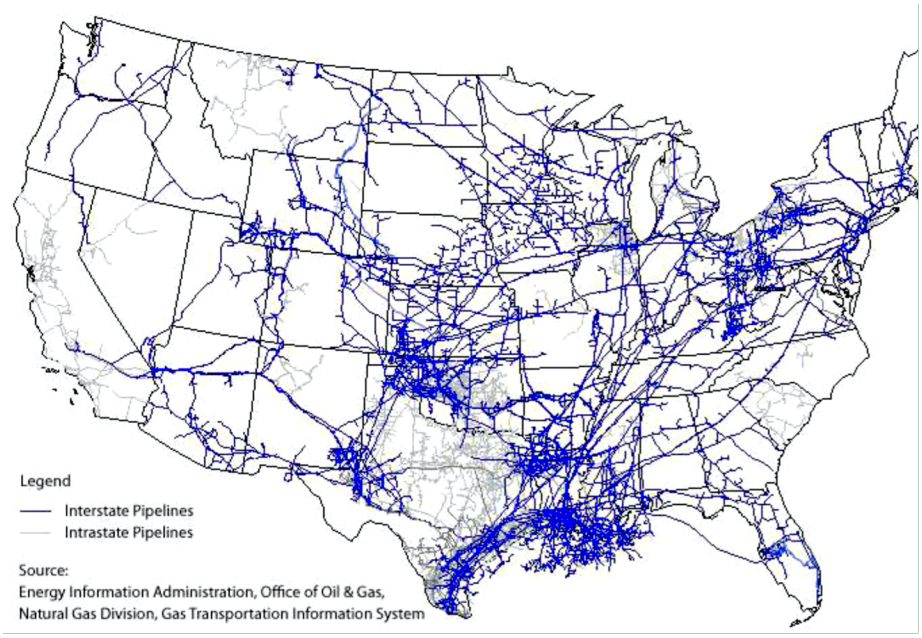

Figure 2. The distribution of natural gas transmission pipelines in the United States [1].

However, these pipelines are susceptible to degradation over their service life. One of the main degradation mechanisms is corrosion, a deterioration of materials by the reactions with its

environments. With high density of natural pipeline networks, any corroded pipeline that is lack of suitable treatment will lead to severe health and environmental hazards associated with huge cost as a result of leakage or burst. The research conducted by Pipeline and Hazardous Materials Safety Administration (PHMSA) from 1988 to 2008 reveals that corrosion, accounts for 18% (3rd highest) among the causes of severe incidents of pipelines while the highest one (25.9%) is for excavation damage [2]; therefore, corrosion remains an import issue in the oil and gas industry over the past thirty years. One of the effective ways to mitigate the risk of internal corrosion is through inspection and maintenance; however, it is too costly to excavate and inspect the entire sections of a pipeline which is typically tens or hundreds of miles.

Prior to applying mitigation and maintenance practices, corrosion prediction in terms of corrosion damage (i.e., corrosion rate, corrosion depth, etc.) is important. Above all, corrosion predictive models can serve as guides and enable engineers to take actions (i.e., maintenance or replacement) proactively for the sake of pipeline integrity management purpose.

Corrosion rate is influenced by many factors such as environmental and operating conditions, material, and geometry. In fact, corrosive matters such as water, CO_2, H_2S, condensates, and Cl^- ions are often unavoidable during the extraction process and thus favor the environment for internal corrosion to happen inside the pipelines.

1.2 Motivation

Up to date, corrosion predictive models can be categorized into three categories: mechanistic, semi-empirical, and empirical depending on the solidity of physical theories behind them [3]. The differences between these categories are shown in Figure 3. Among them, mechanistic models, which are mostly developed in the laboratories, are the most reliable because they have strong theoretical background and solid physics behind it; therefore, they are good for both interpolation and extrapolation predictions. However, sometimes they require parameter tuning and determination before they can be applied to real operating gas pipelines, increasing the difficulty of application in the industry. On the other hand, although empirical models are lack of theoretical background and often data-driven, they are more widely used in the industry compared to mechanistic models because of the ease of application and implementation. However, predictions done by empirical models are skeptical outside the valid range of available data. Semi-empirical models are partly based on theoretical hypothesis and have partly characteristics of both mechanistic and mechanistic models, rendering them also popular in the industry; however, it has the same problem as empirical models that unreliable results are expected for extrapolation.

Pipeline corrosion modeling and integrity management research has been done for many decades, however, two issues have been noticed by the author. Firstly, up to author's knowledge, most state-of-the-art physics-of-failure (PoF)-based models don't take temporal and spatial variability of operating parameters into account for corrosion predictions which deviates from the real situation that operating parameters are changing continuously within an uncertain range. This perspective

is also mentioned in a review study by Heidary et al. [4] who reported that a reliable corrosion assessment model should consider epistemic uncertainty, temporal uncertainty, spatial uncertainty, and inspection errors. Secondly, a study by U.S. Federal Highway Administration (FHWA) in 2002 indicates that the annual cost of corrosion in the United States is approximately $7 billion, among which 52 % is for operation and maintenance [5]. This study reveals another issue about how to implement cost-effective maintenance practices of gas pipelines for pipeline operators. However, nowadays pipeline operators are applying inspection and maintenance actions to ensure the asset integrity based on experience or rule-of-thumb maintenance policies such as Time-based maintenance (TBM), Risk-based maintenance (RBM), or Condition-based maintenance (CBM), but they are usually found to be not cost-effective in the long run. Therefore, in order to establish a reliable pipeline integrity management tool in a cost-effective way, the abovementioned two issues have to be considered and applied for future predictions.

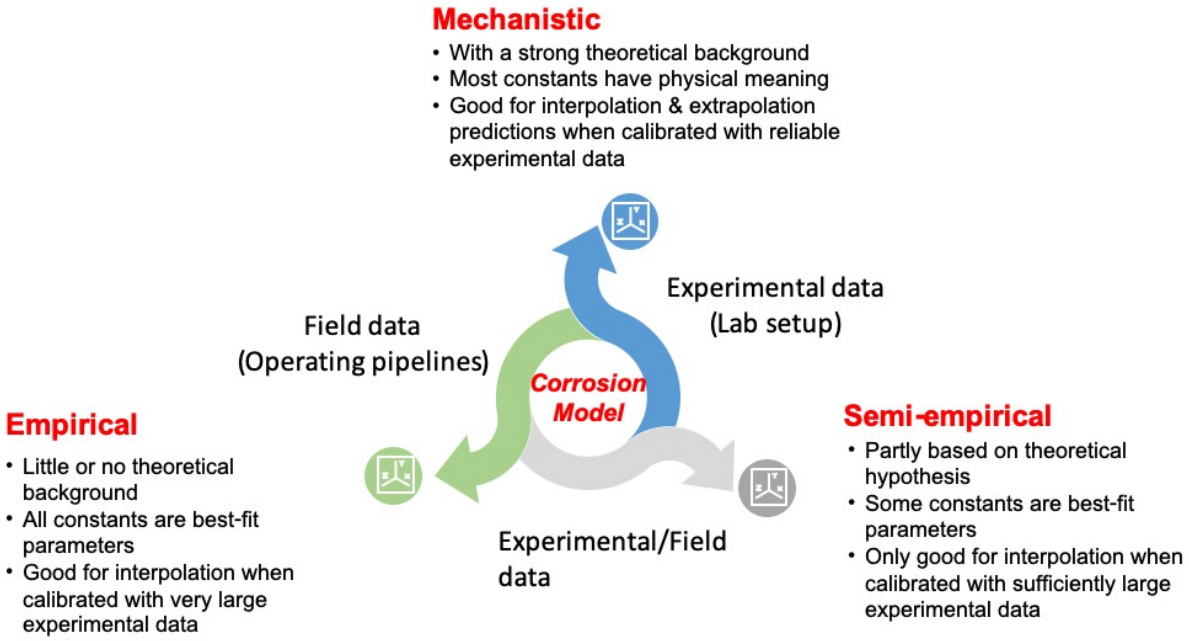

Figure 3. Differences between different categories of corrosion predictive models.

2 Literature Review

2.1 Internal uniform corrosion modeling

Corrosion is the gradual degradation of materials by chemical and/or electrochemical reactions with their environment. Internal corrosion is defined as corrosion that happens on the inner wall of natural gas pipelines when the pipe wall is exposed to corrosive environments such as the combination of water with O_2, H_2S, CO_2, and chloride ions [6]. The extent of corrosion damage is a function of operating conditions. Some combinations of corrosive constituents will lead to severe corrosion, while some will only lead mild or no corrosion, which makes corrosion prediction a difficult task. Fortunately, numerous corrosion predictive models have been developed based on years of research on field experience and laboratory experiments. Different types of corrosion occur at different operating conditions and pipe materials. Uniform corrosion, pitting corrosion, erosion corrosion, microbiologically-influenced corrosion, and corrosion fatigue are common types of internal corrosion in natural gas pipelines.

Uniform corrosion is a type of corrosion that the anodic and cathodic reaction sites occur simultaneously on the entire surface, leading to the uniform reduction of pipe walls. For natural gas pipelines CO_2 and H_2S are two major causes of uniform corrosion because of chemical reactions with water. When dissolved in water, CO_2 is hydrated to become carbonic acid (H_2CO_3) [7]:

$$CO_{2(g)} \Leftrightarrow CO_{2(aq)} \quad (1)$$

$$CO_{2(aq)} + H_2O_{(aq)} \Leftrightarrow H_2CO_{3(aq)} \quad (2)$$

which then dissociates in two steps:

$$H_2CO_{3(aq)} \Leftrightarrow H^+_{(aq)} + HCO^-_{3(aq)} \quad (3)$$

$$HCO^-_{3(aq)} \Leftrightarrow H^+_{(aq)} + CO^{2-}_{3(aq)} \quad (4)$$

H_2S also becomes corrosive when dissolved in water [8]:

$$H_2S_{(g)} \Leftrightarrow H_2S_{(aq)} \quad (5)$$

which then dissociates in two steps:

$$H_2S_{(aq)} \Leftrightarrow H^+_{(aq)} + HS^-_{(aq)} \quad (6)$$

$$HS^-_{(aq)} \Leftrightarrow H^+_{(aq)} + S^{2-}_{(aq)} \quad (7)$$

2.1.1 *de Waard and Milliams model*

In early time, CO_2 corrosion poses significant threat to gas pipelines and therefore has gained more attention. de Waard and Milliams firstly develops an equation and a corresponding nomogram for CO_2 corrosion in wet natural gas pipelines by relating corrosion rate with temperature, partial pressure of CO_2, and scale factor during early 1970s [9]. The nomogram for CO_2 corrosion is shown in Figure 4.

They later simplify the corrosion rate equation for the nomogram with more data and the equation becomes [10]:

$$\log C_{corr} = 5.8 - \frac{1710}{T} + 0.671 \log (pCO_2) \quad (8)$$

where C_{corr} is corrosion rate; T is temperature; pCO_2 is partial pressure of CO_2.

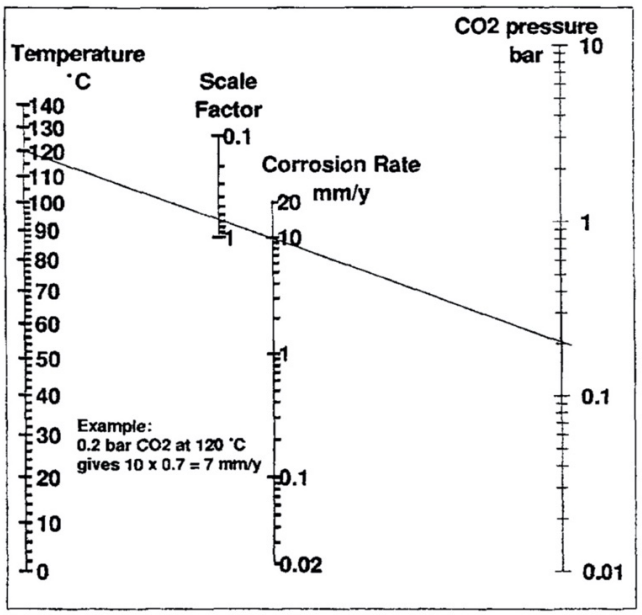

Figure 4. Nomogram for CO_2 corrosion [9].

Moreover, the model is further modified with experiment data to include many other factors such as total pressure, protective layers, pH value, flow velocity, hydrocarbon liquid, and inhibitors (e.g., glycol). These factors are accounted for by multiplying the corrosion rate predicted by equation (8) with correction factors ranging from 0 to 1. That is to say these factors either reduce

or make no change to corrosion rate under certain circumstances. Each factor has a different influence on the predicted corrosion rate:

(1) Effect of total pressure

The increase of total gas pressure will increase corrosion rate, but nonideality will also become more important. Therefore, the effect of fugacity of the gas (F_g) should be considered a correction factor:

$$\log(F_g) = 0.67\left(0.0031 - \frac{1.4}{T}\right)P \qquad (9)$$

where T is temperature; P is total pressure of the gas.

(2) Effect of surface layer

Aqueous CO_2 reacts with steel to form iron carbonate ($FeCO_3$) scales (and Fe_3O_4 under some conditions), which can be protective or non-protective depending on the operating condition:

$$Fe_{(s)} + CO_{2(aq)} + H_2O_{(l)} \rightarrow FeCO_{3(s)} + H_{2(g)} \qquad (10)$$

At lower temperatures (lower than 60℃), the scale is easily removed by flowing liquids and is non- protective. At higher temperature, the scale has a different texture and becomes more protective. The scale correction factor (F_{scale}) can be expressed as:

$$\log(F_{scale}) = 2400\left(\frac{1}{T} - \frac{1}{T_{scale}}\right) \qquad (11)$$

where T is temperature; T_{scale} is scaling temperature above which protective scales start to form i.e., $T > T_{scale}$, otherwise $F_{scale} = 1$. T_{scale} can be written as:

$$T_{scale} = \frac{2400}{6.7 + 0.6\log(fCO_2)} \quad (12)$$

where fCO_2 is fugacity of CO_2.

(3) Effect of pH

With constant volume of water and constant CO_2 pressure, the formation of corrosion byproducts (e.g., $FeCO_3$ and Fe_3O_4) will increase the Fe^{++} concentration, but decrease the H^+ concentration until the solution is saturated with $FeCO_3$ or Fe_3O_4. pH at the onset of $FeCO_3$ or Fe_3O_4 saturation (pH_{sat}) for different temperatures and fugacity of CO_2 can be approximated by:

$$\text{smallest value of} \quad pH_{sat} = 1.36 + \frac{1307}{T + 273} - 0.17\log(fCO_2) \quad and$$
$$pH_{sat} = 5.4 - 0.66\log(fCO_2) \quad (13)$$

The pH correction factor (F_{pH}) is then found to be:

$$\log(F_{pH}) = 0.32(pH_{sat} - pH_{act}) \quad \text{for} \quad pH_{sat} > pH_{act} \quad (14)$$

$$\log(F_{pH}) = -0.13(pH_{act} - pH_{sat})^{1.6} \quad \text{for} \quad pH_{sat} < pH_{act} \quad (15)$$

where pH_{sat} is actual pH.

(4) Effect of velocity

The protective scales will be removed by flowing fluid under some conditions. When wet gas is transported at a superficial gas velocity of 20 m/s, the protective scales will be completely removed and the scale correction factor becomes 1.

(5) Effect of hydrocarbon liquid

Sometimes crude oil present along with gas in gas pipelines during the extraction process. Under this condition, CO_2 corrosion can be inhibited if the steel is oil-wetted as water is entrained in the crude oil. However, light hydrocarbon condensates do not provide any protection like crude oil. The hydrocarbon liquid correction factor (F_{oil}) can be expressed as:

$$F_{oil} = 0 \quad \text{if} \quad \text{water cut} < 30\% \quad \text{and} \quad V_{crude} > 1 \text{ m/s}$$
$$\text{otherwise} \qquad (16)$$
$$F_{oil} = 1$$

where V_{crude} is flow rate of crude oil.

(6) Effect of glycol

Glycol is added to wet gas pipelines to inhibit CO_2 corrosion because glycol can reduce the corrosivity of the water phase and absorb water from the gas phase in a prevention of hydrates formation. The glycol correction factor (F_{glyc}) can be expressed as:

$$\log\left(F_{glyc}\right) = A\log(W\%) - 2A \quad (17)$$

where A is a constant with a value of 1.6 for most glycols; W% is water content of water/glycol mixture in w%.

2.1.2 *Nesic et al. model*

A few years later, Nesic et al. [11–13] develops a mechanistic model for CO_2 corrosion considering electrochemical reactions at the steel surface and transport processes of corrosive species between the steel surface and the bulk solution. Electrochemical reactions, including one anodic reaction and three cathodic reactions, happen when corrosive species contact with the steel surface. The only anodic reaction is iron dissolution:

$$Fe \rightarrow Fe^{2+} + 2e^{-} \quad (18)$$

The three cathodic reactions are hydrogen ion reduction, direct carbonic acid reduction, and direct water reduction:

$$2H^{+} + 2e^{-} \rightarrow H_2 \quad (19)$$

$$2H_2CO_3 + 2e^{-} \rightarrow H_2 + 2HCO_3^{-} \quad (20)$$

$$2H_2O + 2e^- \rightarrow H_2 + 2OH^- \quad (21)$$

The rate for any of the cathodic and anodic reactions can be described in terms of current density *i* (A/m^2). The reaction is referred as "charge transfer controlled" if the rate of the overall corrosion process is limited by the rate of the electrochemical reaction. The charge transfer current density (i_α) can be expressed as:

$$i_\alpha = \pm i_0 \times 10^{\pm(E-E_{rev})/b} \quad (22)$$

where i_0 is exchange current density; E is electrical potential; E_{rev} is reversible potential; b is Tafel slope. The i_0 is a function of temperature, which can be simply expressed in terms of the Arrhenius equation:

$$i_0 = i_0^{ref} e^{-\Delta H/R(\frac{1}{T_k} - \frac{1}{T_{k,ref}})} \quad (23)$$

where i_0^{ref} is reference exchange current density; ΔH is activation enthalpy; T_k is temperature (K); $T_{k,ref}$ is reference temperature (= 298 K); R is gas constant (= 8.314 J/mol·K). In reality, i_0 is also related to concentrations of reactants and the summary of electrochemical parameters for different reactions is listed in Figure 5.

Where the Exchange Current Density is: $i_o = i_{oref} \left(\frac{C_{H^+}}{C_{H^+ref}}\right)^{a_1} \left(\frac{c_{CO_2}}{c_{CO_2 ref}}\right)^{a_2} \left(\frac{c_{H_2CO_3}}{c_{H_2CO_3 ref}}\right)^{a_3} \times e^{\frac{-\Delta H}{R}\left(\frac{1}{T}-\frac{1}{T_{ref}}\right)}$

	i_{oref} $\frac{A}{m^2}$	a_1	$c_{H^+ ref}$ molar	a_2	$c_{CO_2 ref}$ molar	a_3	$c_{H_2CO_3 ref}$ molar	ΔH $\frac{kJ}{mol}$	T_{ref} °C	E_{rev} V	b V
$2H^+ + 2e^- \rightarrow H_2$	0.05	0.5	10^{-4}	0	N/A	0	N/A	30	25	$-\frac{2.3RT}{F}pH$	$\frac{2.3RT}{2F}$
$2H_2CO_3 + 2e^- \rightarrow H_2 + 2HCO_3^-$	0.06	–0.5	10^{-5}	0	N/A	1	10^{-4}	50	20	$-\frac{2RT}{F}pH$	$\frac{2.3RT}{2F}$
$Fe \rightarrow Fe^{2+} + 2e^-$	1	1 for p_{CO_2} <1 bar 0 for p_{CO_2} 1 bar	10^{-4}	2 for pH < 4 1 for 4 < pH < 5 0 for pH > 5	0.0366	0	N/A	37.5	25	–0.488	0.03 for pH < 4 0.08 for 4 < pH < 5 0.12 for pH > 5

Figure 5. Electrochemical parameters for the reactions involved in CO_2 corrosion [11].

When the cathodic reactants are reacted rapidly at the steel surface, the rate of the overall corrosion process is determined by the rate at which these cathodic reactants can be supplied from the bulk solution. At this condition, the reaction is referred to as "diffusion controlled" and the corresponding limiting current density (i_{lim}) can be expressed as:

$$i_{lim\,(A^+)} = k_{m\,(A^+)} F[A^+] \tag{24}$$

where $k_{m\,(A^+)}$ is mass transfer coefficient of reactant A; F is Faraday constant; $[A^+]$ is concentration of reactant A. Given charge transfer current density and limiting current density, the overall current density (i) can be expressed as:

$$i = \frac{1}{\frac{1}{i_\alpha} + \frac{1}{i_{lim}}} \tag{25}$$

As corrosion proceeds the anodic current density is electrically balanced by the cathodic current density at the steel surface and the unknown corrosion potential (E_{corr}) can be found:

$$i_{(H^+)} + i_{(H_2CO_3)} = i_{(Fe)} \tag{26}$$

Once the value of E_{corr} is found, substitute the value E in equation (22) for iron dissolution with E_{corr} can yield corrosion current (i_{corr}). Therefore, CO_2 corrosion rate (CR) can be obtained by Faraday's law:

$$CR = \frac{i_{corr} M_{Fe}}{\rho_{Fe} 2F} \tag{27}$$

where M_{Fe} is molecular mass of iron; ρ_{Fe} is density of iron.

During the corrosion process, when the concentration of Fe^{2+} from corroded steel and that of CO_3^{2-} from dissolved CO_2 are high to an extent i.e., their product exceeds the solubility limit, the precipitation of iron carbonate ($FeCO_3$) occurs according to:

$$Fe^{2+} + CO_3^{2-} \Leftrightarrow FeCO_{3(s)} \tag{28}$$

This nonequilibrium situation is called "supersaturation" ($SS_{(FeCO_3)}$). The higher the supersaturation, the faster the precipitation will happen. $SS_{(FeCO_3)}$ can be defined as:

$$SS_{(FeCO_3)} = \frac{C_{Fe}^{2+} C_{CO_3}^{2-}}{K_{sp(FeCO_3)}} \tag{29}$$

where $K_{sp(FeCO_3)}$ is solubility product constant, a function of temperature and strength.

$$K_{sp(FeCO_3)} = 10^{\left(-59.3498-0.041377\times T_k-\frac{2.1963}{T_k}+24.5724\times logT_k+2.518\times I^{0.5}-0.657\times I\right.} \quad (30)$$

where T_k is temperature in K; I is ionic strength.

The iron carbonate precipitation/growth rate (R_{FeCO_3}) can be modeled mathematically by two equations:

$$R_{FeCO_3} = Ae^{\frac{54.8-123}{RT}K_{sp(FeCO_3)}\left(SS_{(FeCO_3)}^{0.5}-1\right)^2} \quad (31)$$

$$R_{FeCO_3} = Ae^{\frac{52.4-119}{RT}K_{sp(FeCO_3)}\left(SS_{(FeCO_3)}-1\right)\left(1-SS_{(FeCO_3)}^{-1}\right)} \quad (32)$$

where A is surface area available for precipitation per unit volume; R is gas constant; T is temperature; $K_{sp(FeCO_3)}$ is solubility product constant; $SS_{(FeCO_3)}$ is supersaturation. It should be noted that iron carbonate can not only precipitate on the steel surface but also within the pores of a porous surface layer in which A is equal to the surface area of the pore per unit volume. Dense and protective iron carbonate surface layers form when the precipitation rate is larger than the corrosion rate under high temperature (> 50 ℃) and high pH (> 5). Otherwise, non-protective and porous iron carbonate surface layers form instead.

Nesic et al. model gives a clearer picture of corrosion mechanism compared to de Waard and Milliams model because all equations and parameters have physical meanings; however, those parameters have to be determined from experiments.

2.1.3 *Sun and Nesic model*

So far, the previous described two models for uniform corrosion are in "sweet corrosion" (CO_2 corrosion) margin only. Not until 2009 does Sun and Nesic [14] propose a mechanistic model that propagates the application of corrosion modeling to "sour corrosion" (CO_2/H_2S corrosion). Since H_2S is hardly present by itself without CO_2 in a real gas pipeline, so this model predicts uniform corrosion in a mixed CO_2/H_2S environment.

Based on their experimental observations, sulfide layers especially Mackinawite-type sulfides are likely to present at the beginning of the corrosion process by a fast, direct, and heterogeneous reaction at the steel surface called "solid-state reaction":

$$Fe_{(S)} + H_2S \Longrightarrow FeS_{(s)} + H_2 \qquad (33)$$

Due to the presence of this inner mackinawite film, this model assumes that the whole corrosion process is under mass-transfer control and the fluxes of three main corrosive species i.e., CO_2, H_2S, H^+. As corrosion proceeds, the mackinawite film grows and delaminates over time, leading to the formation of the outer mackinawite layer. How these fluxes are transported from the liquid/bulk

solutions to the steel surface through the mackinawite film are keys to simulate the corrosion rate. A schematic diagram of the corrosion process is shown in Figure 6.

Take H_2S for example, three kinds of fluxes are considered:

(1) Convective diffusion through the mass-transfer boundary layer:

$$\mathrm{Flux}_{H_2S} = k_{m,H_2S}(C_{b,H_2S} - C_{o,H_2S}) \tag{34}$$

where k_{m,H_2S} is mass-transfer coefficient for H_2S in the hydro-dynamic boundary layer ($= 1 \times 10^{-4}$ m/s); C_{b,H_2S} is bulk concentration of H_2S in the liquid/bulk solution in mol/m^3; C_{o,H_2S} is interfacial concentration of H_2S at the outer layer/solution interface in mol/m^3.

(2) Molecular diffusion through the liquid in the porous outer layer:

$$\mathrm{Flux}_{H_2S} = \frac{D_{H_2S}\varepsilon\psi}{\delta_{os}}(C_{o,H_2S} - C_{i,H_2S}) \tag{35}$$

$$\delta_{os} = \frac{m_{os}}{\rho_{FeS}\, A} \tag{36}$$

where D_{H_2S} is diffusion coefficient for dissolved H_2S in water ($= 2 \times 10^{-9}$ m^2/s); ε is outer mackinawite layer porosity ($= 0.9$); ψ is outer mackinawite layer tortuosity factor ($= 0.003$); δ_{os} is thickness of the mackinawite layer in m; m_{os} is mass of the mackinawite layer in kg; A is surface area of the steel in m^2; ρ_{FeS} is density of the mackinawite layer in g/m^3.

(3) Solid-state diffusion through the inner mackinawite layer:

$$\mathrm{Flux}_{H_2S} = A_{H_2S} \ln\left(\frac{C_{i,H_2S}}{C_{s,H_2S}}\right) \tag{37}$$

where A_{H_2S} is solid-state diffusion kinetic constant for H_2S ($= 2 \times 10^{-5}$ mol/m^{2}s); C_{s,H_2S} is "near-zero" concentration of H_2S on the steel surface ($= 1 \times 10^{-7}$ mol/m^3).

In a steady state, these three fluxes are equivalent to each other and Flux_{H_2S} becomes:

$$\mathrm{Flux}_{H_2S} = A_{H_2S} \ln\left(\frac{C_{b,H_2S} - \mathrm{Flux}_{H_2S}\left(\frac{\delta_{os}}{D_{H_2S}\varepsilon\psi} + \frac{1}{k_{m,H_2S}}\right)}{C_{s,H_2S}}\right) \tag{38}$$

This flux can be further converted to corrosion rate caused by H_2S (CR_{H_2S}):

$$CR_{H_2S} = \mathrm{Flux}_{H_2S}\, M_{Fe}/\rho_{Fe} \tag{39}$$

where M_{Fe} is molecular mass of iron; ρ_{Fe} is density of iron.

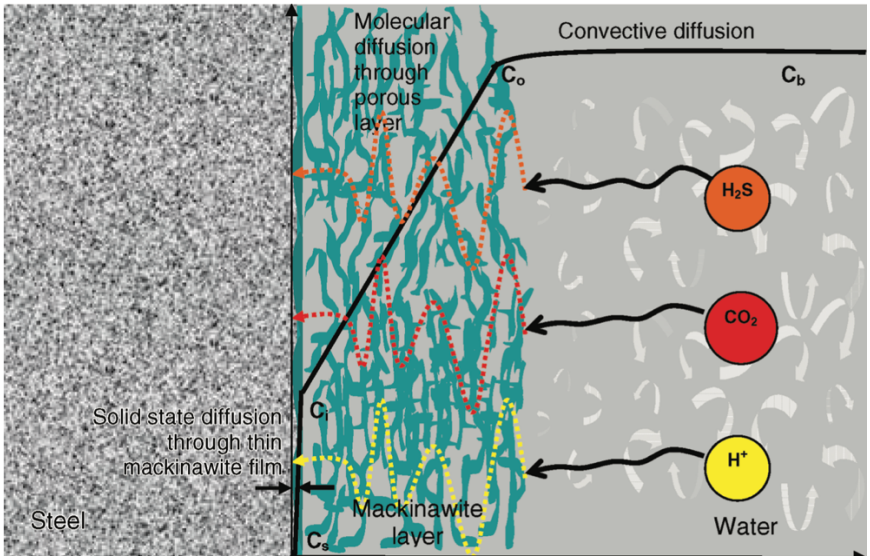

Figure 6. A schematic diagram of CO_2/H_2S corrosion process [14].

The effects of other two corrosive species, namely, CO_2 and H^+ on corrosion follow similar patterns in a calculation of corrosion rate by CO_2 (CR_{H_2S}) and by H^+ (CR_{H^+}). Finally, the total corrosion rate in a mixed CO_2/H_2S environment (CR) is the contribution of these three main corrosive species:

$$CR = CR_{H_2S} + CR_{CO_2} + CR_{H^+} \tag{40}$$

Refer to equation (38), most parameters can be found in handbooks or are already determined via experiments except δ_{os}, which is thickness of mackinawite layer. The thickness changes over time based on the layer formation kinetics and layer damage kinetics:

$$SRR = SFR - SDR \tag{41}$$

where SRR is sulfide layer retention rate in $\mathrm{mol/m^2 s}$; SFR is sulfide layer formation rate in $\mathrm{mol/m^2 s}$; SDR is sulfide layer damage rate in $\mathrm{mol/m^2 s}$.

Since the formation of sulfide layers is a solid-state reaction as shown in equation (33), the supplier of Fe^{2+} is from the steel itself via corrosion process. The SFR is therefore assumed to be corrosion rate (CR). As for SDR, which is assumed to be affected by intrinsic or hydrodynamic stresses, is set to be 0.5CR as half of the formed sulfide layer is lost based on experimental observations. The final expression of SRR becomes:

$$\mathrm{SRR} = \mathrm{CR} - 0.5\mathrm{CR} = 0.5\mathrm{CR} \tag{42}$$

Once SRR is determined, the change in mass of the mackinawite layer (Δm_{os}) in equation (36) can be calculated via:

$$\Delta m_{os} = \mathrm{SRR}\, M_{FeS}\, A\, \Delta t \tag{43}$$

where M_{FeS} is molecular mass of iron sulfide; Δt is time interval.

Sun and Nesic model successfully extends the application margin from CO_2 only to mixed CO_2/H_2S environments; however, assumptions such as: (1) not considering sulfide layer dissolution effect and (2) the whole corrosion process is under mass-transfer control makes the model inaccurate under certain conditions.

2.2 Internal Pitting corrosion modeling

Unlike uniform corrosion, the percentage of cathodic and anodic areas on the steel surface are uneven for pitting corrosion, leading to localized degradation of materials. Usually a small anodic reaction site is surrounded by large local cathodic reaction sites and form a pit. Depending on the types of materials, operating conditions, and environment, pits have different shapes as shown in Figure 7 [15]. Pits usually initiate at places where protective layers break down and fresh materials are exposed. Therefore, the initiation is related to the composition and thickness of protective layers as well as harmful ions such as chloride ions that tend to destroy protective layers. However, pitting corrosion has random nature, which makes it hard to predict. This also explains why many state-of-the-art pitting corrosion predictive models are data driven with small physical foundation.

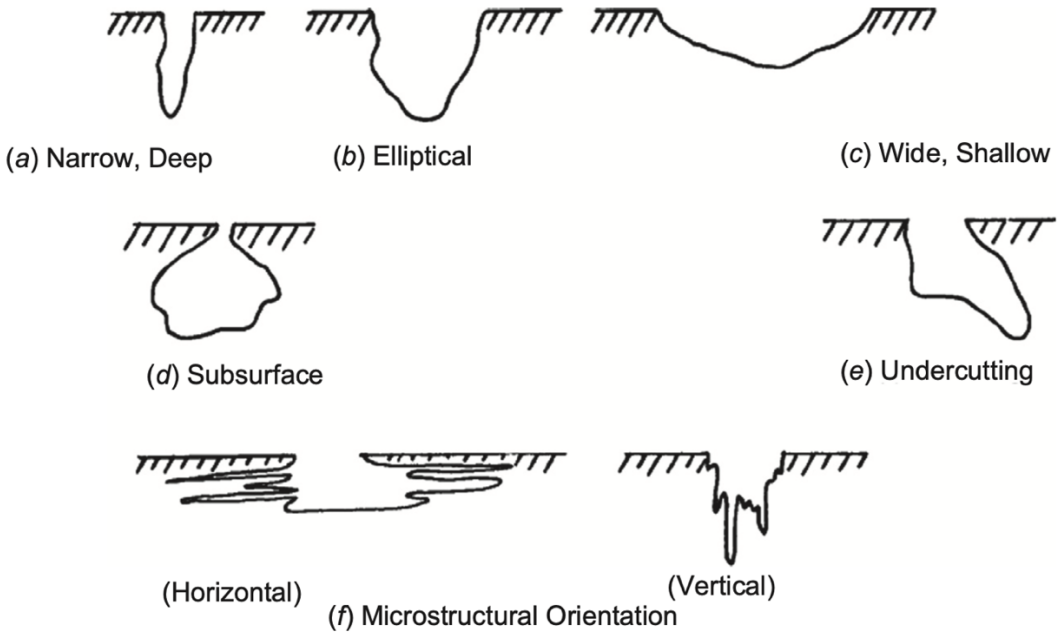

Figure 7. Different shapes of pits [15].

2.2.1 *Common data-driven based models*

According to a review study [4], there are two classes of data-driven based models for pitting corrosion, namely, random variable-based and stochastic process-based models, both of which have their sub-class categories.

2.2.1.1 *Random variable-based models*

Random variable-based models are the most common and easiest for reliability analysis. This category has two sub-classes, namely, linear random variable-based and non-linear random variable-based models depending on whether they can reflect the time-dependent nature of pitting corrosion rate or not.

(1) Linear random variable-based models

A linear random variable-based model estimates pit growth rate for a population of defects by a linear equation:

$$\upsilon_d = \frac{D(t_2) - D(t_1)}{t_2 - t_1} \tag{44}$$

where $D(t_1)$ and $D(t_2)$ is maximum depth of the pit at $t_1$and t_2, respectively; υ_d is pit growth rate of the pit.

Although this model requires only small number of data sets and is used commonly, it does not take into account the time-dependent nature of pitting corrosion. In addition, backward

extrapolation of this model results in negative corrosion initiation time, which violates the physics of corrosion.

(2) Non-linear random variable-based models

On the other hand, a non-linear random variable-based model [16,17] improves the drawback of linear random variable-based model and predicts the maximum defect depth by a power function:

$$D_{max}(t) = k(t - t_0)^{\alpha} \quad (45)$$

where $D_{max}(t)$ is maximum defect depth at time t; t_0 is initiation time of stable pit growth; k is proportionality factor; α is exponent factor (a positive and less than one number).

Random variable-based models are easy to develop and use via regression analysis; however, they do not consider either spatial heterogeneity or temporal variation on corrosion modeling, leading to less realistic predictions for the future. On the contrary, stochastic process-based models show the advancement by dealing with the temporal variability of the corrosion degradation process.

2.2.1.2 *Stochastic process-based models*

Stochastic process-based models have four sub-classes, namely, linear stochastic process-based, non-linear stochastic process-based, Markov process-based, and Gamma process-based models.

(1) Linear stochastic process-based models

A linear stochastic process-based model takes into account the temporal variability by modeling the pit growth rate as a Poisson square wave process (PSWP) [18]. PSWP describes maximum pit depth growth rate (i.e., pulse height) as independent and identically distributed (i.i.d) random variables that are characterized by any specified distributions; pulse durations are characterized as i.i.d random variables that are exponentially distributed. This model estimates the maximum pit depth by:

$$D_{max}(t_{i+1}) = D_{max}(t_i) + Y_i(t_{i+1} - t_i) \quad \text{for} \quad i = 0, 1, \dots, n \tag{46}$$

where $D_{max}(t_i)$ is maximum pit depth at time t, Y_i is maximum pit depth growth rate; n is number of pulses.

Similar to the linear random variable-based model, this model also leads to negative corrosion initiation time after backward extrapolation.

(2) Non-linear stochastic process-based models

Non-linear stochastic process-based models are developed to correct the drawback of linear stochastic process-based models. A general expression of the maximum pit depth by a non-linear stochastic process-based model is given by [18]:

$$D_{max}(t_{i+1}) = D_{max}(t_i) + Y_i[(t_{i+1} - t_0)^{\alpha} - (t_i - t_0)^{\alpha}] \quad \text{for} \quad i = 0, 1, \dots, n \tag{47}$$

where $D_{max}(t_i)$ is maximum pit depth at time t; Y_i is proportionality coefficient of maximum pit depth; α is exponent coefficient; n is number of pulses; t_0 is corrosion initiation time.

Although stochastic process-based models take into account the temporal variability, they do not consider the spatial heterogeneity.

(3) Markov process-based models

Another sub-class of stochastic process-based models is Markov process-based models. A Markov process is a continuous-time stochastic process that follows Markovian property in which the conditional probability of the future state depends only on the present state. Pitting corrosion process can be described by the Kolmogorov differential equations given by [19]:

$$\frac{dP_1(t)}{dt} = -\lambda_1 P_1(t) \tag{48}$$

$$\frac{dP_i(t)}{dt} = -\lambda_{i-1} P_{i-1}(t) - \lambda_i P_i(t) \quad \text{for} \quad i = 2, \dots, N \tag{49}$$

where λ_i is transition rate from state i to $i+1$; $P_i(t)$ is probability of being in state i at time t; N is number of states in which the thickness of the pipeline divided.

For a Markov process-based model, the goal is to predict the probability of being in each state represented by the maximum pit depth at each time. Thus, the difficulties of this model are to find transition rates between states and relate transition rates to corrosion rates with available data that can best describe the corrosion behavior of gas pipelines. Transition rates can be time-dependent

to become non-homogeneous Markov process-based models [20]. Non-homogeneous transition rates can be expressed as:

$$\lambda_j(t) = \frac{\lambda_j(1+\lambda t)}{1+\lambda t^k} \qquad \text{for} \qquad j = 1, 2, \dots, n \tag{50}$$

where λ_j is transition rate from state j to $j+1$; t is exposure time; λ and k are parameters of a specific pitting corrosion in pipe systems.

Similar to stochastic process-based models, Markov process-based models consider the temporal variability but not the spatial heterogeneity.

(4) Gamma process-based models

Last sub-class of stochastic process-based models is Gamma process-based models. The pitting corrosion depth at time t, $d(t)$, can be characterized by a homogeneous gamma process with a time-dependent shape parameter, $\alpha(t)$, and a scale parameter, β. The probability density function of $d(t)$ can be expressed as [21]:

$$f_G(d(t)|\alpha(t-t_0,\beta) = \beta^{\alpha(t-t_0)} \frac{d(t)^{\alpha(t-t_0)-1} e^{-d(t)\beta} I(t)}{\Gamma(\alpha(t-t_0))} \tag{51}$$

where t_0 is corrosion initiation time; $\Gamma(\cdot)$ is gamma function; $I(t)$ is indicator function, which equals to unity if $t > t_0$ or equals to zero if $0 \le t \le t_0$.

As $\alpha(t) > 0$ and $\beta > 0$, which results in the monotonic increasing nature of the gamma process, this process can describe degradation mechanisms such as corrosion well. In other words, it

captures the increasing nature of the defect size. In addition, Gamma process-based models are the most versatile ones among data-driven models because they consider both temporal variability and spatial heterogeneity.

2.2.2 *Mathematical function-based models - Papavinasam model*

Papavinasam et al. [22,23] propose a predictive model that takes operating parameters into account for oil and gas pipelines. The model is developed based on laboratory experiments which are done to simulate real operating conditions as well as field data from real operating pipelines. It can only be used to predict pitting corrosion rate for the location where water is accumulated. Different effects of parameters on pitting corrosion rate are discussed and quantified each of which can influence pitting corrosion rate individually:

(1) Effect of oil:

The influence of oil on pitting corrosion depends on the type of oil-water emulsion. For water-in-oil (W/O) emulsion, as the continuous phase oil has low conductivity, corrosion on the steel surface in contact with W/O emulsion is reduced. However, oil-in-water (O/W) emulsion is likely to facilitate corrosion as water with high conductivity is the continuous phase in contact with the steel surface. The pitting corrosion rate (PCR_{oil}) as a function of contact angle of oil in a water environment is given by:

$$PCR_{oil} = -0.33\theta + 55 \quad (52)$$

where θ is contact angle in degree.

(2) Effect of water:

Wettability of water in the environment with the presence of oil has a large impact on pitting corrosion. An oil-wet surface is immune to corrosion, but a water-wet surface or a mixed-wet surface is not. According to experiments, the wettability of water is related to water percentage (water production rate/ (water + oil production rate) × 100). The pitting corrosion rate (PCR_{water}) as a function of water percentage is given by:

$$PCR_{water} = 0.51W + 12.13 \quad (53)$$

where W is water percentage in %.

(3) Effect of gas:

Besides the presence of oil and water, the production rate of gas would affect the flow rate. The increase of the turbulence flow increases pitting corrosion, which can by modeled by wall shear stress. The pitting corrosion rate (PCR_{gas}) as a function of wall shear stress is given by:

$$PCR_{gas} = 0.19W_{ss} + 64 \quad (54)$$

where W_{ss} is wall shear stress in Pa.

(4) Effect of solids:

Solids influence pitting corrosion in many ways depending on different flow regimes. Under low flow regime, solids may deposit on the steel surface and facilitate underdeposit localized corrosion; under moderate flow regime, solids are likely to remove protective layers in localized areas where pitting corrosion will occur; under high flow regime, solids may promote erosion corrosion. The pitting corrosion rate (PCR_{solid}) as a function of the presence of solids is given by:

$$PCR_{solid} = 25R_{solid} + 50 \quad (55)$$

where R_{solid} is the presence of solids in a pipe (= 1 for presence; = 0 for absence).

(5) Effect of temperature:

The influence of temperature on corrosion is complicated. In general, higher temperature increases corrosion rate because it accelerates chemical and electrochemical reactions of corrosion. However, high temperature also facilitates the precipitation of protective layers and reduce corrosion rate. For pitting corrosion, high temperature increases the diffusivity of pitting species such as chloride ions which may destroy protective layers in localized areas, increasing pitting corrosion rate. The pitting corrosion rate (PCR_T) as a function of temperature is given by:

$$PCR_T = 0.57T + 20 \quad (56)$$

where T is temperature in ℃.

(6) Effect of total pressure:

Pressure has a dual role on corrosion. High pressure may facilitate corrosion if it accelerates the dissolution of steels; however, it may also promote the formation of protective layers as supersaturation condition is met. The pitting corrosion rate (PCR_P) as a function of total pressure is given by:

$$PCR_P = -0.081P_{total} + 88 \quad (57)$$

where P_{total} is total pressure in psi.

(7) Effect of H_2S partial pressure:

H_2S becomes corrosive once it is dissolved in water. Aqueous H_2S has a dual role on corrosion. Higher H_2S partial pressure may increases corrosion rate as H_2S reduction is a key cathodic reaction for corrosion in a H_2S-present environment. On the other hand, Higher H_2S partial pressure may also inhibit corrosion rate as dissolution of H_2S provides required species S^{2-} for the formation of iron sulfide protective layers. The pitting corrosion rate ($PCR_{P_{H_2S}}$) as a function of H_2S partial pressure is given by:

$$PCR_{P_{H_2S}} = -0.54P_{H_2S} + 67 \quad (58)$$

where P_{H_2S} is partial pressure of H_2S in psi.

(8) Effect of CO_2 partial pressure:

Similar to H_2S, CO_2 reduction is one of the main cathodic reactions for corrosion in a CO_2-present environment. However, it also promotes the formation of iron carbonate layers and inhibit corrosion rate. According to Sun and Nesic [14], the formation of iron sulfide is kinetically preferable compared to that of iron carbonate; therefore, the dominant protective layers are mainly iron sulfides in a mixed CO_2/H_2S environment. The pitting corrosion rate ($PCR_{P_{CO_2}}$) as a function of H_2S partial pressure is given by:

$$PCR_{P_{CO_2}} = -0.63P_{CO_2} + 74 \quad (59)$$

where P_{CO_2} is partial pressure of CO_2 in psi.

(9) Effect of sulfate ions:

The effect of sulfate ion on corrosion is predominant only in the presence of H_2S. Once sulfate layers are formed, corrosion rate is inhibited. Experiments show that sulfate ions have little effect on pitting corrosion rate. The pitting corrosion rate ($PCR_{SO_4^{2-}}$) as a function of sulfate ions is given by:

$$PCR_{SO_4^{2-}} = -0.013[SO_4^{2-}] + 57 \quad (60)$$

where $[SO_4^{2-}]$ is concentration of sulfate ions in ppm.

(10) Effect of bicarbonate ions:

According to equation (2), CO_2 can be dissolved in water and form carbonic acid (H_2CO_3), which later will later dissociate into H^+ and HCO_3^- according to equation (3). The dissolution step is why aqueous CO_2 is corrosive; however, if the supply of HCO_3^- is sufficient, shifting the equilibrium of equation (3) to the left and reducing the severity of corrosion. In addition, bicarbonate ions act like a buffer that can absorb H^+ ions and neutralize the acid. The pitting corrosion rate ($PCR_{HCO_3^-}$) as a function of bicarbonate ions is given by:

$$PCR_{HCO_3^-} = -0.014[HCO_3^-] + 81 \quad (61)$$

where $[HCO_3^-]$ is concentration of bicarbonate ions in ppm.

(11) Effect of chloride ions:

Chloride ion is the most potent species in destroying protective layers; therefore, it plays an important role for inducing pitting corrosion. In addition, once a pit is formed, it is likely to accumulate inside a pit and accelerates corrosion rate.

$$PCR_{Cl^-} = 0.0007[Cl^-] + 9.2 \quad (62)$$

where $[Cl^-]$ is concentration of chlorides ions in ppm.

(12) Effect of unconsidered parameters:

There are some minor parameters (e.g., acetic acid) that may influence pitting corrosion but not discovered or considered in this model. Their effects are considered by taking the mean value of

other 11 individual pitting corrosion rate called $\mathrm{PCR_{additional}}$. This effect has small influence on predicted corrosion rate, but it increases the uncertainty of the prediction.

(13) Combined effect:

Although each of the parameter discussed above can individually influence pitting corrosion rate, the ultimate pitting corrosion is the combined effect of all operational parameters. That is to say the influence of each parameter has to be connected in a statistical principle because the driving force for pitting corrosion is a distributed parameter. The ultimate pitting corrosion rate ($\mathrm{PCR_{mean}}$) can be expressed as:

$$\mathrm{PCR_{mean}} = \frac{\mathrm{PCR_{oil}} + \mathrm{PCR}_{water} + \mathrm{PCR}_{gas} + \cdots + \mathrm{PCR}_{SO_4^{2-}} + \mathrm{PCR}_{HCO_3^-} + \mathrm{PCR}_{Cl^-}}{12} \qquad (63)$$

According to the model assumptions, $\mathrm{PCR_{mean}}$ is the resulting pitting corrosion rate at a localized anodic reaction site where protective layers are removed.

(14) Effect of duration:

In general, pitting corrosion rate is not constant during the propagation of pitting corrosion. Many factors (e.g., reformation of protective layers, local increase in pH, etc…) actually lead to a parabolic decrease of pitting corrosion as a function of time. If the operating conditions are constant over years, the average pitting corrosion rate ($\mathrm{PCR_{average}}$) can be expressed as:

$$PCR_{average} = \frac{\frac{PCR_{mean}}{1} + \frac{PCR_{mean}}{2} + \frac{PCR_{mean}}{3} + \cdots + \frac{PCR_{mean}}{t}}{t} \quad (64)$$

where t is number of years.

(15) Effect of flow regime:

Based on the analysis of field data, this model further provides a correction factor in a consideration of flow regime, which is multiplied by $PCR_{average}$. Different kinds of flow regime may happen inside a gas pipeline and influence the water wettability in contact with the steel surface, resulting in the change of corrosion behaviors. Correction factors based on different flow regimes and the pitting corrosion rate (PCR) as a function of flow regime are provide in Table 1.

Table 1. Corrected predicted pitting corrosion rate as a function of flow regime [22].

Flow Regime Type	PCR
Slug Flow	No Change
Plug Flow	$PCR_{average} \times 0.98$
Bubble Flow	$PCR_{average} \times 0.96$
Dispersed Flow	$PCR_{average} \times 0.94$
Oscillatory Flow	$PCR_{average} \times 0.92$
Annular Flow	$PCR_{average} \times 0.90$
Churn Flow	$PCR_{average} \times 0.88$
Wave Flow	$PCR_{average} \times 0.86$
Stratified Flow	$PCR_{average} \times 0.84$

2.3 Pipeline corrosion risk assessment

Risk assessment is to analyze and evaluate the risk associated with damage caused by a certain kind of hazard in terms of the probability of occurrence and the magnitude of the consequence of occurrence. Risk assessment is also central to pipeline integrity management that ensures the maximum availability of pipelines. Corrosion risk is about future failure probabilities of corroded pipelines and consequences of pipeline failure that may lead to asset and personnel loss. Two approaches, namely, deterministic and probabilistic approaches, have been developed for the treatment of pipeline corrosion risk.

2.3.1 *Deterministic framework*

Traditional deterministic approach of risk assessment is based on expert judgement by engineering personnel, which is fallible and subjective for many cases [24]. On the other hand, semi-quantitative (deterministic) approach adopts explicit judgement that scientific treatment or model makes, which is more reliable and objective.

Deterministic corrosion risk assessment of gas pipelines involves the prediction of corrosion rate by any given corrosion models and the determination of pipe minimum allowable wall thickness (MAWT) and nominal pipe wall thickness. On the basis of the assumption that corrosion rate is constant over time, the remaining life (years) at a distance "z" along a pipeline ($R(z)$) can be calculated by:

$$R(z) = \frac{N_{wt} - d(z) - t_{MAWT}}{CR(z)} \tag{65}$$

where N_{wt} is nominal pipe wall thickness; $d(z)$ is cumulative corrosion damage to date at distance z; t_{MAWT} is pipe minimum allowable wall thickness; $CR(z)$ is corrosion rate at distance z by a given corrosion model.

The probability of failure is then determined based on the remaining life values of the pipe. The development of failure criteria relies on expert judgement and may differ among different pipeline operators. An example of deterministic failure probability criteria is shown in Table 2.

Table 2. Demonstration of deterministic failure probability criteria.

Pipeline Remaining Life (years)	Probability of Failure
$\mathbf{R(z) < 5}$	High
$\mathbf{5 < R(z) < 15}$	Medium
$\mathbf{R(z) > 15}$	Low

Although deterministic approach is simple to use and can be applied to the whole pipeline, the prediction is sometimes too conservative as each classification of probability of failure covers a large window of pipeline remaining life, which prevents pipeline operators from applying cost-effective maintenance practices based on the prediction result. Also, its inability to deal with uncertainties of input data exposes the corrosion prediction to the risk of underestimation or overestimation problem.

2.3.2 *Probabilistic framework*

Unlike deterministic approach which takes mean values of input data, probabilistic approach takes uncertainties of input data into account in terms of probability distributions [25,26]. Therefore, the prediction, mostly based on scientific standards or models, considers the information of uncertainty. In other words, extreme conditions are considered, enabling pipeline operators to take suitable actions.

2.3.2.1 *Service limit method*

Service limit method involves the determination of service limit, namely, corrosion allowance of a gas pipeline above which the pipeline fails because of corrosion-induced failure [24]. Probability distributions of cumulative corrosion damage over time are collected or estimated each of which will later be compared to the corrosion allowance to determine if failure event is likely to happen. An analytical expression for failure probability calculation is given:

$$P(C(t) > \lambda) = 1 - \int_0^{\lambda} \phi\big(C(t)\big)dt \tag{66}$$

where λ is corrosion allowance; $C(t)$ is cumulative corrosion damage at time t; ϕ is probability density distribution. Figure 8 shows a schematic diagram of service limit method showing the probability density function of cumulative corrosion damage with respect to corrosion allowance.

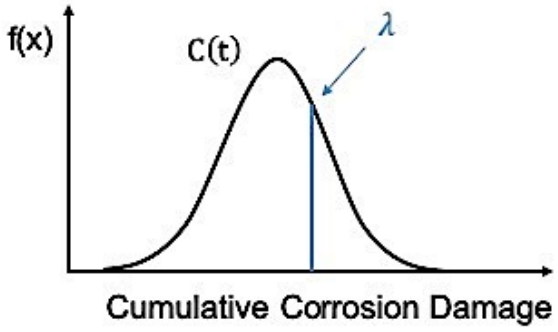

Figure 8. Illustration of service limit method of cumulative corrosion damage.

2.3.2.2 *Reliability analysis method*

A system's reliability can be modeled by considering the performance criteria, i.e., load and resistance [27,28]. A functional relationship between a load and a resistance is called "limit state function" ($G(x)$), which can be expressed as:

$$G(x) = R - L \tag{67}$$

where R is probability density function of resistance (or strength); L is probability density function of load.

The limit state function is negative when the system fails, but is positive when the system is stable. Figure 9 shows a schematic diagram of limit state function of a system with respect to load and resistance. As the results by probabilistic methods such as reliability analysis method are hard to verify experimentally, numerical technique i.e., Monte Carlo simulation is often used to artificially simulate a large number of experiments to obtain outcomes of the model. This technique involves

random sampling of load and resistance random variables (R.V.) from their respective probability distributions and evaluation of whether a failure scenario ($G(x) < 0$) happens for the calculation of failure probability (P_f). The analytical expression of this technique is given by:

$$P_f = \frac{n(G(x) < 0)}{N} \tag{68}$$

where N is number of trials.

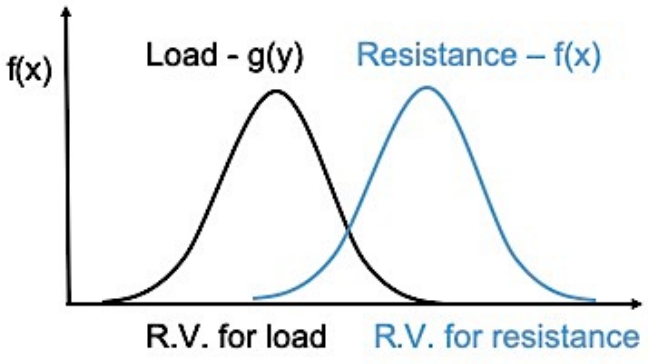

Figure 9. Illustration of reliability analysis method of limit state function of a system.

3 Research objectives

The main objectives of this research are: firstly, develop a corrosion predictive model that considers both temporal and spatial variability of operating for corrosion predictions. Secondly, develop a smart condition-based maintenance algorithm by reinforcement learning using the proposed corrosion predictive model as a pipeline system to be simulated. This research work is a part of the project titled: "**Inference Methodology for Pipeline System Integrity Management**",

which aims at developing a multi-disciplinary science, engineering, and operational approach to find a solution of pipeline integrity. Therefore, the developed corrosion predictive model and maintenance algorithm is/will be integrated into a pipeline system and integrity management (PSIM) software that is currently being developed by our lab to fulfill the corrosion prognosis function of the software.

To address the research contributions that have been done, this dissertation involves three parts in a hierarchical order: Part A - pipeline corrosion predictive model, Part B - smart condition-based maintenance (SCBM) algorithm and Part C - pipeline system and integrity management software as shown in Figure 10.

Each of these topics has respective sub-topics listed as follows:

Part A: Pipeline Corrosion Predictive Model - Chapter 4 to 6

(1) Development of corrosion predictive models for gas pipelines (Chapter 4):

A corrosion predictive model was developed to study the internal corrosion of transmission gas pipelines subject to an aqueous CO_2/H_2S environment. Two common types of corrosion, namely, uniform and pitting corrosion, were considered in the development of the model. The model can predict corrosion rates and depths given operating and environmental parameters.

(2) Modeling of the variability of operating and environmental parameters in gas pipelines (Chapter 4):

Methodology to simulate operating and environmental parameters in operating gas pipelines with both temporal and spatial variabilities were proposed. Considering variability of operating and environmental parameters enables the corrosion predictive models to predict time-evolution probability density functions of corrosion rates and depths.

(3) Model validation with experimental data (Chapter 5):

The proposed uniform corrosion model embedded in the internal corrosion predictive model was validated with the experimental data with respect to pH, flow velocity, temperature, and partial pressure of H_2S. The effects of these parameters on corrosion rates were discussed.

(4) Model application on operating gas pipelines in the field (Chapter 6):

To verify the validity of this model on operating gas pipelines, eight wet gas pipelines in Sichuan province, China were studied, and the predicted corrosion rates were compared with observational corrosion rates. Due to lack of information, the identification of the types of corrosion that these gas pipelines are suffered must be made before the corrosion prediction. A methodology including extreme value analysis and risk curve analysis was applied to identify uniform and pitting corrosion given the pipe wall loss data.

Part B: Smart Condition-based Maintenance (SCBM) of Pipeline Integrity Management - Chapter 7 and 8

(1) Development of smart conditioned-based maintenance (SCBM) algorithm (Chapter 7):

A smart condition-based maintenance management methodology was developed for cost-optimization of maintenance actions by a reinforcement learning (RL) algorithms. Due to lack of data, the developed internal corrosion predictive model was used to simulate the environment (pipeline) and reacted with the agent (maintenance planner).

(2) Case study (Chapter 8):

The results by the proposed maintenance planner were compared to those by the traditional periodic maintenance policy. The main difference between results by two methodologies was discussed.

Part C: Pipeline System Integrity Management (PSIM) Software - Chapter 9 and 10

(1) Description of the PSIM software framework (Chapter 9):

A risk-based pipeline integrity management tool that integrates data, methods, and technologies into a dynamic pipeline health and monitoring management software developed in our lab was introduced. The software can firstly do integrity assessment based on a variety of evidence including real monitoring data and inspection; secondly, predict pipe segment health with corrosion prognostic function; last but not least, optimize the sensor placement by inference probability models based on the damage (i.e. corrosion) detection in gas pipelines at a specific location.

(2) Development of the corrosion prognosis function (Chapter 9):

The proposed internal corrosion predictive model along with an external corrosion model composed of two corrosion models, namely, pitting corrosion and stress corrosion cracking models, were integrated into the software to fulfil the corrosion prognostic function.

(3) Case study (Chapter 10):

A system-level pipeline integrity management analysis was done on Hybrid Causal Logic Analyzer (HCLA), a software platform that combines Boolean logic-based probability risk assessment (PRA) methods such as event sequence diagrams (ESDs) and fault trees (FTs) with Bayesian networks (BNs), for the calculation of pipeline failure probabilities. A case study was then done to demonstrate the results of its dynamic pipeline network probabilistic health assessment function.

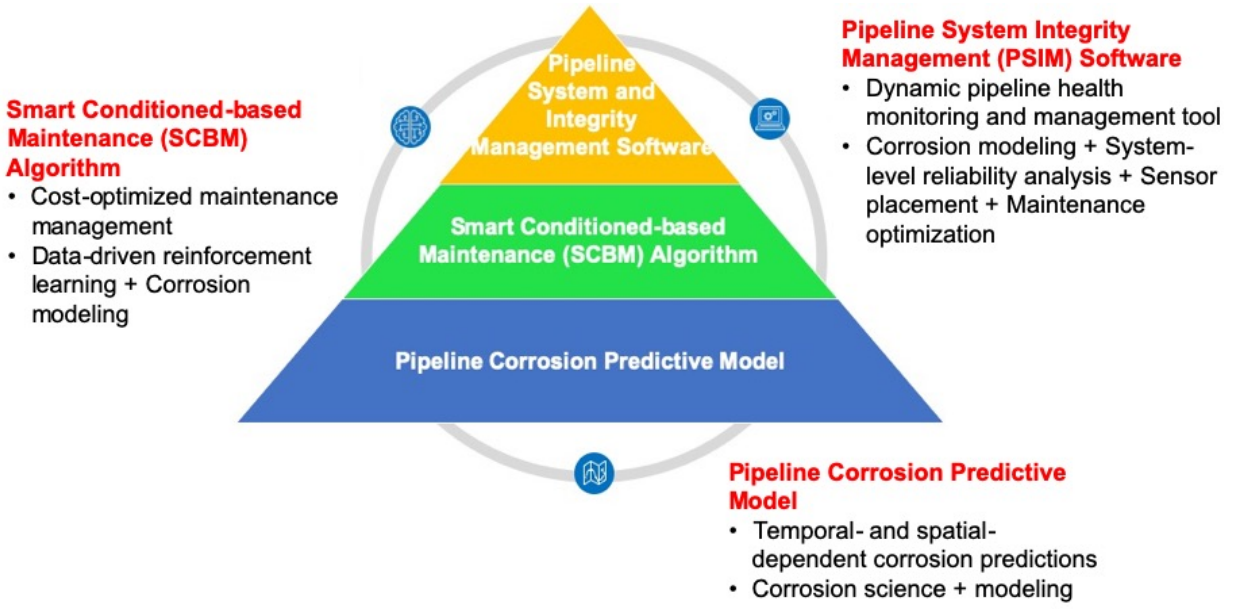

Figure 10. Hierarchy of three topics covered in this research.

It should be mentioned that the parts of the work described here have been published on Journal of Natural Gas Science and Engineering [29], uploaded to ResearchGate [30], or presented at the Probabilistic Safety Assessment and Management (PSAM 14) [31,32], Proceedings of the ASME 2019 International Mechanical Engineering Congress and Exposition (IMECE2019) [33], and 2019 Boston COMSOL Conference [34].

Part A

4 Development of Gas Pipeline Corrosion Predictive Models

The goal of corrosion predictive models is to predict whether a pipeline is susceptible to a particular type of corrosion in a given environment; if yes, estimate corrosion rate and depth that the corrosion will proceed. This chapter described the development of corrosion predictive models of natural gas pipelines for internal corrosion including uniform and pitting corrosion. In addition, two methodologies were introduced to consider temporal and spatial variabilities of operating parameters on corrosion modeling.

4.1 Internal corrosion model

The proposed internal corrosion predictive model includes two predictive models for uniform and pitting corrosion types, respectively. A schematic diagram of the model flow chart is shown in Figure 11. The model inputs are operating parameters of pipelines (e.g., operating temperature, gas pressure, flow velocity, pH, etc.), while the model outputs are corrosion rate or corrosion depth as a function of time.

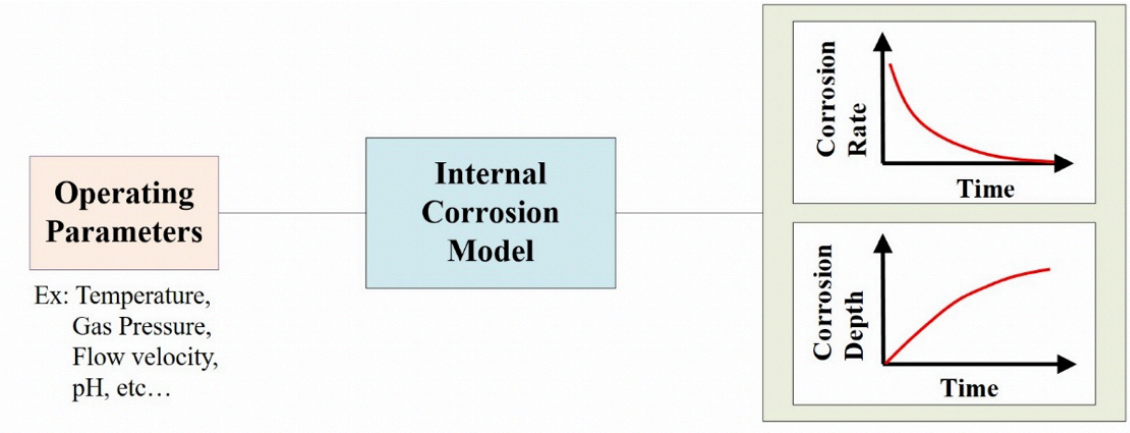

Figure 11. The flow chart of the internal corrosion predictive model.

4.1.1 *Uniform corrosion*

This research proposed a uniform corrosion model, which is a physics-based model for mild steels in an aqueous CO_2/H_2S environment. It can be used to estimate the corrosion rate as a function of time to reflect the time-dependent nature of uniform corrosion. The model describes uniform corrosion in a 'phenomenological' sense in terms of two stages based on the formation of protective layers. Stage I simulates the corrosion rate to be time-independent under the assumption of the absence of protective layers. According to experimental observations in Zheng et al.'s study [8], this stage only exists for a short time (i.e., transition time, t_0), usually in several hours. On the other hand, the Stage II simulates the corrosion rate to be time-dependent due to growth or annihilation of protective layers. Specifically, the corrosion rate decreases over time because protective layers act as diffusion barriers for corrosive species. A schematic diagram of predicted uniform corrosion rate as a function of time is shown in Figure 12.

4.1.1.1 *Modeling Stage I*

Several chemical reactions immediately take place in pipelines made of mild steels subjected to an aqueous CO_2/H_2S environment. A corrosive environment is then formed due to these chemical reactions. Typical chemical reactions in an aqueous CO_2/H_2S environment and their equilibrium equations are shown in Table 3. The equilibrium constants of chemical reactions from other literature are shown in

Table 4 and will be used to calculate concentrations of corrosive species.

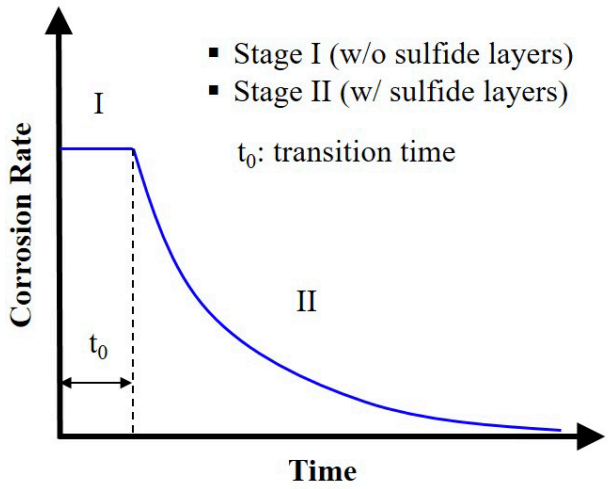

Figure 12. Predicted uniform corrosion rate as a function of time.

Table 3. Typical chemical reactions in an aqueous CO_2/H_2S environment and their equilibrium equations.

Reaction	**Chemical Reaction**	**Equilibrium Equation**	**Unit**
Dissolution of carbon dioxide	$CO_{2(g)} \Leftrightarrow CO_{2(aq)}$	$K_{CO_2} = \frac{[CO_{2(aq)}]}{pCO_{2(g)}}$	molar/bar
Carbon dioxide hydration	$CO_{2(aq)} + H_2O_{(l)} \Leftrightarrow H_2CO_{3(aq)}$	$K_{hyd} = \frac{K^f_{hyd}}{K^b_{hyd}} = \frac{[H_2CO_3]}{[CO_{2(aq)}]}$	-
Carbonic acid dissociation	$H_2CO_{3(aq)} \Leftrightarrow H^+_{(aq)} + HCO_3^-{}_{(aq)}$	$K_{ca} = \frac{[HCO_3^-][H^+]}{[H_2CO_3]}$	molar
Bicarbonate ion dissociation	$HCO_3^-{}_{(aq)} \Leftrightarrow H^+_{(aq)} + CO_3^{2-}{}_{(aq)}$	$K_{bi} = \frac{[CO_3^{2-}][H^+]}{[HCO_3^-]}$	molar
Dissolution of hydrogen sulfide	$H_2S_{(g)} \Leftrightarrow H_2S_{(aq)}$	$K_{H_2S} = \frac{[H_2S_{(aq)}]}{pH_2S_{(g)}}$	molar/bar
Hydrogen sulfide dissociation	$H_2S_{(aq)} \Leftrightarrow H^+_{(aq)} + HS^-_{(aq)}$	$K_{HS} = \frac{[HS^-][H^+]}{[H_2S_{(aq)}]}$	molar
Water dissociation	$H_2O_{(l)} \Leftrightarrow OH^-_{(aq)} + H^+_{(aq)}$	$K_w = [OH^-][H^+]$	$molar^2$

Table 4. Equilibrium constants of chemical reactions.

Equilibrium Constant
$K_{CO_2} = \frac{14.5}{1.00258} \times 10^{-(2.27 + 5.65\times10^{-3}T_f - 8.06\times10^{-6}T_f^2 + 0.075I)}$
$K_{hyd} = 2.58 \times 10^{-3}$
$K_{ca} = 387.6 \times 10^{-(6.41 - 1.594\times10^{-3}T_f + 8.52\times10^{-6}T_f^2 - 3.07\times10^{-5}pCO_2\times14.5 - 0.4772I^{0.5} + 0.118I)}$
$K_{bi} = 10^{-(10.61 - 4.97\times10^{-3}T_f + 1.331\times10^{-5}T_f^2 - 2.624\times10^{-5}pCO_2\times14.5 - 1.166I^{0.5} + 0.3466I)}$
$K_{H_2S} = 10^{-(634.27 + 0.2709T_k - 0.11132\times10^{-3}T_k^2 - \frac{16719}{T_k} - 261.9\times log(T_k))}$
$K_{HS} = 10^{(782.43945 + 0.361261T_k - 1.6722\times10^{-4}T_k^2 - \frac{20565.7315}{T_k} - 142.741722\times ln(T_k))}$
$K_w = 10^{-(29.3868 - 0.0737549T_k + 7.47881\times10^{-5}T_k^2)}$

*T_f is the temperature in degrees Fahrenheit; T_k is the absolute temperature in Kelvin; pCO_2 is the partial pressure of CO_2 in psi; I is the ionic strength in molar.

In addition to chemical reactions, several electrochemical reactions may subsequently occur on the steel surface in contact with the corrosive environment. Typical electrochemical reactions including anodic and cathodic reactions in an aqueous CO_2/H_2S environment are shown in Table 6. It can be seen that there is only one anodic reaction (i.e., iron dissolution) but four cathodic reactions (i.e., hydrogen ion reduction, direct carbonic acid reduction, direct hydrogen sulfide reduction). Every electrochemical reaction contributes to current densities consisting of charge transfer current density (i_α) and mass transfer limiting current density (i_{lim}). Depending on the rate-determining process, these electrochemical reactions are either under charge transfer control only or under both charge transfer and mass transfer control.

Table 5. Typical electrochemical reactions including anodic and cathodic reactions in an aqueous CO_2/H_2S environment.

Reaction	Electrochemical Reaction	Type	Reaction No.
Iron dissolution	$Fe^{2+}_{(s)} \rightarrow Fe^{2+}_{(aq)} + 2e^-$	Anodic	Reaction (1)
Hydrogen ion reduction	$2H^+_{(aq)} + 2e^- \rightarrow H_{2(g)}$	Cathodic	Reaction (2)
Direct carbonic acid reduction	$2H_2CO_{3(aq)} + 2e^- \rightarrow H_{2(g)} + 2HCO_3^-{}_{(aq)}$	Cathodic	Reaction (3)
Direct hydrogen sulfide reduction	$2H_2S_{(aq)} + 2e^- \rightarrow H_{2(g)} + 2HS^-_{(aq)}$	Cathodic	Reaction (4)
Direct water reduction	$2H_2O_{(l)} + 2e^- \rightarrow H_{2(g)} + 2OH^-_{(aq)}$	Cathodic	Reaction (5)

Table 6 shows the expressions of charge transfer current density and limiting current density of electrochemical reactions, which will be used for current density calculation in this research. Table 6 shows that iron dissolution and direct water reduction are under charge transfer control only because there is an unlimited supply of ferric ions on the steel surface and an unlimited supply of water in an aqueous CO_2/H_2S environment. Hydrogen ion reduction, direct carbonic acid reduction, and direct hydrogen sulfide reduction are under charge transfer control in the beginning and later become mass transfer control because the supply of corrosive species from the bulk solution is slower than the consumption of them at the steel surface after a certain time. A concentration gap is thus formed between the steel surface and the bulk solution.

For the anodic reaction (Reaction (1)), the overall anodic current density (i_a) is equal to the charge transfer current density ($i_{\alpha(a)}$), whereas for the cathodic reactions (Reaction (2)-(4)), the overall cathodic current density (i_c) is consisted of the charge transfer current density ($i_{\alpha(c)}$) and the limiting current density ($i_{lim(c)}$) in a parallel expression given by equation (25). As corrosion proceeds the anodic current density is electrically balanced by the cathodic current density at the steel surface, and corrosion potential (E_{corr}) can be found:

$$i_{(H^+)} + i_{(H_2CO_3)} + i_{(H_2S)} + i_{(H_2O)} = i_{(Fe)} \tag{69}$$

where $i_{(Fe)}$ is current density of Reaction (1); $i_{(H^+)}$ is current density of Reaction (2); $i_{(H_2CO_3)}$ is current density of Reaction (3); $i_{(H_2S)}$ is current density of Reaction (4); $i_{(H_2O)}$ is current density of Reaction (5).

Once the value of E_{corr} is found, substitute the value E in equation (22) for iron dissolution with E_{corr} can yield corrosion current density(i_{corr}), which is the charge transfer current density at the corrosion potential for the anodic reaction (i.e., iron dissolution). According to the electrochemical model [7], the corrosion current density can be converted into the corrosion rate at Stage I (CR_I) in mm/y given by:

$$CR_I = \frac{i_{corr} M_{Fe}}{\rho_{Fe} 2F} \tag{70}$$

where M_{Fe} is molecular mass of iron (= 55.85 g/mol); ρ_{Fe} is density of iron (= 7.86 g/cm^3); F is Faraday constant (= 96500 C/mol). Further unit correction is needed for the corrosion rate to be in the unit of mm/y.

Table 6. Charge transfer current density and limiting current density of electrochemical reactions.

Charge Transfer Current Density (A/m^2)		
No.	Exchange Current Density, $i_{\alpha 0}$	Current Density, i_α
(1)	$1 \times \left(\frac{3.5 \times 10^6[HS^-]}{1 + 3.5 \times 10^6[HS^-]}\right) \times e^{\frac{-37500}{R}\left(\frac{1}{T_k} - \frac{1}{293}\right)}$	$i_{\alpha 0,Fe} \times 10^{\left(\frac{E + 0.488}{2.3RT_k/1.5F}\right)}$
(2)	$0.5 \times \left(\frac{[H^+]}{10^{-4}}\right)^{0.5} \times e^{\frac{-30000}{R}\left(\frac{1}{T_k} - \frac{1}{298}\right)}$	$-i_{\alpha 0,H^+} \times 10^{-\left(\frac{E+2.3RT_kpH/F}{2.3RT_k/0.5F}\right)}$
(3)	$0.06 \times \left(\frac{[H^+]}{10^{-5}}\right)^{-0.5}\left(\frac{[H_2CO_3]}{10^{-4}}\right) \times e^{\frac{-50000}{R}\left(\frac{1}{T_k} - \frac{1}{293}\right)}$	$-i_{\alpha 0,H_2CO_3} \times 10^{-\left(\frac{E+2RT_kpH/F}{2.3RT_k/0.5F}\right)}$
(4)	$1.5 \times 10^{-4} \times \left(\frac{[H^+]}{10^{-4}}\right)^{-0.5}\left(\frac{[H_2S]}{10^{-4}}\right)^{0.5} \times e^{\frac{-60000}{R}\left(\frac{1}{T_k} - \frac{1}{293}\right)}$	$-i_{\alpha 0,H_2S} \times 10^{-\left(\frac{E+2.3RT_kpH/F}{2.3RT_k/0.5F}\right)}$
(5)	$1 \times 10^{-6} \times \left(\frac{[H^+]}{10^{-4}}\right)^{-0.5}\left(\frac{[H_2S]}{10^{-4}}\right)^{-0.1} \times e^{\frac{-90000}{R}\left(\frac{1}{T_k} - \frac{1}{293}\right)}$	$-i_{\alpha 0,H_2O} \times 10^{-\left(\frac{E+2.3RT_kpH/F}{2.3RT_k/0.5F}\right)}$
Limiting Current Density (A/m^2)		
(2)	$i_{lim(H^+)} = k_{m(H^+)}F[H^+]$	
(3)	$i_{lim(H_2CO_3)} = F[CO_2]f_{H_2CO_3}\sqrt{D_{H_2CO_3}K_{hyd}K_{hyd}^f}$	
(4)	$i_{lim(H_2S)} = k_{m(H_2S)}F[H_2S]$	

*E is the potential in V; $k_{m(H^+)}$ and $k_{m(H_2S)}$ are the mass transfer coefficients of H^+ and H_2S in m/s; F is Faraday constant (= 96500 C/mol); $f_{H_2CO_3}$ is the flow factor of carbonic acid; $D_{H_2CO_3}$ is the diffusion coefficient of aqueous carbonic acid (= 1.3×10^{-9} m^2/s at 25℃).

4.1.1.2 *Modeling Stage II*

At the beginning of Stage II, the formation of protective layers starts by a direct and fast heterogeneous solid-state reaction as expressed by equation (33). The primary protective layers are sulfide layers of mackinawite. Due to the presence of protective layers, the corrosion process is assumed to be under mass transfer control, and the corrosion rate is time-dependent at this stage.

During the corrosion process at Stage II, the diffusion of corrosive species (i.e., CO_2, H_2S, and H^+) and release of Fe^{2+} are taking place in the CO_2/H_2S aqueous system. However, they fail to consider the effect of sulfide layer dissolution, which is significant at low pH environment. This research considers that effect in the corrosion modelling and demonstrates the uniform corrosion process at Stage II in Figure 13. The corrosion rate is related to the diffusion processes of corrosive species between the steel surface and the bulk solution, which can be quantified by their fluxes. Adopting the Sun and Nešic's model [14], the steady-state H_2S flux (ϕ_{H_2S}), CO_2 flux (ϕ_{CO_2}), and H^+ flux (ϕ_{H^+}) in mol/(m^2s) are expressed as:

$$\phi_{H_2S} = A_{H_2S} \ln\left[\frac{C_{b(H_2S)} - \phi_{H_2S}\left(\frac{\delta}{D_{H_2S}\epsilon\varphi} + \frac{1}{k_{m(H_2S)}}\right)}{C_{s(H_2S)}}\right] \quad (71)$$

$$\phi_{CO_2} = A_{CO_2} \ln\left[\frac{C_{b(CO_2)} - \phi_{CO_2}\left(\frac{\delta}{D_{CO_2}\epsilon\varphi} + \frac{1}{k_{m(CO_2)}}\right)}{\frac{Flux_{CO_2}}{D_{H_2CO_3}\epsilon\varphi K_{hyd}^f K_{hyd}}}\right] \quad (72)$$

$$\phi_{H^+} = A_{H^+} \ln \left[\frac{C_{b(H^+)} - \phi_{H^+} \left(\frac{\delta}{D_{H^+} \epsilon \varphi} + \frac{1}{k_{m(H^+)}} \right)}{C_{s(H^+)}} \right] \quad (73)$$

where ϕ_{H_2S}, ϕ_{CO_2}, and ϕ_{H^+} are the fluxes of H_2S, CO_2, and H^+ in mol/(m^2s); $k_{m(H_2S)}$, $k_{m(CO_2)}$, and $k_{m(H^+)}$ are the mass transfer coefficients of H_2S, CO_2, and H^+ in m/s; $C_{b(H_2S)}$, $C_{b(CO_2)}$, and $C_{b(H^+)}$ are the bulk concentration of H_2S, CO_2, and H^+ in the liquid phase in mol/m^3; ε is the outer mackinawite layer porosity (= 0.9); ψ is the outer mackinawite layer tortuosity factor (= 0.003); δ is the thickness of mackinawite layers in m; A_{H_2S}, A_{CO_2}, and A_{H^+} are the solid state diffusion kinetic constants for H_2S, CO_2, and H^+ (= 2×10^{-5}, 4×10^{-4}, and 2×10^{-6} mol/(m^2s)); $C_{s(H_2S)}$ and $C_{s(H^+)}$ are the near zero concentration of H_2S and H^+ on the steel surface (= 1×10^{-7} mol/m^3); δ is the thickness of mackinawite layers in m; D_{H_2S}, D_{CO_2}, $D_{H_2CO_3}$, and D_{H^+} are aqueous diffusion coefficients for H_2S, CO_2, H_2CO_3, and H^+, which were computed via Einstein's relation [7]:

$$D_i = D_{ref(i)} \left(\frac{T_k}{T_{k,ref}} \right) \left(\frac{\mu_{ref(H_2O)}}{\mu_{H_2O}} \right), \quad i = H_2S, CO_2, H_2CO_3, \text{and } H^+ \quad (74)$$

where $D_{ref(H_2S)}$, $D_{ref(CO_2)}$, $D_{ref(H_2CO_3)}$, and $D_{ref(H^+)}$ are reference aqueous diffusion coefficients for H_2S, CO_2, H_2CO_3, and H^+ (= 2×10^{-9}, 2.8×10^{-8}, 2.8×10^{-8} ,and 1.96×10^{-9} m^2/s at 25℃); T_k is the temperature in K and $T_{k,ref}$ is the reference temperature (= 298 K), respectively; μ_{H_2O} is the water dynamic viscosity and $\mu_{ref(H_2O)}$ is the reference water dynamic viscosity (= 1.002×10^{-4} Pa·s at 25℃), respectively.

Flux of each corrosive species can be converted into an individual corrosion rate:

$$CR_{H_2S} = \frac{\phi_{H_2S} M_{Fe}}{\rho_{Fe}} \quad (75)$$

$$CR_{CO_2} = \frac{\phi_{CO_2} M_{Fe}}{\rho_{Fe}} \quad (76)$$

$$CR_{H^+} = \frac{\phi_{H^+} M_{Fe}}{2\rho_{Fe}} \quad (77)$$

where CR_{H_2S}, CR_{CO_2}, and CR_{H^+} are the corrosion rate of H_2S, CO_2, and H^+ in mm/y; M_{Fe} is the molar mass of iron (= 55.85 g/mol); ρ_{Fe} is the density of iron (= 7.86 g/cm^3). Finally, the total corrosion rate in Stage II (CR_{II}) is the sum up of CR_{H_2S}, CR_{CO_2}, and CR_{H^+} as they are main corrosive species in CO_2/H_2S aqueous environment.

$$CR_{II} = CR_{H_2S} + CR_{CO_2} + CR_{H^+} \quad (78)$$

It should be noted that unit correction is needed for the corrosion rate to be in the unit of mm/y.

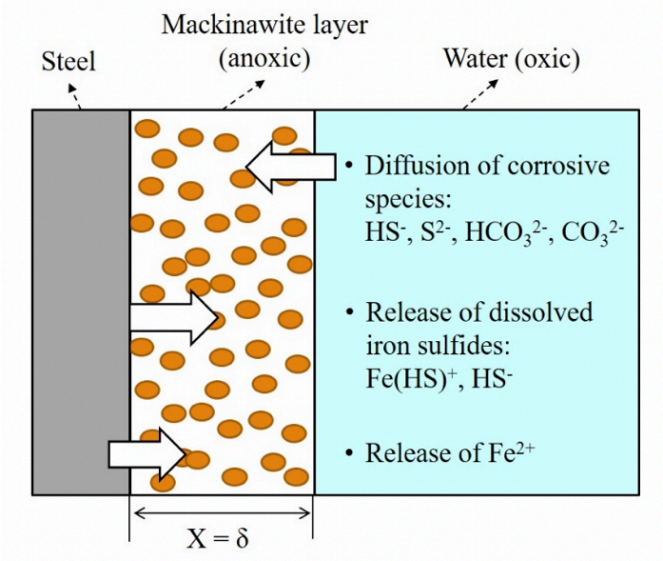

Figure 13. Schematic diagram of the Stage II corrosion process in a CO_2/H_2S aqueous system.

During the corrosion process at state II, the thickness of protective layers (i.e., mainly sulfide layers) will either grow or annihilate depending on the tradeoff between layer formation and layer damage effects. Therefore, whether formation or damage effect of sulfide layers dominates is determined by the sulfide layer retention rate (SRR) in mol/(m^2s) at every time interval, which can be represented as:

$$\mathrm{SRR} = \mathrm{SFR} - \mathrm{SDR} \tag{79}$$

where SFR is the sulfide layer formation rate; SDR is the sulfide layer damage rate. As the unlimited supply of ferric ions of sulfide layers is the steel itself, SFR is assumed to be the corrosion rate at Stage II ($\mathrm{CR_{II}}$). On the other hand, SDR is the sum up of sulfide layer mechanical damage rate ($\mathrm{SDR_M}$) and the sulfide layer dissolution rate ($\mathrm{SDR_D}$). $\mathrm{SDR_M}$ is influenced by the

effect of intrinsic growth stresses and the effect of extrinsic hydrodynamic forces. A sulfide layer mechanical damage coefficient (α), ranging from 0 to 1, is used to model SDR_M as:

$$SDR_M = \alpha \times CR \tag{80}$$

α is simulated to be a function of temperature, pH, flow velocity, and partial pressure by a Bayesian Network (BN) model. BN is a good tool to model the influences between random variables by cause-consequence dependencies [35]. According to experimental observations by Sun and Nesic [14], sulfide layer mechanical damage effect is found to be related to temperature, pH, flow velocity, and partial pressure of H_2S, all of which are set to be mutually independent parents of the child node α. The quantification of joint probability tables requires the modeling results with experimental data obtained by the proposed model, the data from other literature and expert opinions. An example of the BN model for α value assessment is displayed in Figure 14. It can be seen that this BN model is in a discrete framework with the states of each node uniformly distributed. This particular example shows that the estimated α value is likely to be between 0 to 0.2 with 60% probability and between 0.2 to 0.4 with 40% probability when the flow velocity is between 500 to 750 rpm with 100% probability; the pH level is between 5 to 6 and 6 to 7 with the same probability; the temperature is between 25 to 50℃ with 100% probability; the partial pressure of H_2S is between 10 to 100 and 100 to 1000 mbar with the same probability.

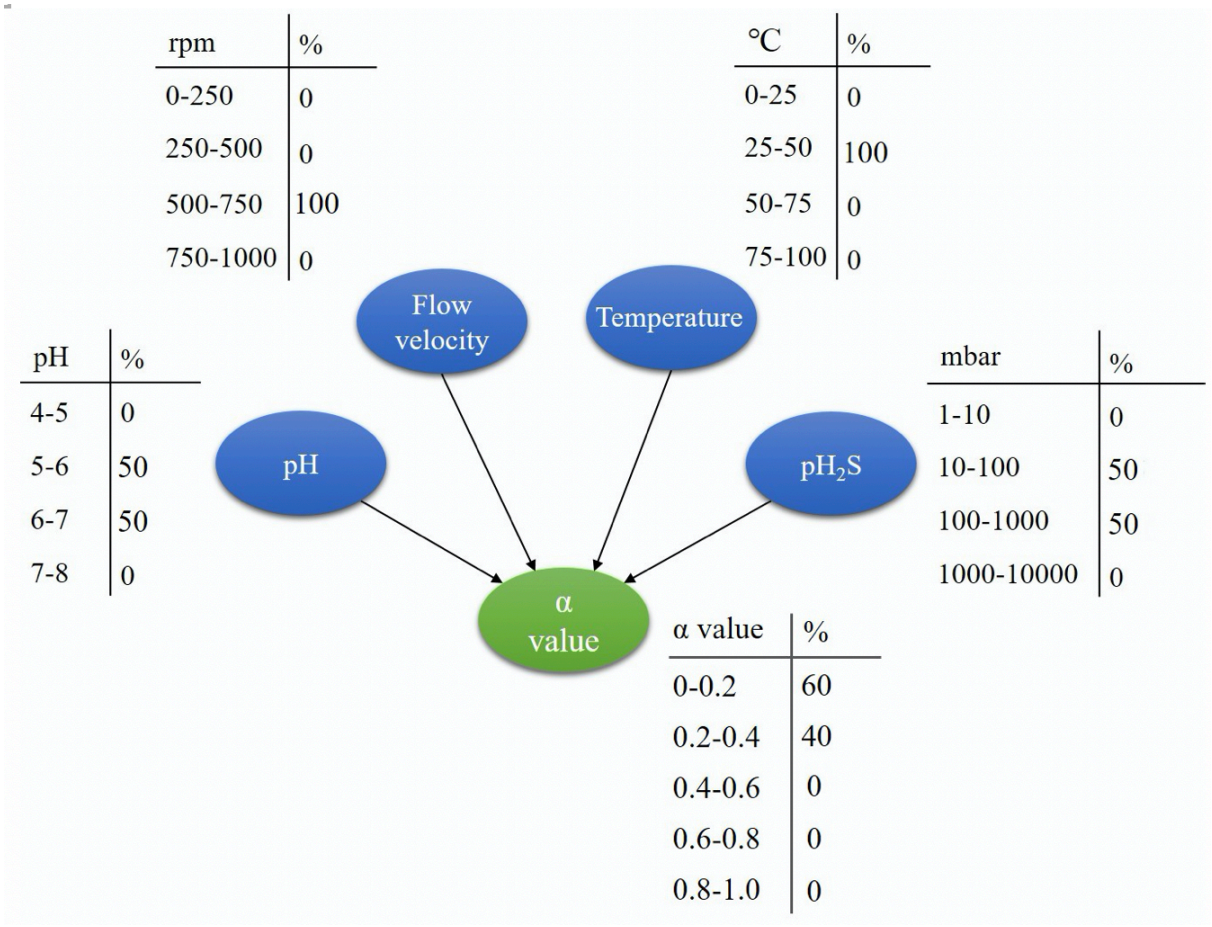

Figure 14. An example of the BN model for α value assessment.

For SDR_D, the initial mackinawite sulfide layers in the aqueous H_2S system is reported to dissolute into $Fe(HS)^+$ and HS^- at a rate as a function of pH, temperature, and ionic strength under certain conditions [36,37]. This dissolution rate is a first-order equation with a hydrogen ion concentration-dependent term in acid solutions and a hydrogen ion concentration-independent term in neutral to alkaline solutions.

$$SDR_D = k_1[H^+] + R(k_2) \quad (81)$$

where $R(k_2)$ is the H^+ concentration-independent term contributing to the dissolution rate of mackinawite in mol/(cm^2·min); $[H^+]$ is the hydrogen ion concentration in mol/cm^2.

k1 and k_2 are rate constants in cm/min and mol/(cm^2·min), respectively. k_1 and k_2 are functions of temperature in Arrhenius form as:

$$k_1 = (26 \pm 1) \times 10^3 \exp\left(\frac{-28451}{RT_k}\right) \quad (82)$$

$$k_2 = (4.2 \pm 0.1) \times 10^{-4} \exp\left(\frac{-30125}{RT_k}\right) \quad (83)$$

where T_k is the temperature in K; R is the gas constant (= 8.314 J/(mol·K)).

According to Pankow and Morgan's study [38], an anaerobic region will form and facilitate the non-oxidative dissolution when mackinawite sulfide layers originally form in the aqueous H_2S system, whereas oxygen in the water solution facilitates the oxidation of dissolved iron sulfides. Therefore, a concentration gradient is developed between the anaerobic region and the oxic region, triggering the non-oxidative dissolution of mackinawite. This dissolution is described by $R(k_2)$, the dissolution rate of mackinawite in neutral to alkaline solutions, and it can be expressed as:

$$R(k_2) = \left(1 - \frac{c}{c_s}\right) k_2 \quad (84)$$

where c is the concentration of dissolved mackinawite in mol/cm^3; c_s is the saturation concentration (= 2×10^{-9} mol/cm^3 at the natural water pH).

To simplify the problem, $R(k_2)$ is treated as a production term in a one-dimensional diffusion problem. Two boundary conditions, namely, c = 0 when X = 0 and $c = c_s$ when $X = \infty$ are used to obtain the steady-state solution as:

$$c = c_s\left(1 - \exp\left[-\left(\frac{2k_2}{D_m c_s r}\right)^{0.5} X\right]\right) \tag{85}$$

where X is the thickness of mackinawite sulfide layers in m; r is the radius of mackinawite particles; D_m is the diffusion coefficient of dissolved mackinawite (= 3×10^{-3} cm^2/min).

Once CR_{II} and SDR including SDR_M and SDR_D are calculated via the abovementioned steps, SRR can be obtained for each time interval. At time interval Δt, SRR is converted to the change of sulfide layer thickness ($\Delta\delta$) in m, which can be expressed as:

$$\Delta\delta = \frac{SRR \times M_{FeS} \times \Delta t}{\rho_{FeS}} \tag{86}$$

where M_{FeS} is the molecular mass of mackinawite (= 87.91×10^{-3} kg/mol); ρ_{FeS} is the density of mackinawite (= 4840 kg/m^3).

To generate a series of predicted corrosion rate over time, the abovementioned steps were repeated until the target time was reached. The flow chart of the detailed calculation procedures of the uniform corrosion model is shown in Figure 15. Firstly, calculated CR_I for Stage I given operating

parameters, which is time independent. Secondly, calculated CR_{II} for Stage II by solving equations (71)-(78) with δ being 0 at the beginning. Then, SRR and $\Delta\delta$ were calculated via equations (79)-(86), which were used to update δ and CR_{II} for each time interval Δt. It should be noted that this model assumes that $CR_I > CR_{II}$ as protective layers at Stage II play the role of diffusion barrier, inhibiting the corrosion process. Finally, these steps were repeated until the target time was reached.

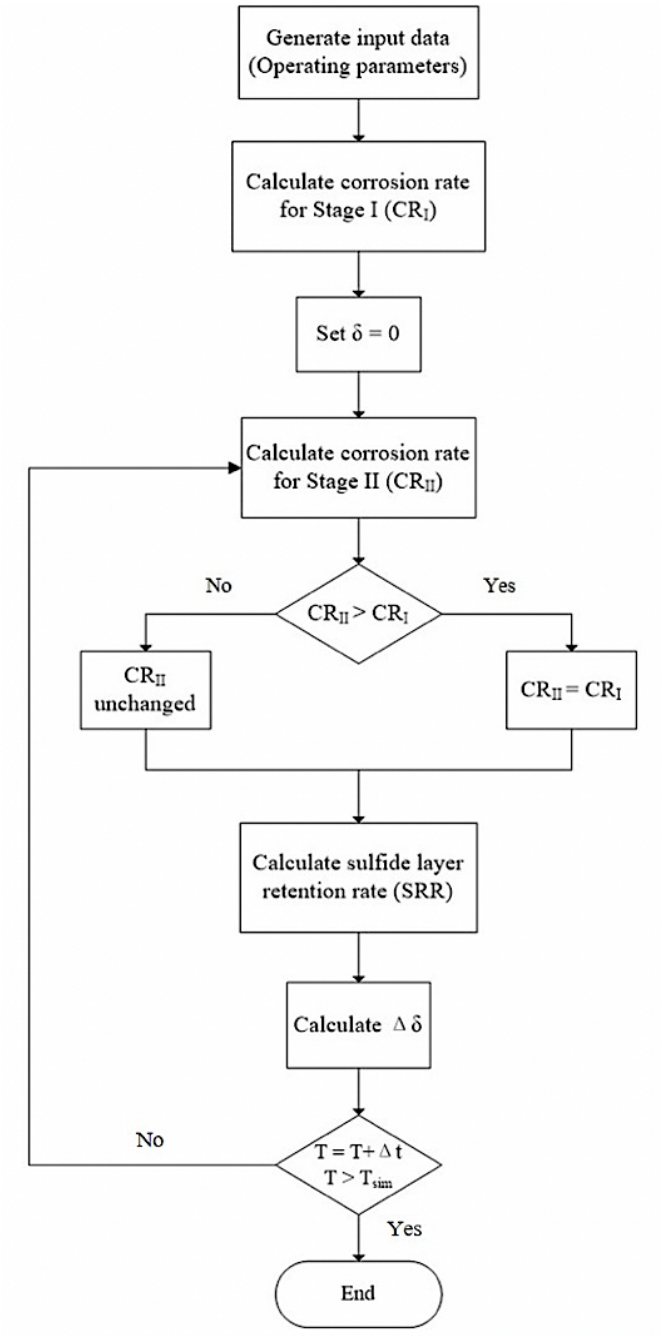

Figure 15. The flow chart of the detailed calculation procedures of the uniform corrosion model.

4.1.2 *Pitting corrosion*

This research simulated the pitting corrosion behavior given operating parameters by the Papavinasam model [22,23] because this model is time-dependent and also able to reflect the influences of numerous operating parameters on corrosion rate. In addition, it is applicable to nature gas pipelines made of mild steels and subjected to aqueous CO_2/H_2S environment, which matches our research scopes. The mathematical expression of the time-independent mean pit growth rate (PCR_{mean}) is expressed as equation (63) and the time-dependent average pitting corrosion rate over a time interval ($PCR_{average}$) is expressed as equation (64), respectively. A number of changes that have been made in this research in based on the Papavinasam model are described as follows:

(1) In order to simulate the instantaneous pitting corrosion rate at a certain time, the original corrosion rate equation is modified and written as:

$$PCR_t = \frac{PCR_{mean}}{t} \tag{87}$$

where t is time in years.

(2) In a consideration of daily variability of operating parameters, this model can predict daily mean pit growth rate as a function of time. A schematic diagram of predicted pitting corrosion rate as a function of time is shown in Figure 16.

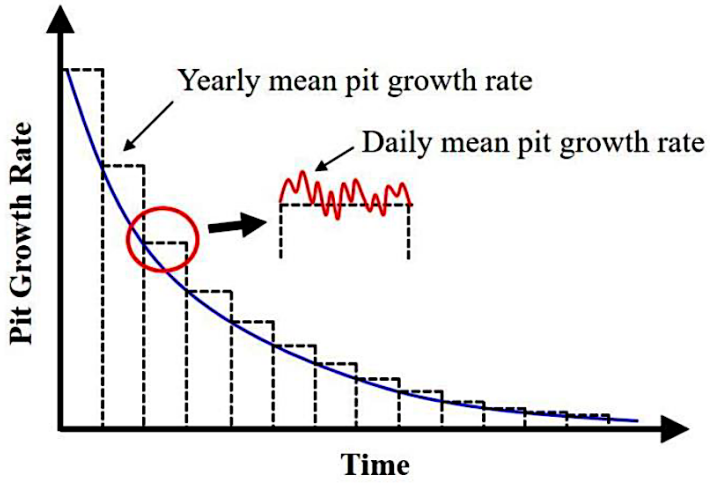

Figure 16. A schematic diagram of predicted pitting corrosion rate as a function of time.

4.2 Modeling the variability of operating parameters

Most of the time, operating parameters of a nature gas pipeline are changing all the time within an uncertain range temporally and spatially. Taking both temporal and spatial variabilities into account enables the application of the proposed corrosion model from deterministic to probabilistic framework.

4.2.1 *Temporal variability*

To consider the temporal variability and simulate a series of time-varying operating parameters for corrosion predictions, a methodology was proposed, all of which will become inputs of the proposed corrosion predictive model. Each time-varying operating parameter was simulated by Poisson process. Specifically, the duration of time is described by Exponential distribution; the

magnitude is described by a particular distribution based on observations; the number of each time interval is described by Poisson distribution in which the lambda value is fixed to be 1/day for every operating parameter in a simulation of daily variability. The schematic diagram of the Poisson process for the modelling of operating parameters is shown in Figure 17.

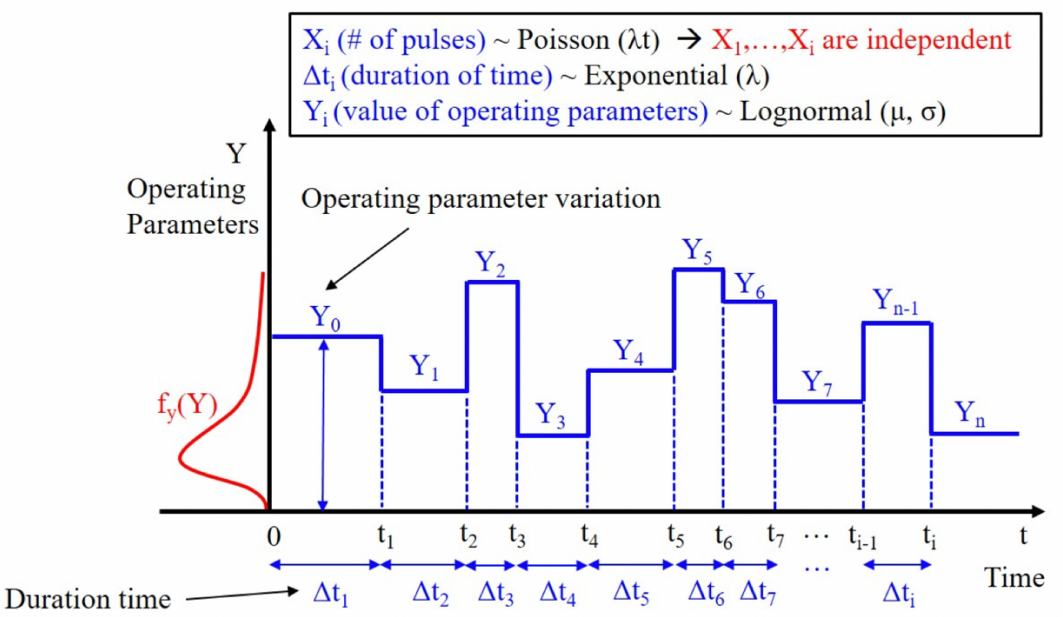

Figure 17. The schematic diagram of the Poisson process for operating parameters modeling.

Given time-varying operating parameters as model inputs, a Monte Carlo simulation was then performed to generate the time-evolution probability density functions of corrosion predictions. A detailed flow chart of the proposed methodology on corrosion predictions in probabilistic framework is displayed in Figure 18. The flow chart shows that:

Step 1: Specified distributions of all operating parameters are determined based on field observations or literature.

Step 2: Poisson process with lambda equaling 1/day is used to simulate the operating parameters such as Temperature, pCO_2, pH, etc. A value for each parameter is randomly selected based on its probability distribution using Monte Carlo sampling.

Step 3: Step 2 is repeated for all the operating parameters to generate time histories operating parameters that are used in generating corrosion rate as a function of time

Step 4: These time histories operating parameters are taken as inputs for the corrosion predictive model.

Step 5: The above processes are repeated for a large of number of times to generate the probability distributions of corrosion rate at different time.

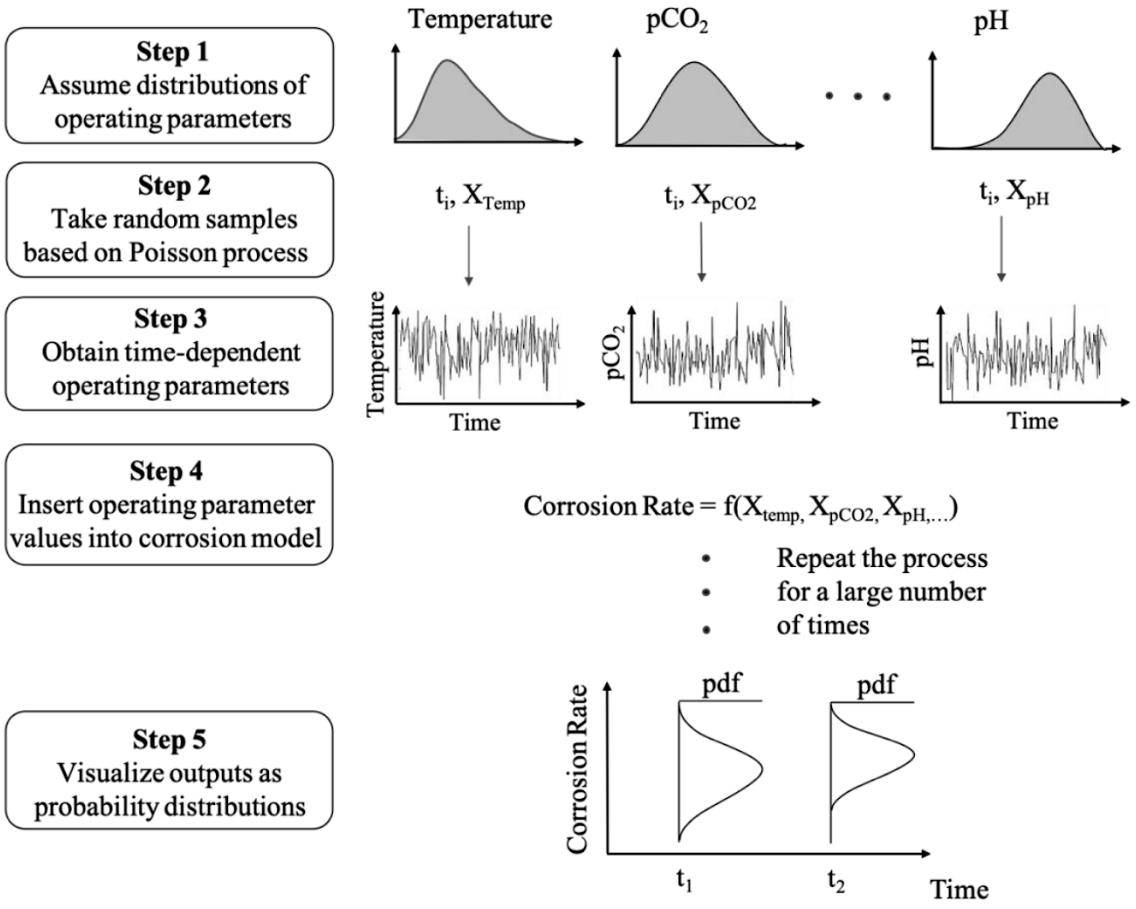

Figure 18. A detailed flow chart of the proposed methodology on corrosion predictions in a probabilistic framework.

4.2.2 *Spatial variability*

A typical nature gas pipeline is usually tens of miles long. Therefore, it can be imagined that operating parameters are different at various locations along the pipe. Spatial variability of operating parameters is thus also important on corrosion predictions. This issue has been reported in previous studies by other scientists and engineers. For example, operating temperature is likely

to decrease with increasing distance from the inlet due to heat exchange with the pipe material; operating pressure also shows a same trend of decreasing where compressors are located. Moreover, Kale et al. [26] indicates the decreasing efficiency of corrosion inhibitors along the pipe if the inhibitors are added from the inlet.

In this research, besides locations at near inlet, at near outlet, and at midpoint, the basic design variables (e.g., pipe length, bent, and diameters) were assumed not to be relevant to the spatial variability. An example of the effect of spatial variability of operating parameters on corrosion predictions is depicted in Figure 19. This figure shows that the probability density functions of predicted corrosion rate by the proposed uniform corrosion model are different at three different sites inside a pipe. This result is similar to Droguett et al.'s finding [39] that different failure rate can occur if the data is collected from systems exposed to different operational, design, and maintenance conditions. Therefore, it is reasonable to say that the presence of variation of corrosion predictions in a reflection of spatial variability of operating parameters in this research is the result of inherent population variability of the corrosion predictions as the operating conditions are different. In other words, on a pipeline system point of view, predicted corrosion rate at every site along a pipeline is inherently different, each of which can be viewed as a sub-population.

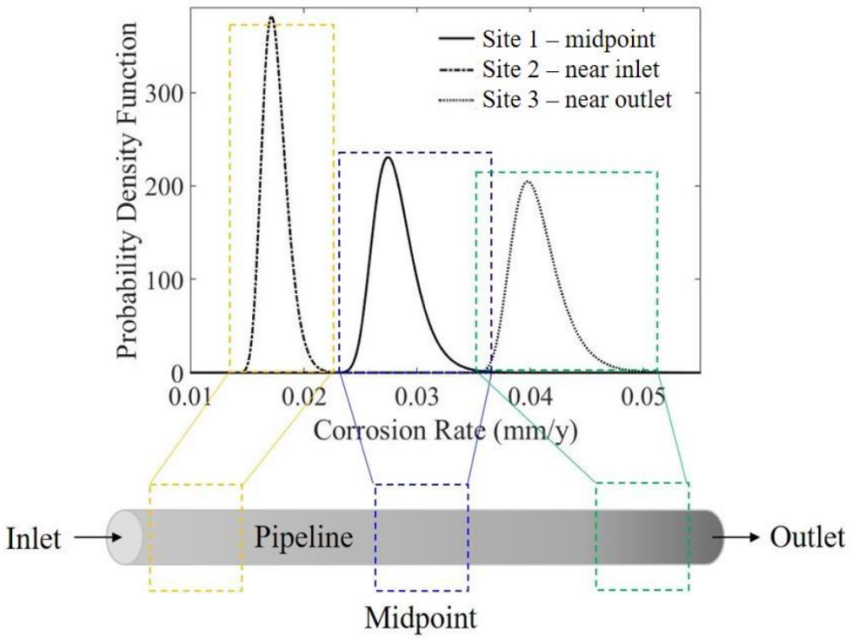

Figure 19. Location-dependent probability density functions of corrosion rate predictions.

Bayesian estimation method, specifically, non-homogeneous analysis was applied to address the non-homogeneity of predicted corrosion rate considering spatial variability of operating parameters. A Bayesian data analysis package called R-DAT [40] was used to estimate the parametric population variability distribution (i.e., a probability distribution of corrosion rate that can represent the general corrosion rate for the whole pipe with location-varying operating conditions. A schematic diagram of the Bayesian estimation method for the parametric population variability distribution is shown in Figure 20.

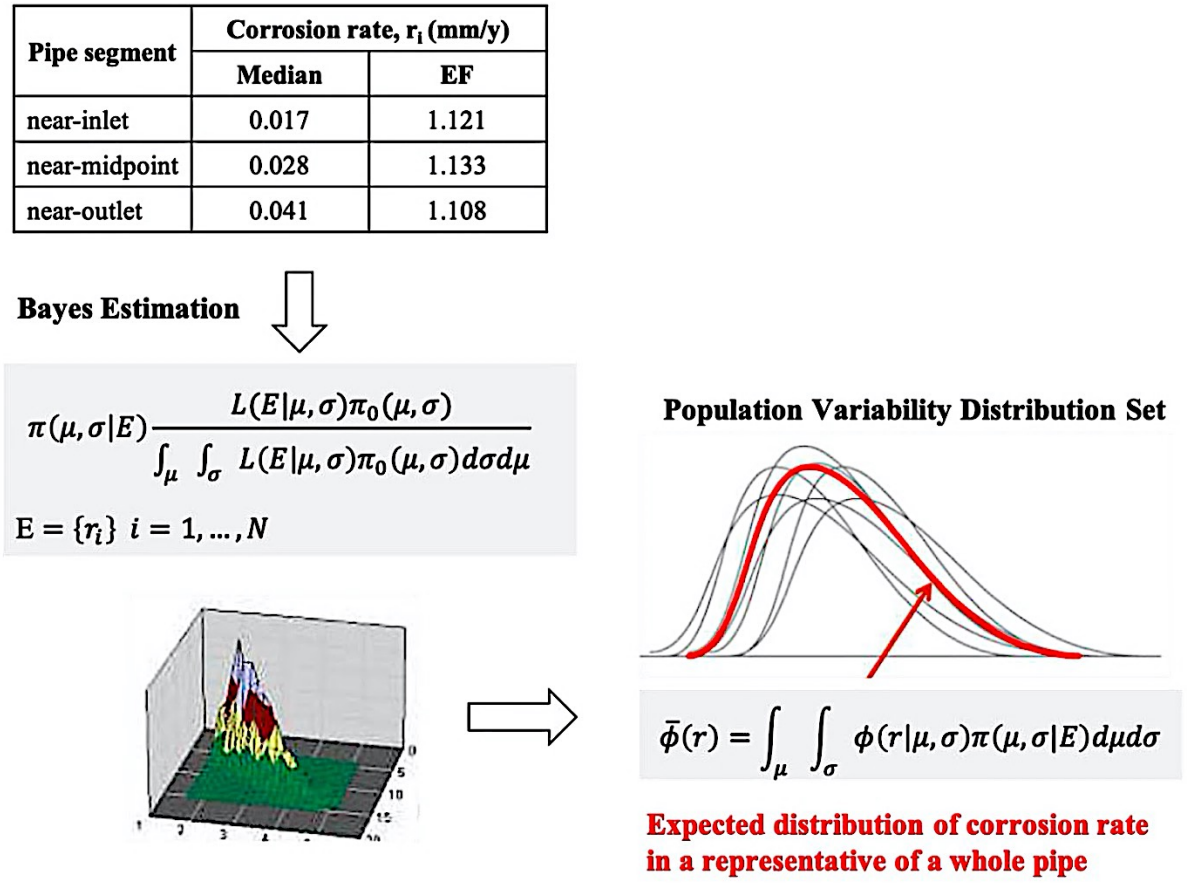

Figure 20. Bayesian estimation method of corrosion predictions considering the spatial variability of operating parameters.

The detailed process of calculating the parametric population variability distribution was described as follows: Firstly, a form of the parametric population variability distribution of corrosion rate, $\emptyset(r)$, was assumed (i.e., Lognormal distribution in R-DAT [40]) and given as:

$$\emptyset(\mathrm{r}) = \emptyset(\mathrm{r}|\theta) \quad \text{where} \quad \theta = (\mu, \sigma) \tag{88}$$

where r is corrosion rate; θ is a set of parameters (i.e. μ and σ for Lognormal distribution). Secondly, evidence or information, E, which is composed of predicted corrosion rate predictions considering spatial variability of operating parameters as shown in the top table in Figure 20, was used to estimate θ by Bayes theorem, which can be expressed as:

$$\pi(\theta = \mu, \sigma|E) = \frac{L(E|\mu, \sigma)\pi_0(\mu, \sigma)}{\int_\mu \int_\sigma L(E|\mu, \sigma)\pi_0(\mu, \sigma)d\sigma d\mu} \tag{89}$$

where $\pi(\mu, \sigma|E)$ is the posterior probability of θ given E; $\pi_0(\mu, \sigma)$ is the prior probability of θ. $L(E|\mu, \sigma)$ is the likelihood function, which can be expressed as:

$$L(E|\mu, \sigma) = \prod_{i=1}^{n} L(r_i|\mu, \sigma) \quad \text{where} \quad L(r_i|\mu, \sigma) = \int_r L(r_i|r)\emptyset(r|\mu, \sigma)dr \tag{90}$$

where r_i is corrosion rate predictions considering spatial variability of operating parameters. Finally, the mean parametric population variability distribution of corrosion rate was considered the average of all possible $\emptyset(r)$ given E denoted by $\overline{\emptyset}(r)$:

$$\overline{\emptyset}(r) = \int_\mu \int_\sigma \emptyset(r|\mu, \sigma)\pi(\mu, \sigma|E)d\sigma d\mu \tag{91}$$

The calculated $\overline{\emptyset}(r)$ is the general parametric population variability distribution in representative of a corrosion rate distribution for the whole pipe with the location-changing operating conditions. In practical, the proposed methodology of corrosion predictions considering spatial variability and

temporal variability of operating parameters should be applied together for corrosion modeling on nature gas pipelines. Only if all possible variability is considered in the modeling can models provide comprehensive and unbiased predictions.

4.3 Conclusions

This chapter introduced the two internal corrosion models (i.e., one for uniform corrosion and one for pitting corrosion) for natural gas pipelines. The common advantage of these models is that they are all correlated with operating parameters, enabling the study of the effect of operating parameters on corrosion rates. In addition, this trait allows us to consider temporal and spatial variabilities of operating parameters on corrosion modeling in which the predicted results are believed to be more reliable.

5 Model Validation with Experimental Data

A model has to be calibrated and validated for its applicability before it can be used. Therefore, this chapter is to test the validity of the proposed uniform corrosion predictive model, a modified model from the Sun and Nesic model [14], for predicting instantaneous corrosion rate given operating parameters of nature gas pipeliens. The predicted results were compared with the experimental data in H_2S/CO_2 and pure H_2S aqueous systems with respect to pH level, flow velocity, temperature, and partial pressure of H_2S in a deterministic framework presented in the literature [14,41].

5.1 Model comparison

As described before, the proposed uniform corrosion model is a modified model based on the electrochemical model and the Sun-Nešic model; therefore, a comparison between two models are needed. There are several improvements of the proposed model compared to the Sun-Nešic model, which are summarized as follows:

(1) The Sun-Nešic model assumes that the sulfide layers start to form at the beginning of the corrosion process, while the proposed model describes the corrosion process by two stages in which the sulfide layers only form at Stage II.

(2) The Sun-Nešic model assumes that the sulfide layer mechanical damage rate is a constant for sulfide layer damage effect; the proposed model treats the sulfide layer mechanical damage

rate as a variable and defines a sulfide layer mechanical coefficient by a BN model, in which the coefficient is influenced by the pH level, flow velocity, temperature, and partial pressure of H_2S.

(3) The Sun-Nešic model does not take into account the sulfide layer dissolution effect, but the proposed model does.

5.2 Results and discussion

The comparison between the predicted results by the proposed model and the Sun-Nesic model with the experimental data is shown in Figure 21. The predicted corrosion rates by the proposed model are denoted by solid lines; the predicted corrosion rates by the Sun-Nesic model are denoted by dashed lines; the experimental data are denoted by dots.

The results show that most model predictions by the proposed model reasonably agree with the experimental data, displaying the trends of corrosion rate drop over time, except for the condition pH=4. On the other hand, model predictions by the Sun-Nešic model only agree with the experimental data at few test conditions. Specifically, most of their predictions largely overestimate initial corrosion rates due to the invalid assumption that sulfide layers start to form at the beginning of the corrosion process, whereas predicted initial corrosion rates by the proposed model are more reasonable. In addition, the Sun-Nešic model can not reflect the change of pH level and flow velocity due to the negligence of sulfide layer dissolution effect and the constant mechanical damage rate assumptions.

It can be seen from Figure 21 that the influences of different parameters on the corrosion rates are dependent on protective layers, each of which can be described in terms of Stage I and II as follows:

(1) Effect of pH

Figure 21(a) demonstrates the effect of pH level in a range between 4 to 6 on the corrosion rates. At stage I where protective layers are absent, decreasing pH level increases the hydrogen reduction of cathodic reactions, resulting in a rise in initial corrosion rates; at Stage II where protective layers are present, decreasing pH level increases the sulfide layer dissolution rate and the sulfide layer mechanical damage rate, leading to an increase of the corrosion rates. It should be noted that the proposed model should be used with cautions when pH level is down to 4 where the corrosion rates increase over time, whereas they usually decrease over time at other test conditions. This can be explained by the enhanced galvanic corrosion between ferrite (α) and pearlite ($\alpha + Fe3C$) phases in mild steels as Fe3C is an electronic conductor, which was not taken into account in the proposed model. The enhanced galvanic corrosion takes effect before sulfide layers are formed and thus increases corrosion rates at the initial stage [42].

(2) Effect of flow velocity

Figure 21(b) shows the effect of flow velocity between 60 and 600 rpm on the corrosion rates. At Stage I, increasing the flow velocity accelerates the transport of corrosive species to the metal surface, leading to a rise in the initial corrosion rates; at Stage II, increasing flow velocity

enhances the sulfide layer mechanical damage rate as a result of increasing extrinsic hydrodynamic forces, leading to a rise in the corrosion rates.

(3) Effect of temperature

Figure 21(c) illustrates the effect of temperature between 50℃ and 90℃ on the corrosion rates. At Stage I, increasing temperature accelerates electrochemical and chemical reactions as well as transport processes of corrosive species, leading to a rise in the initial corrosion rates. At Stage II, the enhancement of the supply of ferric ions for the sulfide layer formation outweighs the increase of the sulfide layer dissolution rate by increasing temperature. Therefore, the corrosion rates actually show a decreasing trend with increasing temperature.

(4) Effect of partial pressure of H_2S

Figure 21(d) displays the effect of H_2S partial pressure between 4 and 70 mbar on the corrosion rates. H_2S is one of the corrosive species and also a supplier of S^{2-} ions for sulfide layer formation. At Stage I, increasing H_2S partial pressure results in the increasing initial corrosion rates due to the enhancement of the direct reduction of H_2S. At Stage II, increasing H_2S partial pressure in the range between 4 and 70 mbar results in the increasing corrosion rates. Similar to a study by Singer et al. [43], where the H_2S partial pressure is in the range between 10 and 150 mbar, the corrosion rates all show an increasing trend with increasing H_2S partial pressure. However, this increasing trend turns into a decreasing trend when H_2S partial pressure is as high as 0.3 bar due to the acceleration of the formation of protective sulfide layers [41].

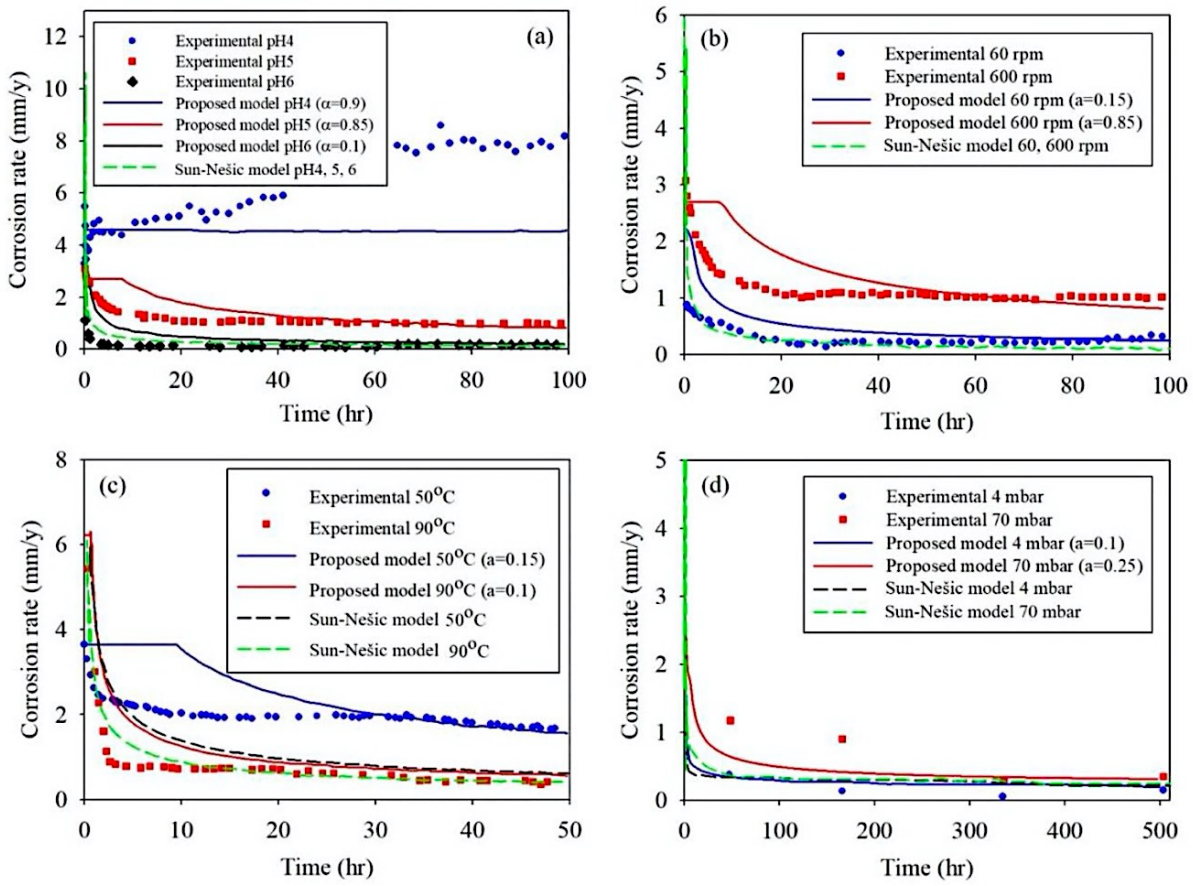

Figure 21. Corrosion rate as a function of time with respect to different environmental factors: (a) pH 303 level (Conditions: pH_2S = 54 mbar, T = 80℃, stirring rate = 600 rpm for pH = 4 and 5, and 400 304 rpm for pH = 6), (b) flow velocity (Conditions: pH_2S = 54 mbar, T = 80℃, pH = 5), (c) temperature 305 (Conditions: pH_2S = 0.88 bar at 50℃, pH_2S = 0.3 bar at 90℃, pH = 4.2 to 4.7, stirring condition), 306 and (d) partial pressure of H_2S (Conditions: pCO_2 = 2 bar, T = 70℃, pH = 4.2 to 4.9, flow velocity 307 = 0.3 m/s.). Experimental data taken from previous literature [14,41].

5.3 Conclusions

To sum up, the proposed corrosion model for uniform corrosion is able to predict reasonably accurate corrosion rate with respect to different operating parameters as a function of time. The initial corrosion rates agree with the experimental better than the Sun-Nesic model due to the

consideration of the absence of protective layers at Stage I. Although, the predicted corrosion rates at Stage I may have larger deviations compared to those at Stage II, the result is acceptable as corrosion modeling in real operating gas pipelines emphasizes on long-term prediction (i.e., years).

6 Model Application on Operating Gas Pipelines in The Field

As one of the goals of this study is to develop a corrosion predictive model that can be applied to real operating gas pipelines, this chapter aims at validating the applicability of the proposed corrosion predictive model on operating gas pipelines in the field as a case study. Here, eight wet gas gathering pipelines in Sichuan Province, China were studied [44]. Comparisons were made between the model predictions and the observational data in terms of probability measures. Bayesian estimation was used for updating in consideration of model errors.

6.1 Description of the pipeline systems

According to [44], all the pipelines were made of 20 Gauge steels, defined by China National Standard GB/T688, and they were mainly used for transporting CH_4 ($\geq$ 94%) with a small amount of H_2S (1.7 ~ 2.3%) and CO_2 (0.5 ~ 2.0%). These pipelines were diagnosed to be under attack by internal corrosion in which corrosion rates data was generated by metal magnetic memory testing and ultrasonic guided wave methods. According to the definition by Pots et al. [45], these pipelines were operated in the sour regime ($pCO_2/pH_2S < 20$) in which the pCO_2/pH_2S ratios were in the range of 0.3 ~ 0.9; therefore, the proposed corrosion predictive model including an uniform model and a pitting model should be a suitable tool in this case. The basic design variables relevant to these pipelines are given in Table 7 and the operating variables are given in Table 8. It should be noted that the pipe parameters provided in [44] were deterministic in the first place; therefore, in this study each variable was assigned a specified type of distribution and a coefficient of variance

(COV) based on suggestions in other literature [25,46] in order to transform the problem into a probabilistic framework.

6.1.1 *Corrosion control measures*

As corrosion damage in gas pipelines is irreversible, uncensored corrosion often leads to lost production, downtime for maintenance or repair, and even casualties for worst cases. Therefore, pipeline operators implement several kinds of control measures to mitigate the corrosion. One of the common measures for internal corrosion is corrosion inhibitor treatment [47]. The mitigation level of corrosion inhibitor on corrosion rate depends on the inhibition efficiency (E%), which is usually determined through laboratory studies. A mathematical expression of the inhibition efficiency (E%) is given as:

$$\mathrm{E\%} = \frac{\mathrm{CR_{un}} - \mathrm{CR_{inh}}}{\mathrm{CR_{un}}} \times 100 \tag{92}$$

where $\mathrm{CR_{un}}$ is uninhibited corrosion rate (i.e., the predicted corrosion rate by the proposed corrosion model in this case); $\mathrm{CR_{inh}}$ is inhibited corrosion rate.

Corrosion rate drop due to corrosion inhibitor treatments is not unlimited, instead, the inhibition efficiency is reported to depend on the concentrations of corrosion inhibitors i.e., the higher the concentration of corrosion inhibitors, the higher the inhibition efficiency [48]. In addition, if corrosion rate is down to a certain level (e.g., 0.1 mm/y), the inhibition efficiency decreases accordingly. As shown in Table 8, two classes of inhibition efficiency were assumed depending

on the threshold corrosion rate 0.1 mm/y, above which the inhibition efficiency was uniformly distributed in the range between 60 to 95 %, whereas the inhibition efficiency was uniformly distributed in the range between 25 to 50 % when the corrosion rate is below the threshold corrosion rate.

Equation (92) can be used to calculate CR_{inh} given CR_{un} and E% or vice versa; however, CR_{inh} is not available all the time during the pipe operation in practical. Injection pump failures, inhibitor unavailability due to human errors, or poor quality of inhibitors, etc. may lead to unavailability of corrosion inhibitors, rendering the corrosion rate uninhibited. The inhibitor availability can be modeled by a mathematical expression to calculate the overall corrosion rate CR_{tot}:

$$CR_{tot} = f \times CR_{inh} + (1 - f) \times CR_{un} \quad (93)$$

where f is availability of corrosion inhibitors (i.e., fraction of time corrosion inhibitors is available).

Table 7. Basic design variables of eight gas pipelines.

Variables	**Data**								
	Type	**COV**	**Mean**						
			No.1	No.2	No.3	No.4	No.5	No.6	No.7	No.8
L (km)	Normal	0.05	12.26	2.69	2.82	2.47	2.16	3.52	8.41	7.84
D (mm)	Normal	0.05	159	108	108	108	108	108	219	273
d (mm)	Normal	0.05	8	6	6	6	6	6	8	8
t (y)	Normal	0.05	17	7	6	7	6	8	20	20

* L is the length; D is the diameter; d is the thickness; t is the operating time of the pipe

Table 8. Operating variables of eight gas pipelines (partly [44])

Variables	**Data**									
	Type	**COV**	**Mean**							
			No.1	No.2	No.3	No.4	No.5	No.6	No.7	No.8
T_in (K)	Lognormal	0.10	301	301	301	301	301	301	301	301
T_out (K)	Lognormal	0.10	298	298	298	298	298	298	299	298
P_in (MPa)	Lognormal	0.15	5.1	2.1	2.8	5.4	2.1	2.1	5.0	5.1
P_out (MPa)	Lognormal	0.15	3.2	1.8	2.5	4.9	1.8	1.8	3.7	3.8
pH_2S_in (MPa)	Lognormal	0.15	0.089	0.036	0.049	0.093	0.045	0.044	0.108	0.110
pH_2S_out (MPa)	Lognormal	0.15	0.041	0.031	0.044	0.085	0.038	0.038	0.080	0.082
pCO_2_in (MPa)	Lognormal	0.15	0.041	0.013	0.029	0.044	0.030	0.039	0.046	0.065
pCO_2_out (MPa)	Lognormal	0.15	0.026	0.011	0.026	0.040	0.026	0.033	0.034	0.049
V (m/s)	Lognormal	0.10	2	2	2	2	2	2	2	2
pH	Lognormal	0.05	6.58	6.58	6.58	6.58	6.58	6.58	6.58	6.58
Cl^- ($\times 10^3$ ppm)	Lognormal	0.15	91	91	91	91	91	91	91	91
Inhibitor Availability (%)	Uniform	Lower limit			85	Upper limit				95
Inhibitor Efficiency (%)	Uniform				60/25					95/50
R_{solid}	Uniform				0					1

* "Operating parameter_in" denotes the operating parameter at the inlet; "Operating parameter_out" denotes the operating parameter at the outlet.
* T is the temperature; P is the operating pressure; pH_2S is the partial pressure of H_2S (=P × mol% H_2S/100); pCO_2 is the partial pressure of CO_2 (=P × mol% CO_2/100); V is the flow velocity; pH is the pH level; Cl^- is the concentration of chloride ions.

6.1.2 *Temporal and spatial variabilities*

Applying a corrosion model for field purposes requires the execution to be in a probabilistic framework in order to take into account the uncertainties of operation and basic design variables. Therefore, the proposed methodologies to consider temporal and spatial variabilities of operating parameters described in "**Chapter 4.2: Modeling the variability of operating parameters**" were applied on the given data for eight pipelines.

For temporal variability of operating parameters, specifically, each operating parameter was modeled by a Poisson process with daily-varying values (i.e., $\lambda = 1/\text{day}$) following assumed probability distribution in Table 8 where the target time is the operating time for each pipeline. The schematic diagram of the Poisson process for the modelling of operating parameters is shown in Figure 17. Readers are referred to "**Chapter 4.2.1: Temporal variability**" for more details.

To make simulated operating parameters more realistic, the operating parameters were modeled to be fully-correlated on a basis of a proposed correlation matrix shown in Figure 22 where temperature and pressure were assumed to be highly and positively correlated compared to others [49]. By repeating this process for every operating parameter, a number of series of operating parameter as a function of time for each pipeline were created.

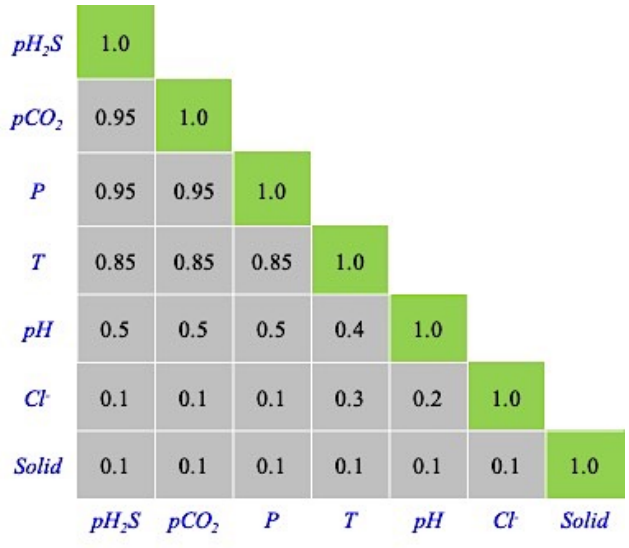

Figure 22. The proposed correlation matrix of operating parameters.

For spatial variability of operating parameters, only operating temperature, operating pressure, partial pressure of H_2S, and partial pressure of CO_2, were considered. In other words, these operating parameters were location dependent where they are higher at the inlet and lower at the outlet as shown in Table 8. Three locations, namely, at near inlet, at midpoint, and at near outlet were considered for location-dependent corrosion predictions, all of which were later used to calculate population variability distribution of corrosion rate in a representative of a whole pipe. The same process was then repeated for each studied pipeline. Reader are referred to "**Chapter 4.2.2: Spatial variability**" for more details.

A picture of the R-DAT software interface showing the settings of prior distribution of corrosion rate for pipeline No.2 is illustrated in Figure 23 as an example. In this case, the prior distribution of corrosion rate was assumed to follow Lognormal distribution with median (Median) and error

factor (EF) as main parameters, both of which are described by an estimate (Estimate) and a range factor (RF).

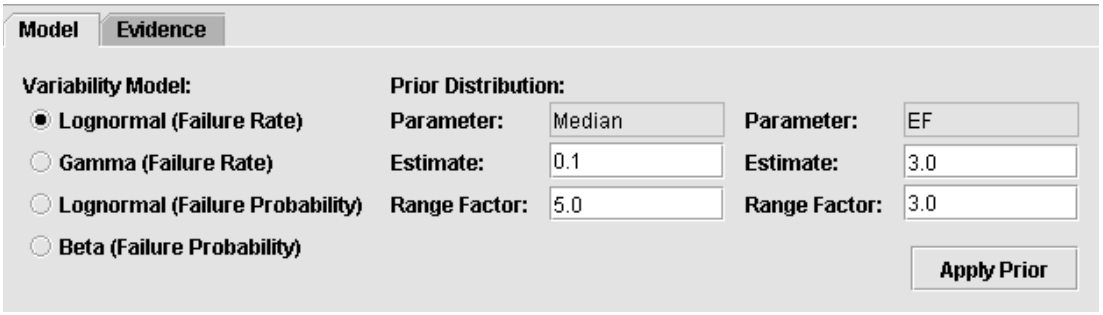

Figure 23. R-DAT software interface of prior distribution setting for pipeline No.2 [40].

Figure 24 shows the R-DAT software interface of evidence setting for pipeline No.2. As described before, predicted corrosion rates considering temporal variability of operating parameters at near inlet, at midpoint, and at near outlet were considered as evidences in a calculation of population variability distribution of corrosion rate. Their corresponding median, EF, 95th percentile, and 5th percentile values were provided as inputs to the software. This process was repeated for the eight pipelines to be studied.

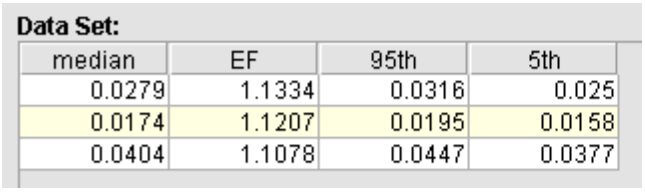

Figure 24. R-DAT software interface of evidence setting [40].

6.1.3 *Determination of corrosion type*

In [44], remaining pipe wall thickness of each pipeline was measured by metal magnetic memory testing and ultrasonic guided wave methods, both of which belong to non-destructive testing (NDT). The corresponding corrosion depth was calculated by subtracting the remaining wall thickness from the original pipe wall thickness, while the corresponding corrosion rate was calculated by dividing the corrosion depth with the operating time under the assumption of linear corrosion growth. However, neither metal magnetic memory testing nor ultrasonic guided wave method reveals the information of geometric characteristics of corrosion defects and pipe wall appearance. In addition, no information about the type of corrosion from which these pipelines were suffered was provided in [44]. Therefore, prior to applying corrosion models for corrosion predictions, corrosion type has to be determined for each pipeline.

This study adopted two statistical methodologies, namely, extreme value analysis and risk curve method for the identification of corrosion types between uniform and pitting corrosion with corrosion rate data. Each methodology was described in the following paragraphs and the results of each methodology were compared for mutual verification.

6.1.3.1 *Extreme value analysis*

Extreme value analysis has been widely used to predict pitting corrosion [50,51] because it accounts for the random nature of pitting corrosion. Specifically, it is found that maximum pit depth or pit growth rate caused by pitting corrosion can be well fitted by Gumbel distribution.

Therefore, in this study Gumbel distribution was used to fit corrosion rate data with a threshold of $R^2 = 95$. If a Gumbel distribution fitting on the corrosion rate data of a pipe has $R^2 \geq 95$, this pipe is determined to mainly suffer pitting corrosion. Otherwise, it mainly suffered uniform corrosion. The steps for extreme value analysis were described as follows:

Step 1: Collect data (e.g., corrosion rate or depth) and arrange data in ascending order.

Step 2: Compute the cumulative probability distribution of the data ($F(y)$) using the average rank method given by:

$$F(y) = \frac{i}{N + 1} \tag{94}$$

where i is rank of the data in an ascending order; N is total number of data points.

Step 3: Fit the data by Gumbel distribution given by [50] with linear regression:

$$x = -\alpha[\ln(-\ln F(y))] + \lambda \tag{95}$$

where x is data; α is scale parameter; λ is location parameter.

Step 4: Estimate the parameters α and λ. The probability density function of Gumbel distribution can be expressed as:

$$f(y) = \frac{1}{\alpha}\exp[-y - \exp(-y)] \tag{96}$$

where $y = \frac{x-\lambda}{\alpha}$ and $\alpha > 0$.

If the data cannot be well fitted by Gumbel distribution, the data was then analyzed by EasyFit 5.6 software [52] to find the best-fit probability distribution for it.

6.1.3.2 *Risk curve method*

Risk curve method is widely used in risk analysis to describe the relationship between complementary cumulative frequency (CCF) and the magnitude of an accident in order to find the safety index (D). This method was applied to the field of corrosion to determine if large-scale corrosion is likely to happen by Kasai et al. [53]. Specifically, there are three analogies between an accident and corrosion: the magnitude of the accident is analogous to the magnitude of corrosion rate or depth; the frequency of accident is analogous to the probability of occurrence of corrosion; the time domain (i.e., observation period) of accidents is analogous to the spatial domain (i.e., area of object that suffers corrosion). The typical log-log plot of a risk curve (i.e., amount of damage vs. CCF) is generally convex, but there is a linear relationship in the large-scale damage region, which can be regarded as deeper corrosion depth region. The mathematical expression of this region is shown as:

$$F(h) \propto h^{-D} \quad (97)$$

where $F(h)$ is complementary cumulative probability (i.e., CCP); h is magnitude of corrosion rate or depth, and D is safety index (also known as decreasing ratio of large-scale corrosion in this case). Equation (97) shows that CCP decreases with increasing h in a power law form by D power. In other words, large D corresponds to the scenario that extremely large-scale damage of corrosion is less likely to happen (the case for uniform corrosion), whereas smaller D corresponds to the scenario that extremely large-scale damage of corrosion is more likely to happen (the case for pitting corrosion).

6.1.4 *Corrosion prediction*

Based on the results of mutual verification by extreme value analysis and risk curve method, a corrosion type of each pipeline was identified. Then, the pipeline that mainly suffered uniform corrosion was modeled by the uniform corrosion predictive model described in Section 4.1.1, while the pipeline that mainly suffered pitting corrosion was modeled by the pitting corrosion predictive model described in Section 4.1.2. Operating parameters that considered temporal and spatial variabilities were regarded as inputs to the two corrosion predictive models in the calculation of probability density function of corrosion rate. Due to the consideration of both temporal and spatial variabilities of operating parameters, the predicted population variability distribution of corrosion rate of each pipeline is therefore time and location-dependent.

6.2 Results and discussion

Results and discussion including the results of corrosion type identification for each pipeline, model performance and model performance considering model errors by Bayesian estimation as well as the comparison of corrosion predictions between different models were described in the following paragraphs.

6.2.1 *Corrosion type identification*

The results of extreme value analysis for pipeline No.1 to No.8 are shown in Figure 25. Based on the definition that Gumbel distribution fitting of corrosion rate with $R^2 \geq 95$ is denoted as pitting corrosion, whereas that with $R^2 < 95$ is denoted as uniform corrosion. In other words, pipelines No.1, No.3, No.7, and No.8 are identified to mainly suffer pitting corrosion where their corrosion rates can be well described by Gumbel distribution, while pipelines No.2, No.4, No.5, and No.6 are identified to mainly suffer uniform corrosion based on extreme value analysis results. Corrosion rates of pipelines No.2, No.4, No.5, and No.6 were then analyzed by EasyFit 5.6 software [52] and found that the best-fit probability distribution is Generalized Extreme Value (GEV) distribution.

The results of risk curve method for pipeline No.1 to No.8 are shown in Figure 26. According to [53], there is no strict rule of how large D should be to be classified as large. However, two groups of D were observed from the results, namely, $D < 4$ and $D > 10$. Therefore, the risk curve of corrosion rate with $D < 4$ is denoted as pitting corrosion, whereas that with $D > 10$ is denoted as

uniform corrosion. In other words, pipelines No.1, No.3, No.7, and No.8 are identified to mainly suffer pitting corrosion, while pipelines No.2, No.4, No.5, and No.6 are identified to mainly suffer uniform corrosion based on risk curve method results.

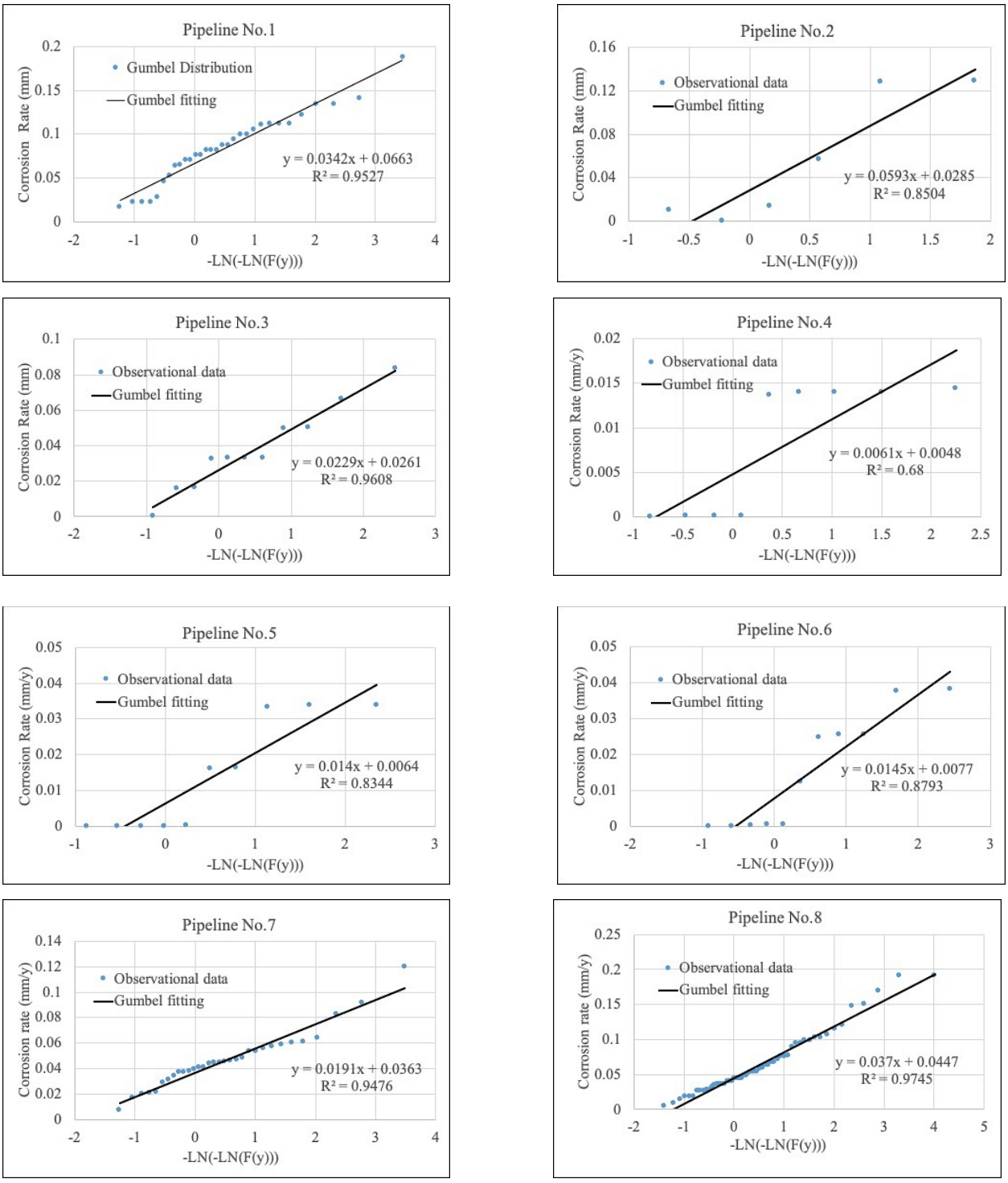

Figure 25. Results of extreme value analysis for pipeline No.1 to No.8.

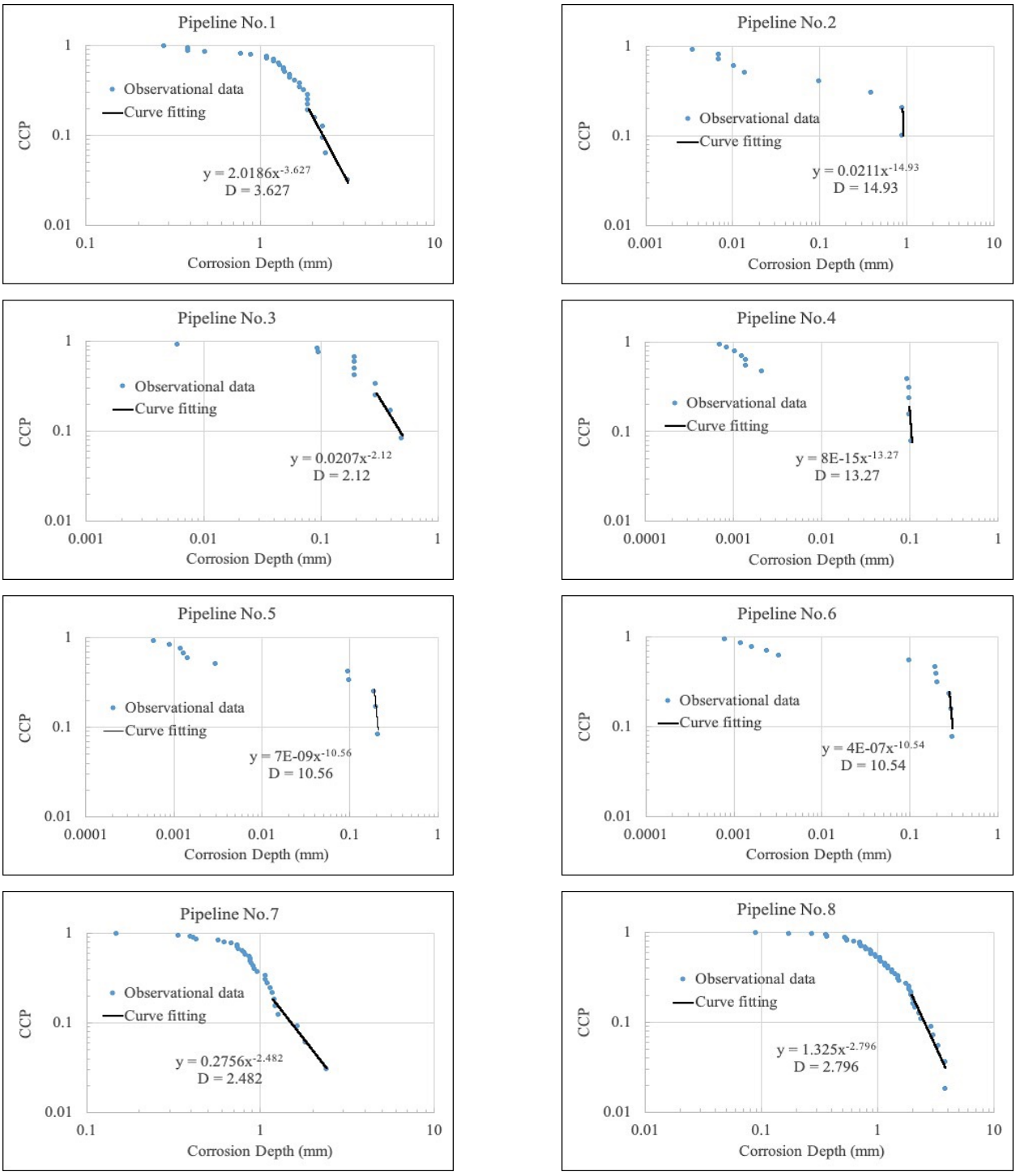

Figure 26. Results of risk curve method for pipeline No.1 to No.8.

The detailed results of corrosion type identification for all the pipelines are arranged and illustrated in Table 9. The results by extreme value analysis and risk curve method are actually mutually verified, indicating the suggested conclusion that pipelines No.1, No.3, No.7, and No.8 mainly suffer pitting corrosion, while pipelines No.2, No.4, No.5, and No.6 mainly suffer uniform corrosion. However, it should be noted that since this conclusion was made by statistical analysis based on the available data, there are other information of the pipelines that weren't revealed by the available data. For example, although analysis results show that pipelines No.2, No.4, No.5, and No.6 suffer uniform corrosion, it does not rule out the possibility that these pipelines do not have corrosion defects caused by pitting corrosion. Instead, it only implies that they are likely to have more areas affected by uniform corrosion than pitting corrosion, which were captured by the inspection tools.

In addition, Table 9 shows that three out of four pipelines that were identified to mainly suffer pitting corrosion, namely, pipelines No.1, No.7, and No.8 have been operated much longer than others (i.e., more than 10 years). In other words, older pipelines are found to be more likely to suffer uniform corrosion than younger ones. It can be explained by the film-breaking mechanism [54], stating that local breakdown of protective layers, mostly due to the presence of chloride ions or mechanical stresses at the defects on the protective layer, is the main cause of pit initiation. Since older pipelines are likely to have more defects on the protective layers after long time of operation, it is reasonable to speculate that they are more vulnerable to pitting corrosion as a result of local film breakdown according to the analysis results.

Table 9. Results of corrosion type identification for pipelines No.1 to No.8.

Methodology	Parameter	Pipeline			
		No.1	**No.3**	**No.7**	**No.8**
Extreme value analysis	Corrosion type	Pitting			
	Distribution type	Gumbel			
	Scale parameter, α	0.035	0.024	0.020	0.038
	Location parameter, λ	0.070	0.033	0.039	0.047
Risk curve method	Safety index, D	3.63	2.12	2.48	2.79

Methodology	Parameter	Pipeline			
		No.2	**No.4**	**No.5**	**No.6**
Best-fit by EasyFit 5.6 [52]	Corrosion type	Uniform			
	Distribution type	Generalized Extreme Value			
	Scale parameter, σ	0.019	0.007	0.014	0.013
	Location parameter, μ	0.016	0.004	0.008	0.007
	Shape parameter, κ	0.480	0.054	-0.092	0.018
Risk curve method	Safety index, D	14.93	13.27	10.56	10.54

6.2.2 *Model performance*

Model performance was tested by comparing the prediction results by the proposed model with the observational data (i.e., corrosion rate). Graphical expressions as well as statistical metrics of the prediction results and the observational data were compared and discussed.

Firstly, the model considered only temporal and spatial variabilities of operating parameters. The graphical comparison in terms of probability distribution between the predicted corrosion rates and the observational corrosion rates of pipelines No.1, No.3, No.7, and No.8 for pitting corrosion is shown in Figure 27. It shows that the observational corrosion rates of pitting corrosion follow Gumbel distribution, while the predicted corrosion rates follow Lognormal distribution obtained from EasyFit 5.6 software [52]. Except for pipeline No.3, the model predictions of pipelines No.1,

No.7, and No.8 agree well with the observational data. The probability distributions of model predictions tend to have longer tails compared to the observational corrosion rates due to the consideration of spatial variability of operating parameters from the inlet to the outlet, which covered a broad range of operating parameters, whereas the observational corrosion rates were assumed to be randomly measured from certain sections of the pipeline, meaning only a limited range of operating parameters was considered.

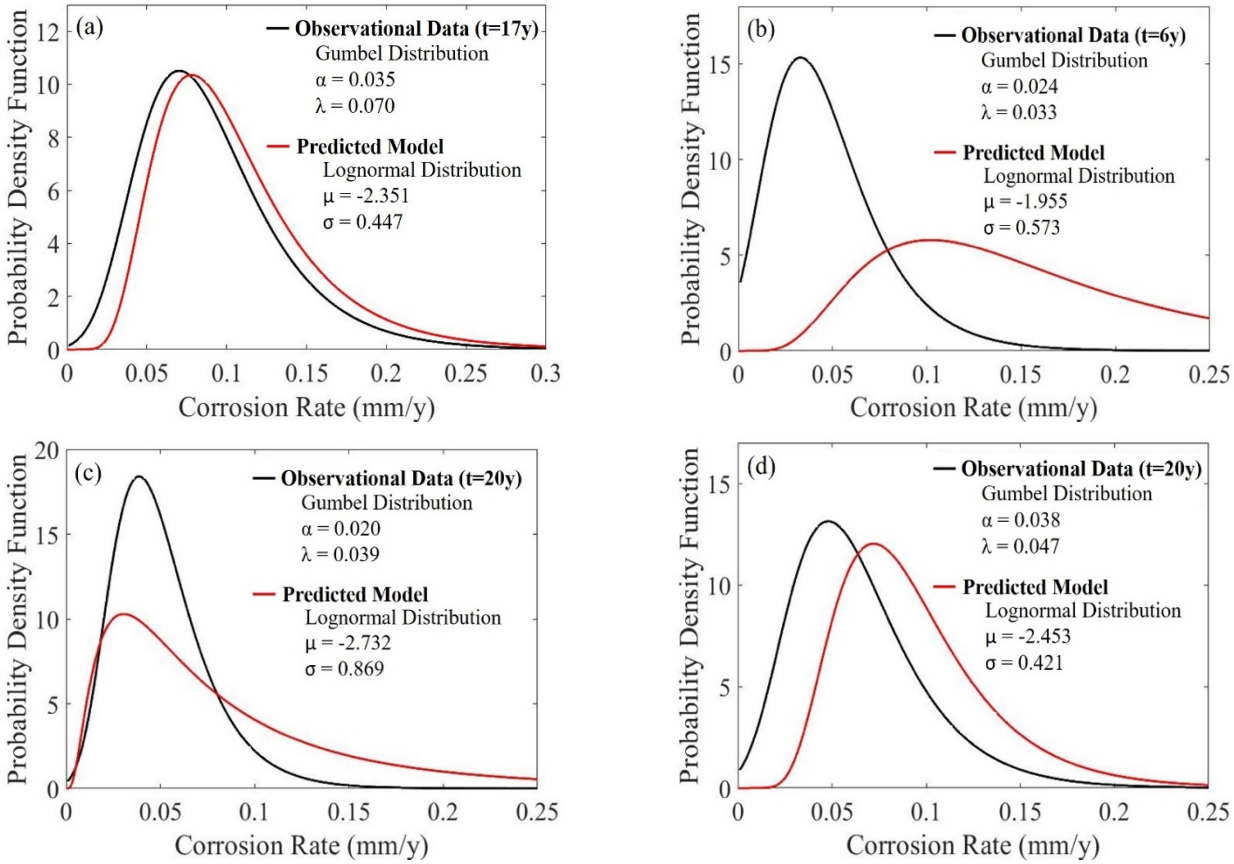

Figure 27. Comparison between the predicted corrosion rates with the observational corrosion rates of pipelines (a) No.1, (b) No.3, (c) No.7, and (d) No.8 for pitting corrosion.

Comparison of statistical metrics (i.e., median, mean, mode, and standard deviation) between model predictions and the observed corrosion rates was also done and displayed in Figure 28. Figure 28 shows that most of the differences between the model predictions and the observed corrosion rates are within a factor of 2, indicating a decent accuracy of the corrosion model for pitting corrosion.

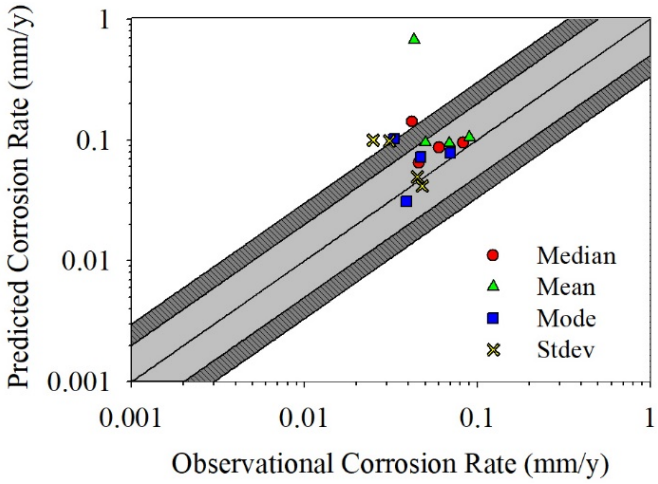

Figure 28. Model predictions vs. Observational data of pipelines No.1, No.3, No.7, and No.8 in terms of statistical metrics for pitting corrosion.

The graphical comparison in terms of probability distribution between the predicted corrosion rates and the observational corrosion rates of pipelines No.2, No.4, No.5, and No.6 for uniform corrosion is shown in Figure 29. It shows that the observational corrosion rates of uniform corrosion follow Generalized Extreme Value distribution, while the predicted corrosion rates follow Lognormal distribution. Only one out of four model prediction agree relatively well with

the observational corrosion rates, while the rest model predictions tend to overestimate the corrosion rates.

Comparison of statistical metrics between model predictions and the observed corrosion rates was depicted in Figure 30, which shows that the majority of mean, median, and mode values of model predictions are larger than observational corrosion rates with a factor of 3 and even 4.

To sum up, the model considering temporal and spatial variabilities of operating parameters can predicted decently accurate corrosion rates for pitting corrosion; however, the model predictions of uniform corrosion are not as accurate as those for pitting corrosion. This finding implies that for the pipelines that were identified to mainly suffer uniform corrosion, namely, pipelines No.2, No.4, No.5, and No.6 may have been under attack by other kinds of corrosion, all of which also play import roles and influence the corrosion behavior in the pipelines. Therefore, a correction of the existing model was applied and described in the next section.

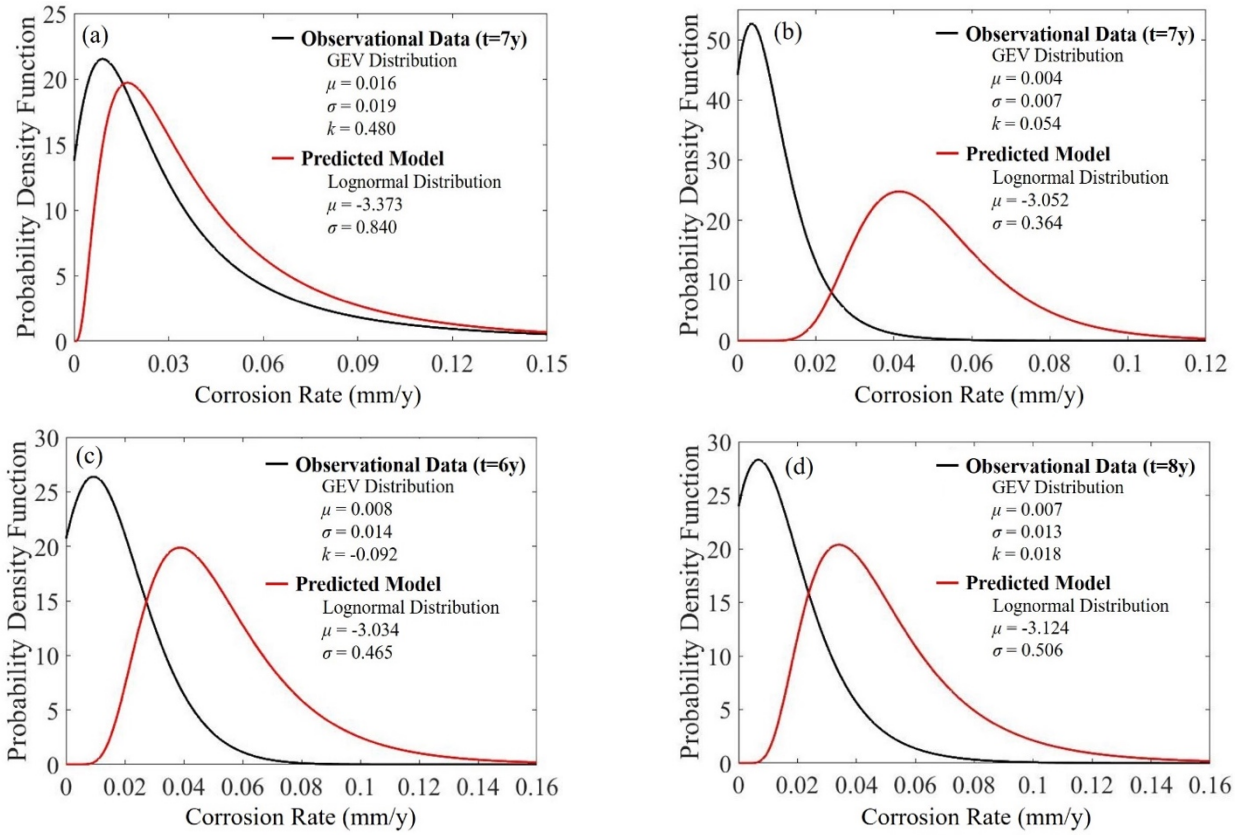

Figure 29. Comparison between the predicted corrosion rates with the observational corrosion rates of pipelines (a) No.2, (b) No.4, (c) No.5, and (d) No.6 for uniform corrosion.

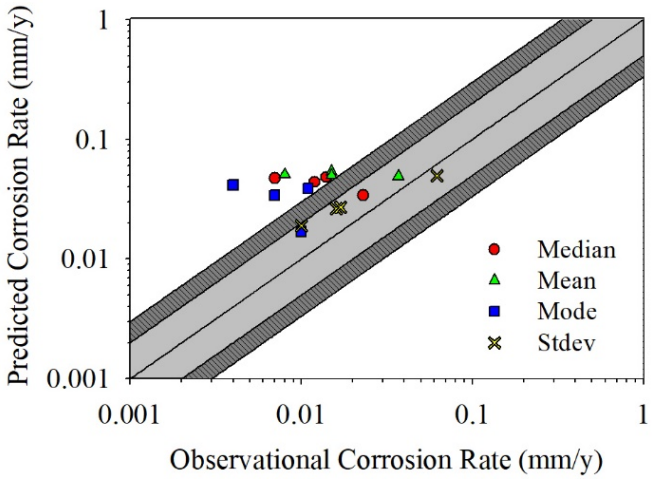

Figure 30. Model predictions vs. Observational data of pipelines No.2, No.4, No.5, and No.6 in terms of statistical metrics for uniform corrosion.

6.2.3 *Model performance with model errors*

Model errors were taken into account by Bayesian estimation to do model calibration. Model errors in this case study come from the assumptions of the model or factors that are not considered for corrosion modelling. For example, pipelines were identified to mainly suffer only uniform and pitting corrosion by extreme value analysis and risk curve method; however, besides uniform and pitting corrosion, other types of corrosion such as erosion corrosion, microbiologically-influenced corrosion, corrosion fatigue, Top-of-Line corrosion were not considered in this case study. Most importantly, the lack of historical operation information about the pipelines in terms of maintenance practices and repair certainly influences the model predictions.

A schematic diagram showing the display of model errors between observational corrosion rates and model predictions is illustrated in Figure 31. In Figure 31, E_n is the deviation of median values between the predicted corrosion rates and the observational corrosion rates for prediction n; EF is the error factor. Bayesian estimation method introduced in Section 4.2.2 was applied to quantify the model errors in the form of probability distributions. Specifically, parameteric probability distributions of model errors of four pipelines for pitting corrosion and those of four pipelines for uniform corrosion were calculated, respectively. Once the model errors for each pipeline was obtained, Monte Carlo simulation was used to correct the predicted corrosion rates with model errors to obtain the updated corrosion rates, which were analyzed by EasyFit 5.6 software [52] to find the best-fit probability distributions.

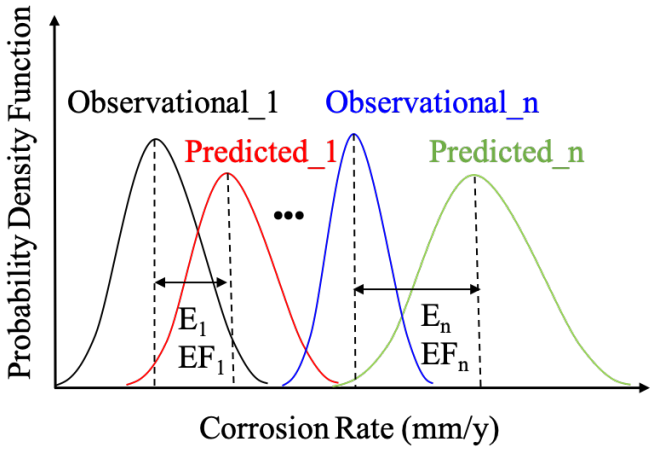

Figure 31. A schematic diagram showing the display of model errors between observational corrosion rates and model predictions.

Figure 32 and Figure 34 show the graphical comparison between the updated corrosion rates with the observational corrosion rates for pipelines No.1, No.3, No.7, and No.8 after considering model errors for pitting corrosion and that between the updated corrosion rates with the observational corrosion rates for pipelines No.2, No.4, No.5, and No.6 after considering model errors for uniform corrosion, respectively. The results show that both uniform and pitting corrosion predictions agree well with the observational corrosion rates, which can be verified by the comparison of statistical metrics between model predictions and observational corrosion rates shown in Figure 33 and Figure 35. Most deviations of statistical metrics are reduced to around or within a factor of 2, indicating a significant improvement in corrosion predictions.

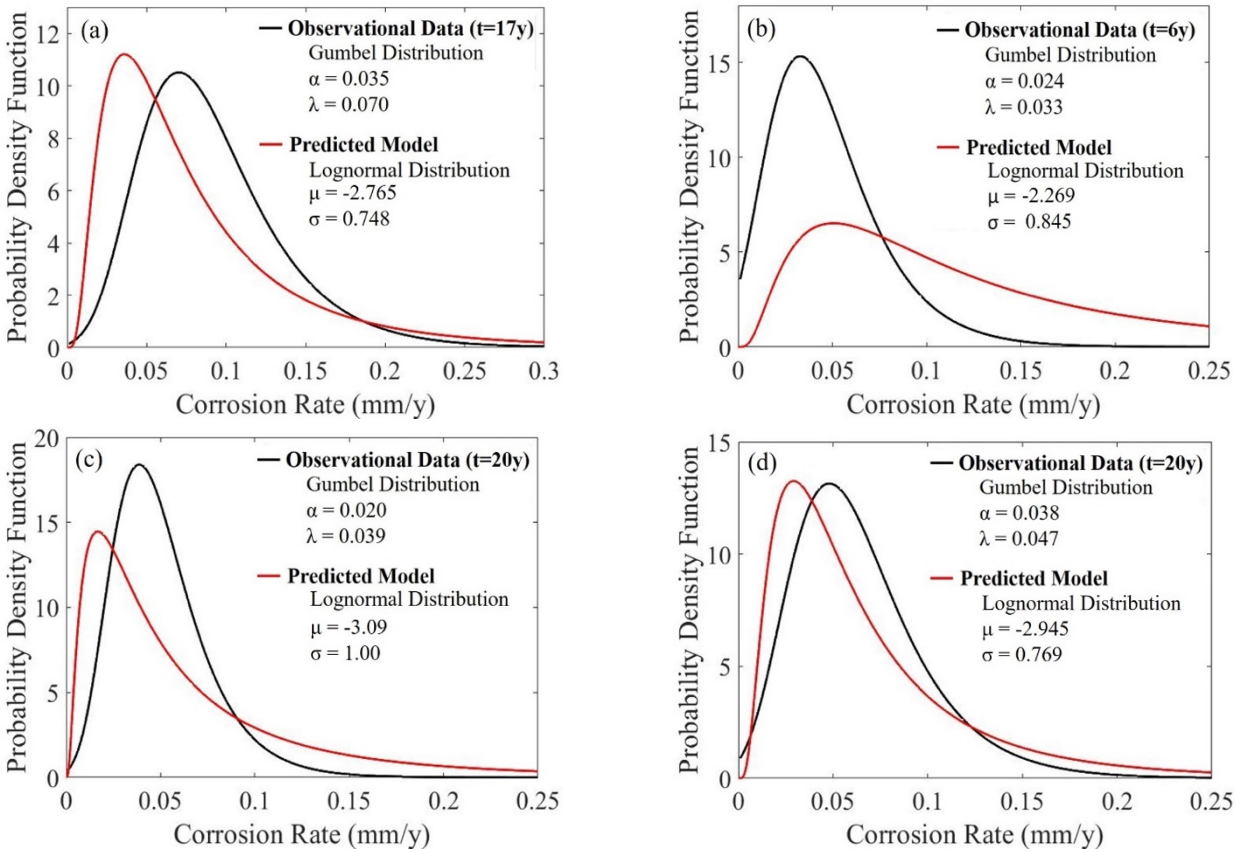

Figure 32. Comparison between updated corrosion rates with observational corrosion rates of pipelines (a) No.1, (b) No.3, (c) No.7, and (d) No.8 considering model errors for pitting corrosion.

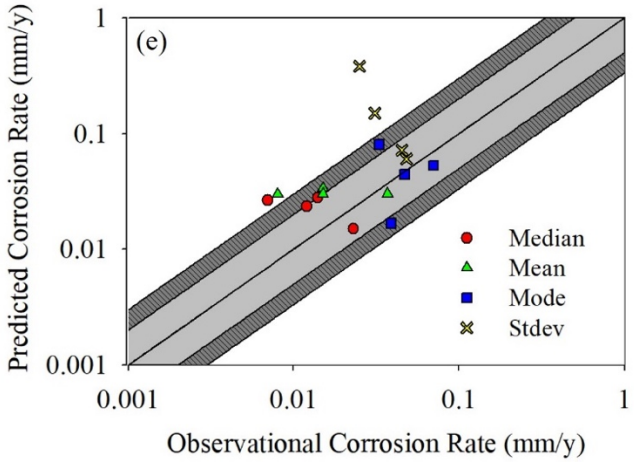

Figure 33. Model predictions vs. Observational data for pipelines No.1, No.3, No.7, and No.8 in terms of statistical metrics after considering model errors for pitting corrosion.

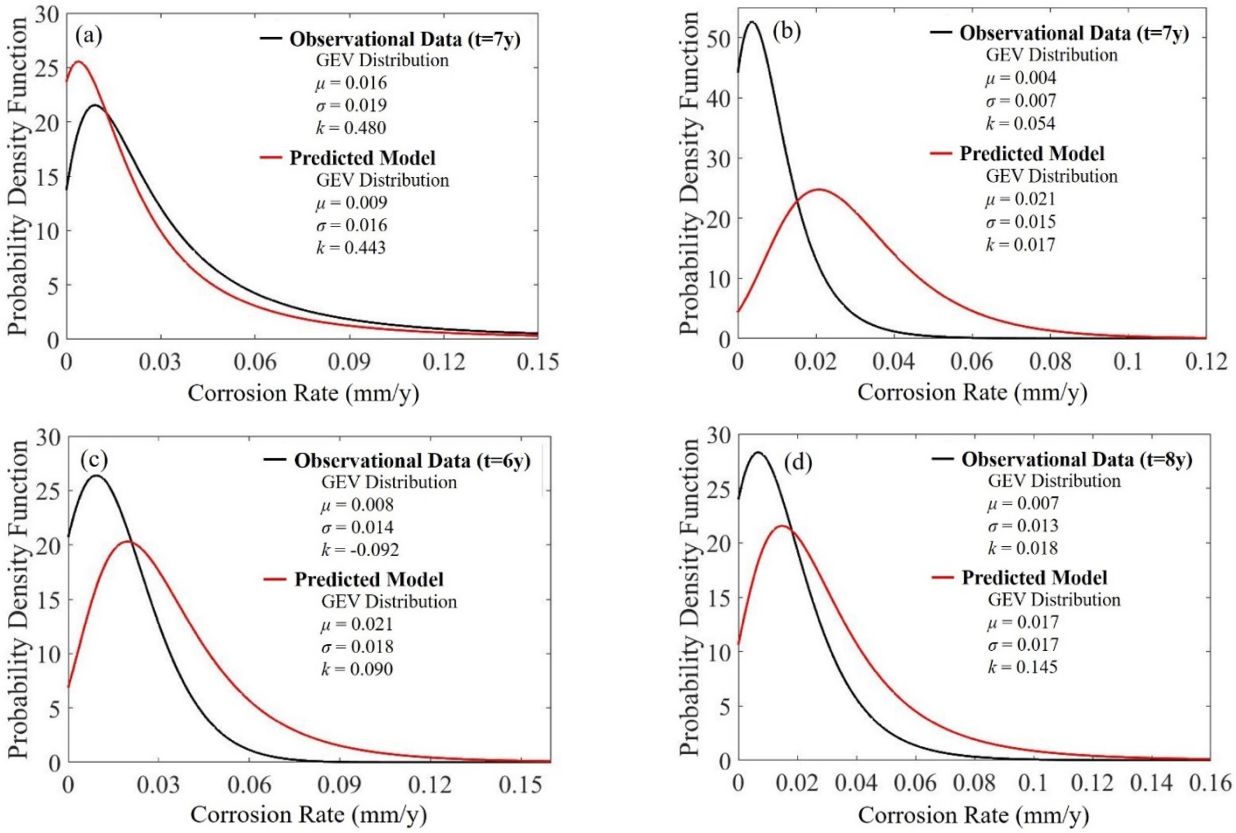

Figure 34. Comparison between updated corrosion rates with observational corrosion rates of pipelines (a) No.2, (b) No.4, (c) No.5, and (d) No.6 considering model errors for uniform corrosion.

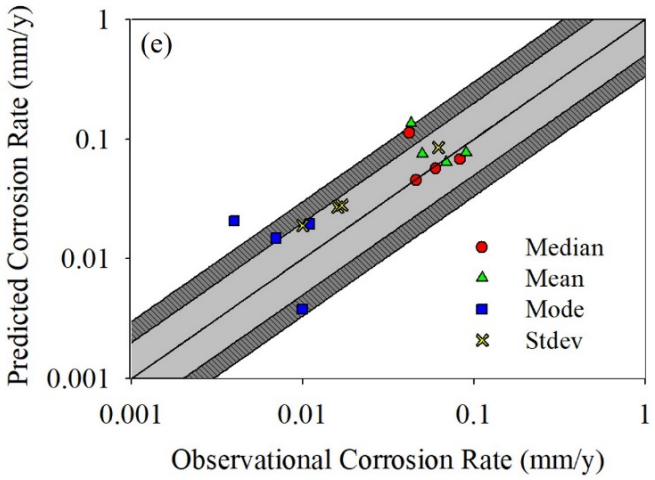

Figure 35. Model predictions vs. Observational data for pipelines No.2, No.4, No.5, and No.6 in terms of statistical metrics after considering model errors for uniform corrosion.

6.2.4 *Model comparison with other existing models*

In the oil and gas industry, engineering criteria have been used for corrosion evaluation. For example, National Association of Corrosion Engineers (NACE) proposed Wet Gas Internal Corrosion Direct Assessment SP0110 (WG-ICDA SP0110) [55] for wet gas pipelines subjected to internal corrosion, which suggests that corrosion rate can be calculated by corrosion predictive models such as the Anderko model [56], the Crolet model [57], the de Waard and Milliams model (D-M model) [10], or the SWRI model [58].

In order to compare the model performance of the proposed corrosion model for uniform corrosion with other existing models, the D-M model and the SWRI model were used to predict corrosion rates given operating parameters of pipelines No.2, No.4, No.5, and No.6. It should be noted that, this comparison considered only temporal variability of operating parameters. The obtained predicted corrosion rates by each model was inserted into EasyFit 5.6 software [52] to find best-fit probability distributions. The comparison between model predictions and observational data in terms of mean and median values by different models is shown in Figure 36. The result shows that the proposed corrosion model for uniform corrosion outperforms the D-M model and the SWRI model in this case. Among three models, the D-M model is most likely to overestimate corrosion rates and the highest absolute deviation is as large as 1 mm/y. This can be explained by the fact that the D-M model doesn't consider the effect of H_2S that can decrease corrosion rate as a result of the formation of protective sulfide layers.

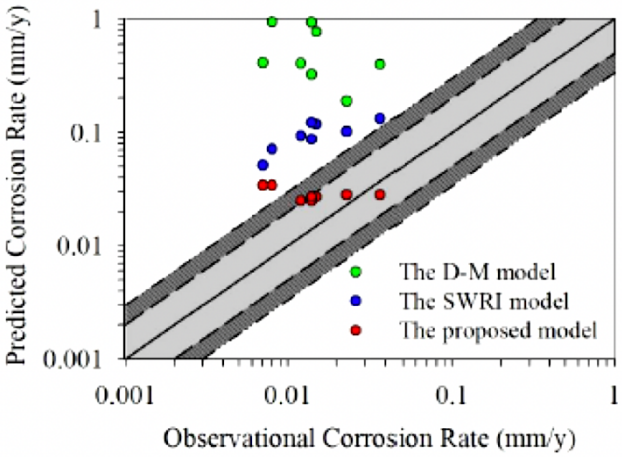

Figure 36. Model predictions vs. Observational data of pipelines No.1 to No.8 in terms of mode values for different corrosion predictive models.

6.3 Conclusions

The application of the proposed model on operating gas pipelines was validated through a case study of eight operating pipelines in Sichuan Province, China. Consideration of temporal and spatial variabilities of operating parameters consolidated the validity of the proposed model on field applications. In other hand, temporal variability of operating parameters enables the model to simulate the effect of time-varying operating parameters on corrosion rate, while spatial variability of operating parameters enables the model to simulate location-dependent corrosion rate. Results show that model predictions considering only temporal and spatial variabilities of operating parameters agree with the observational corrosion rates better for pitting corrosion than uniform corrosion. Further model calibration on model errors largely improves the model performance as most deviations of statistical metrics are reduced to around or within a factor of 2.

Comparison of model performance with other models, namely, the D-M model and the SWRI model shows that the proposed model for uniform corrosion outperforms them in this case study.

Part B

7 Smart Condition-Based Maintenance with Reinforcement Learning for Dry Gas Pipeline Subject to Internal Corrosion

Integrity management is closely related to maintenance practices. A cost-effective way of making maintenance decisions is in demand. This chapter discussed two proposed smart condition-based maintenance management methodologies by reinforcement learning (RL) algorithms, namely, Q-learning and Sarsa(λ) to optimize corrosion maintenance costs over the life of a pipeline. Test study and sensitivity analysis were done to compare the model performances of Q-learning, Sarsa(λ), and traditional periodic maintenance policy.

7.1 Introduction

In this era, the advancement of the Internet of Things (IoT), cloud computing, and communication and actuation technologies facilitates the development of intelligent cyber-physical systems (CPSs). Numerous applications of CPSs have been studied such as self-driving cars, smart buildings, smart electric grids, smart infrastructures, and smart manufacturing and production. These systems are integrated with computer systems with self-learning capability that can communicate and interact with physical components [59]. CPSs are found to benefit the implementation of complicated asset integrity management as the collection of data by IoT can be processed immediately and provide accurate, in-time information about conditions of an infrastructure [60]. For example, a gas pipeline embedded with a decision-making agent can

immediately analyze the collected data and predict the level of corrosion, which can facilitate pipeline operators in making maintenance or repair decisions.

Among many data-driven techniques for the development of Artificial Intelligence (AI), reinforcement learning (RL) is found to be well suited to formulate the asset integrity management problems. In general, RL observes and interacts with the environment by trial and error; therefore, after adequate trainings, it is capable of making decisions to achieve the goal in an optimal way even in an uncertain environment that is new to the RL agent. There are three extraordinary characteristics of RL algorithms: RL algorithms learn from historical and online data monitored and collect by IoT; RL can deal with delayed consequences of applying maintenance actions; RL algorithms are designed to interact and learn in a stochastic environment with unpredictable operating and environmental conditions. The abovementioned three characteristics have make RL attract more and more attention in asset integrity and management in recent years.

Many studies have been done using RL to solve asset integrity and management problems. For example, for the manufacturing systems, Xanthopoulos et al. [61] used policy-based Q-Learning algorithm to find the optimal joint production/maintenance policy that can minimize the inventory level but and reduce the cost. Sensitivity analysis was done to study the influences of arrival rate, deterioration failure rate, and maintenance rate on various maintenance management practices to find the best parameter combinations. Wei and Qi [62] designed a policy-based Q-Learning algorithm to build a maintenance scheduler using a two-machine-one buffer system. The maintenance scheduler was trained to choose actions among produce, idle, and maintenance in a

goal to maximize the average reward. For large infrastructure systems, Aissani et al. [63] used a Sarsa (Sate-Action-Reward-State-Action) algorithm to build a maintenance scheduler that can maximize the system availability and the production efficiency for an oil refinery. They found the RL maintenance scheduler is more cost-effective than the preventive maintenance and the corrective maintenance in making maintenance practice decisions. Moreover, Compare et al. [64] used a Sarsa algorithm to train a RL agent to find best part flow strategy in terms of repair and purchase actions in a gas turbine plant. Results show that RL agent increased the reliability of the gas turbine plant by reducing the probability of forced outages.

Another large-scale infrastructure that requires the integrity management during its operation is gas transmission pipelines. These pipelines are about 3 million miles in total length in the United States as reported by U.S. Energy Information Administration in 2017 and corrosion is one of the main threats to their integrity. In addition, according to NACE, 80% of annual corrosion-related cost, roughly 7 billion US Dollar, is spent on corrosion-related maintenance. Therefore, how to implement pipeline integrity management in a cost-effect way has been a significant issue for pipeline operators.

7.2 Objectives

To date, numerous approaches have been proposed on maintenance management of gas transmission pipelines including time-based maintenance (TBM), risk-based maintenance (RBM), and condition-based maintenance (CBM) [65]. According to the definitions, TBM strategy

performs maintenance based on a calendar schedule already planned in advance. This strategy is similar to periodic maintenance in which each specific maintenance is done over a specific time interval; RBM strategy performs maintenance on the component with the largest risk of failure. It is a more economical methodology than TBM as maintenance resources only apply to the most vulnerable component but not all components; CBM strategy monitors actual conditions of the system and make maintenance decisions based on the conditions of the systems. For example, CBM will decide what maintenance actions to take when there are indicators showing the performance is decreasing or potential failure is coming. Among these three maintenance strategies, condition-based practice is found to be more cost-effective over other two strategies [66].

In view of optimal corrosion maintenance management problem, this study proposed a corrosion maintenance scheduler on gas transmission pipelines by integrating a RL algorithm into a CBM framework. The new methodology is thus called smart-CBM because it is equipped with the power of AI in making maintenance decisions for cost-effective purposes. Higher level of system reliability is also maintained to ensure that corrosion-related failures, such as leak or burst, will not happen during the operation.

7.3 Overview of the RL maintenance scheduler

The proposed maintenance scheduler integrates the internal corrosion modeling with the data-driven and model-free RL algorithms to optimize the maintenance management on a transmission gas pipeline. It should ensure the asset integrity and extend the lifetime of the asset while

minimizing the maintenance costs. In general, a RL agent interacts with an uncertain environment and learn via try and error to achieve a goal. During the interaction, the RL agent firstly observes the signals from the environment and decides what actions to take. That action will then influence the environment and update the environment. Once the agent takes another observation of the environment, it gets new information and a reward signal corresponding to the previous action it takes. Ideally, the agent learns from the reward signal it receives after applying the action to the environment so that it can optimize the decision making in the future to reach maximum rewards.

These processes are repeated many times until the agent learns when to and how to choose actions on a cost-effective point of view. A schematic diagram showing RL agent and environment interaction is displayed in Figure 37.

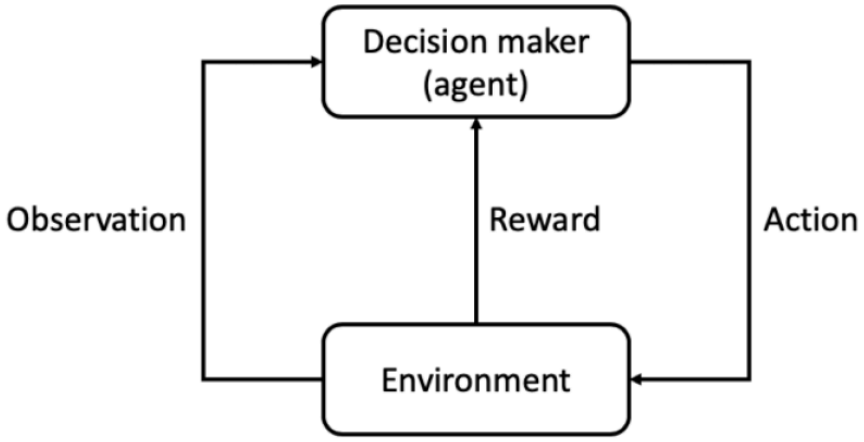

Figure 37. Interaction between a RL agent and the environment.

In this study, a proposed framework of SCBM of a gas transmission pipeline for the development of a maintenance scheduler is shown in Figure 38. The proposed SCBM framework like other RL algorithms has an agent and an environment that are interacting to reach the goal. The environment is a segment of a gas transmission pipeline, which is in operation under stochastic environmental and operational parameters. The internal corrosion takes place in the pipeline during the operation. Once the corrosion is built up to a certain level, failures such as leak or burst will happen and cause catastrophic losses to the human life and property. The proposed corrosion predictive model for internal corrosion described in **"Chapter 5.1 Internal corrosion model"** and the reliability model described in "**Chapter 3.3 Pipeline corrosion risk assessment"** was used to simulate the environment. On the other hand, the agent is a maintenance scheduler aims at preventing the pipeline failures from happening and meanwhile minimizing the maintenance costs. The interaction between the environment and the agent is that, firstly, the environment updates the agent with up-to-date pipe information (e.g. corrosion depth, length, probability of leak, probability of burst) as well as costs (i.e., reward function) on monthly basis. Then, agents will each time select one out of four maintenance actions, namely, internal coating, corrosion inhibitors, cleaning pigs, and repair/replacement or do nothing and interact with the environment. Finally, after enough training, the agent should be able to suggest the best possible action at specific condition to maintain the pipeline integrity while keeping the goal of minimizing the cost. The main idea is to pre-train the maintenance planner with our model and then train it with real data when it is available. Finally, this maintenance planner should be mature enough to be applied on real operating gas transmission pipelines. This process is called transfer learning.

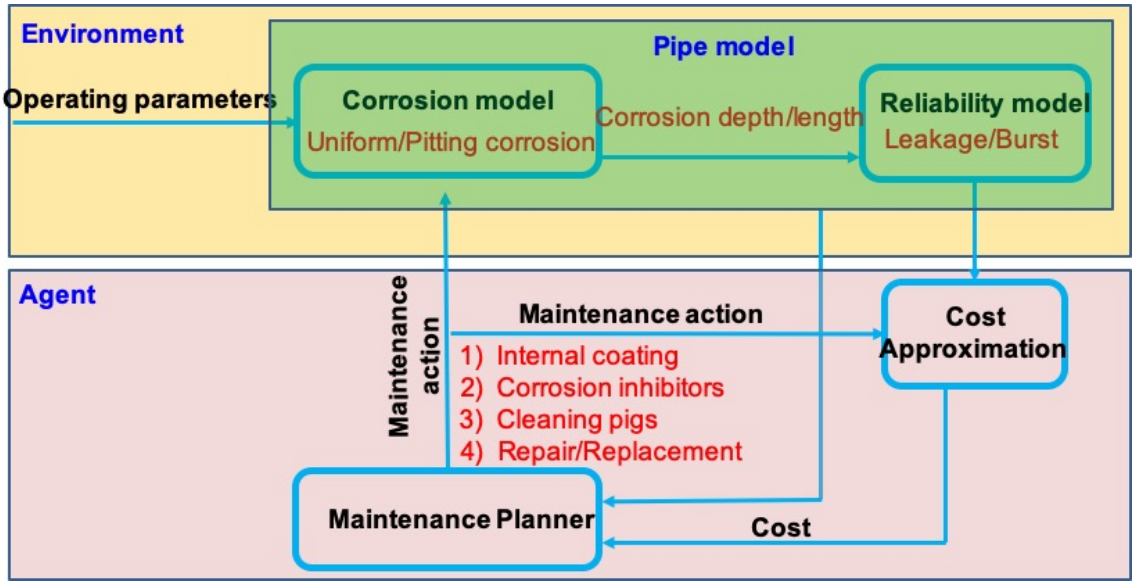

Figure 38. The overview diagram of the proposed model framework of maintenance scheduler.

RL framework can be mathematically formulated by a Markov Decision Process (MDP) defined by a tuple (S,A,R,T) in which S is a set of states, A is a set of actions, R is a reward function, and T is a transition probability function [67]. For maintenance management of gas pipeline, S is the health conditions of the pipe (e.g., corrosion depth and length) that can be used to summarize the historical information of the environment (i.e., pipe in this case). A is the maintenance actions, including pigging, batch corrosion inhibitor, internal coating, and replacement that the agent can take at a certain state to mitigate corrosion. In addition, do nothing is also an option for the agent to avoid forced action situations. R is the rewards associated with the costs of maintenance action, costs of pipeline failures, and bonus of pipeline life extension. The rewards can give the agent feedbacks about how the maintenance action it takes affect the health state of the pipe. It should

be noted that we do not need T here as our developed agent is model-free; therefore, it knows nothing about the environment. In other words, the agent does not know how S is changing in the environment; instead, what it knows is the monthly observation (or updated information) from the environment and the corresponding rewards.

7.4 Methodology and Implementation

This section describes implementation details of the proposed methodology. This section covers three topics, namely, the development of the environment (i.e., pipeline internal corrosion model), the development of the RL maintenance scheduler, and the evaluation methodology and metrics.

7.4.1 *Development of the environment*

The environment is a segment of a demonstrative gas transmission pipeline system, which is assumed to be straight and 1-mile long in length. The pipeline is made of mild steels and is mainly used for transporting natural gas (i.e., CH_4) with small amount of corrosive gases (i.e., CO_2 and H_2S) and elements (i.e., Cl^-) that are introduced during the extraction and collection of natural gases. The pipeline is suffering internal corrosion during the operation in which two common types of corrosion, namely uniform corrosion and pitting corrosion, are assumed to be the main mechanisms of the internal corrosion.

At this stage, the problem is confined to one corrosion defect on the pipe surface; however, the proposed approach is also applicable to other assets under single or multiple defects.

It can be seen from Figure 38 that the environment consists of the simulation of operating parameters and the pipe model, which is composed of an internal corrosion model and a reliability model. Each of them will be described in the following sub-sections.

7.4.1.1 *Simulation of operation parameters with stochastic process*

The inputs of the internal corrosion model in simulation of the demonstrative gas pipeline are operating parameters. Therefore, first of all, time-series operating parameters should be provided to the internal corrosion model to simulate the propagation of corrosion inside the pipeline. The operating condition inside a gas pipeline is very complex as the operating parameters are changing all the time within an uncertain range. Due to the lack of data, the time-series operating parameters were simulated by the proposed methodology described in **"Chapter 5.2 Modeling the variability of operating parameters"**, which takes temporal variability of operating parameters into account. The operating parameters of the demonstrative gas pipeline are shown in Table 10. They are operating temperature (T), total pressure (P), partial pressure of CO_2 (pCO_2), partial pressure of H_2S (pH_2S), flow velocity (V), pH, chloride ion concentration (Cl^-), sulfate concentration (SO_4^{2-}), probability of solid presence (R_{solid}). These parameters were considered stochastic and were assigned specified probability distributions followed by coefficient of variations (COVs).

Table 10. Operating parameters of the internal corrosion model in simulation of the demonstrative gas pipeline.

Variables	Type	Mean	COV
T (K)	Normal	308	0.10
P (bar)	Lognormal	56.6	0.15
pH_2S (bar)	Lognormal	3	0.15
pCO_2 (bar)	Lognormal	4	0.15
V (m/s)	Lognormal	5	0.10
pH	Lognormal	4	0.06
Cl^- (ppm)	Lognormal	150000	0.15
SO_4^{2-} (ppm)	Lognormal	2000	0.15
R_{solid}	Uniform	**Upper limit**	**Lower limit**
		1	0.5

7.4.1.2 *Corrosion degradation model*

Internal corrosion defects inside a pipeline may grow in the radial, circumferential and axial directions; however, most common engineering practices only consider the corrosion depth (d) and length (l) for simplicity [25]. In this study, we also described the corrosion defect by depth and length, and a schematic diagram of a rectangular-like shaped corrosion defect is shown in Figure 39.

To simulate internal corrosion in the demonstrative gas pipeline subjected to an aqueous CO_2/H_2S environment, the proposed internal corrosion predictive model described in **"Chapter 5.1 Internal corrosion model"** was adopted. This corrosion model takes time-series operating parameters as

inputs and returns corrosion rate as a function of time. It should be noted that the predicted corrosion rate by the proposed internal corrosion predictive model is the rate of depth that the pipe wall loses (i.e., corrosion depth rate) due to internal corrosion. As for the corrosion length rate, since there are still no reliable models, this study simulated the corrosion length rate for internal corrosion by a linear growth model, which states that corrosion length propagates linearly over time with a constant corrosion length rate, and this assumption is also used in other study [68] to study the reliability of corroded gas pipelines .

This study considered only uniform and pitting corrosion for internal corrosion; therefore, the accumulated corrosion depths over time were calculated by summing up the daily corrosion rates over total time of operation for uniform and pitting corrosion, respectively. The expressions of corrosion depths for uniform and pitting corrosion are given as:

$$d_{UC}(t) = \sum_{i=1}^{N} \frac{CR_i(t)}{365} \tag{98}$$

$$d_{PC}(t) = \sum_{i=1}^{N} \frac{PCR_i(t)}{365} \tag{99}$$

where $d_{UC}(t)$ and $d_{PC}(t)$ are corrosion depths at time t by uniform corrosion and pitting corrosion, respectively, in mm; $CR_i(t)$ is corrosion rate at time t by uniform corrosion in mm/y; $PCR_i(t)$ is corrosion rate at time t by pitting corrosion in mm/y; N is number of days.

Synergistic effect of different types of corrosion is very complicated; therefore, in practice, many internal corrosion problems are treated in consideration of their combination effect. According to a study [49], the total internal corrosion depth can be expressed as the sum of uniform and pitting corrosion depths given by:

$$d_c(t) = d_{UC}(t)W_{UC} + d_{PC}(t)W_{PC} \quad (100)$$

where $d_c(t)$ is total corrosion depth at time t due to uniform and pitting corrosion in mm; W_{UC} and W_{PC} are weight of uniform and pitting corrosion (i.e., in this case, they are considered equally weighted).

Same to the corrosion depth, the total corrosion length is also the summation of corrosion length rate over time and can be expressed as:

$$l_c(t) = LGR \times \frac{t}{365} \quad (101)$$

where $l_c(t)$ is total corrosion length at time t in mm; LGR is corrosion length rate in mm/y; t is time in days.

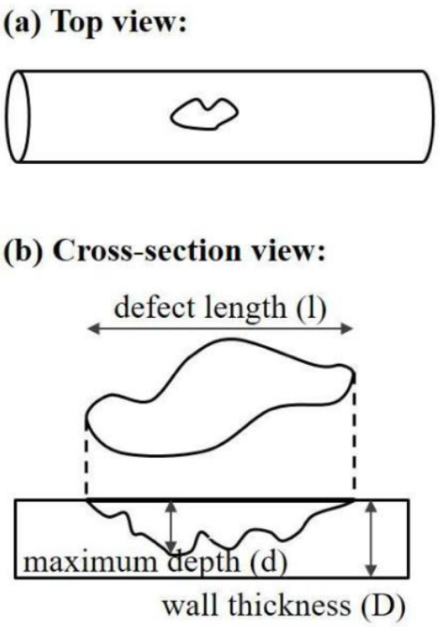

Figure 39. A rectangular-like shaped corrosion defect in the pipeline in (a) Top view and (b) Cross-section view.

7.4.1.3 *Pipeline mechanical and reliability model*

Corrosion defects inside the gas pipeline pose threats to the pipe integrity by deteriorating the pipe strength. As corrosion proceeds, the pipe becomes weaker and unreliable. In this study, two common types of corrosion-related failures, namely, leak and burst were considered in calculation of pipe failure probability or reliability.

Specifically, corrosion defects thin the pipe wall, resulting in leak when through-wall defects are formed. In addition, corrosion defects propagate in different dimensions and reduce the pipe strength, rendering the pipe vulnerable to burst when the remaining strength (or burst pressure) is lower than the operating pressure [68]. Several burst pressure models have been developed over

the past few decades of years [25], including ASME B31G [69], DNV RP-F101 [70], CSA Z662-07 [71], RAM PIPE REQUAL [72], etc. The common characteristics of these standards are that they consider longitudinal-oriented corrosion defects. Moreover, the burst pressure calculation is related to burst stress as a result of the geometry of existing corrosion defects and the pipe property. This study chose ASME B31G standard because it is easy to implement and the prediction result is not too conservative compared to other burst pressure standards according to [25]. The burst pressure calculation by ASME B31G standard can be expressed as:

$$P_b^{B31G} = \sigma_h \frac{2w}{D} = \sigma_f \left[\frac{1-\frac{A}{A_0}}{1-\frac{A}{MA_0}}\right](\frac{2w}{D}) = (1.1\sigma_y)(\frac{2w}{D})\left[\frac{1-A/A_0}{1-\frac{A}{A_0}/M}\right] \quad (102)$$

where P_b^{B31G} is burst pressure by ASME B31G; σ_h is hoop stress; σ_f is flow stress; w is pipe wall thickness; D is pipe outer diameter; A is surface area of corrosion defect; A_0 is original surface area of the pipe; M is Folias factor. M is related to the geometry of the corrosion defects and the pipe itself and can be expressed as:

$$M = \sqrt{1+0.8(\frac{l}{D})^2(\frac{D}{w})} \quad for \quad \sqrt{0.8(\frac{l}{D})^2(\frac{D}{w})} \leq 4 \quad (103)$$

$$M = \infty \quad for \quad \sqrt{0.8(\frac{l}{D})^2(\frac{D}{w})} > 4 \quad (104)$$

The ratio $\frac{A}{A_0}$ is a geometry term of corrosion defect and pip. As corrosion defect is assumed to be two-dimensional, which can be described by corrosion depth and length, according to ASME B31G standard, $\frac{A}{A_0}$ can be expressed as:

$$\frac{A}{A_0} = \frac{\left(\frac{2}{3}\right) ld}{lw} = \frac{2d}{3w} \tag{105}$$

where l is corrosion length; d is corrosion depth.

After the determination of burst pressure, probability of failure for leak and burst can be calculated via the reliability model described in "**Chapter 3.3.2.2 Reliability analysis method**", respectively with Monte Carlo simulation. Specifically, probability of leak is the probability that the corrosion depth is larger than the corrosion allowance, which is usually defined as 80% of the pipe wall thickness [73]. The expression of probability of leak is given as:

$$POF_{leak} = \frac{n[(\lambda - d_{max}) < 0]}{N} \tag{106}$$

where POF_{leak} is probability of leak; d_{max} is maximum corrosion defect; λ is corrosion allowance; N is number of trials.

The expression of probability of burst is given as:

$$POF_{burst} = \frac{n\left[\left(P_b - P_{op}\right) < 0\right]}{N} \tag{107}$$

where P_b is burst pressure; P_{op} is operating pressure of the pipe.

In order to determine if the pipe fails or not in a scenario given POF_{leak} and POF_{burst}, Binomial distribution was used to simulate this process. Leak and burst events are assumed mutually independent for simplicity. Therefore, two parallel simulations were done using the Binomial distribution in which one simulated leak event with POF_{leak} and the other one simulated burst event with POF_{burst}. Finally, the failure event means either one of the failures happens, and the environment is in the failure state.

7.4.2 *Development of the smart condition-based maintenance scheduler*

This section discussed the development of the maintenance scheduler. As stated before, MDP, which consists of a state space, an action space, a reward function, and a state transition function is the mathematical formulization of our RL-based maintenance scheduler. However, it should be noted that although the state transition function was modeled by the proposed internal corrosion model, the maintenance scheduler has no access to it because it is model-free. Therefore, every element of the maintenance scheduler was introduced except the state transition function.

Two RL algorithms were developed in this study. Firstly, Q-learning learning algorithm was applied to develop the maintenance scheduler for optimal corrosion maintenance policy. Then, the

results by the Q-learning maintenance scheduler and the traditional periodic maintenance policy were compared. Moreover, sensitivity analysis was done to study the effect of model parameters on the model performance. Finally, Sarsa algorithm was developed and applied to the problem in order to compare the model performance of Q-learning and Sarsa algorithms.

7.4.2.1 *State space*

The state space can be understood as the health condition of the environment to which the maintenance scheduler has access during inspection. Due to Markov property, which states that the future state depends only on the current state and the current action, each state should contain all the historical information of the environment so that the maintenance scheduler can predict the next state given the action.

As the environment was modeled to be a gas transmission pipe subjected to internal corrosion, the state must include the information of the pipeline in terms of corrosion level. Corrosion level was described by two metrics, namely, corrosion depth and corrosion length as the corrosion was assumed to propagate in two dimensions in this study. Max-normalization was done by dividing the corrosion depth with the maximum corrosion depth and dividing the corrosion length with the maximum corrosion length to obtain the corrosion depth percent (CDP) and the corrosion length percent (CLP), respectively. The maximum corrosion depth was defined as the pipe wall thickness, but the maximum corrosion length is trickier to determine as the pipe length is much longer than a corrosion defect. Therefore, here the maximum corrosion length was estimated by running the

corrosion simulation under the given operating conditions without any maintenance for 40 years. The reason of applying normalization is to remove the maintenance scheduler's dependency on the pipeline's parameters in order to become a more generic model. The expressions of CDP and CLP are given as:

$$CDP = \frac{corrosion\ depth}{maximum\ corrosion\ depth} \tag{108}$$

$$CLP = \frac{corrosion\ length}{maximum\ corrosion\ length} \tag{109}$$

According to our definition to the maintenance scheduler, it has the access to the environment only through monthly inspections. State variable consists of CDP and CLP only cannot provide the maintenance scheduler with enough information to predict next state because it does not know if the corrosion is propagating at the moment or is inhibited by any mitigation method. Therefore, another metric called corrosion rate presence (CRP) was added to the state variable to check if the corrosion process continues or not by comparing the inspected CDP and CLP with those of the previous month. CRP is a Boolean variable defined as follows:

$$CRP = \begin{cases} 0 & if \quad CDP_{t-1} = CDP_t \quad or \quad CLP_{t-1} = CLP_t \\ 1 & if \quad CDP_{t-1} \neq CDP_t \quad or \quad CLP_{t-1} \neq CLP_t \end{cases} \tag{110}$$

where t is time in months.

The state space of the maintenance scheduler consist were discretized into 24 states in terms of CDP, CLP, and CRP, and the table of all possible state spaces is shown in Table 11. Besides these 24 states, two terminal states were considered, namely, failure state and replacement state, each of which stops the simulation and terminates the ongoing scenario.

Table 11. Discretized state spaces of the maintenance scheduler.

CRP	CDP / CLP	0%-20%	20%-40%	40%-60%	60%-100%
0	0%-33%	0	1	2	3
0	33%-66%	4	5	6	7
0	66%-100+%	8	9	10	11
1	0%-33%	12	13	14	15
1	33%-66%	16	17	18	19
1	66%-100+%	20	21	22	23

7.4.2.2 *Action space*

The main task of a maintenance scheduler is to take maintenance actions to mitigate the corrosion. In this study, the maintenance scheduler can choose four maintenance actions, namely, batch corrosion inhibitor, internal coating, cleaning pigging, and replacement. In addition to four maintenance actions, it can also chose do nothing and let the corrosion proceeds if it thinks there is no need to do maintenance depending on the health condition of the pipeline. These maintenance actions are summarized in Table 12. Strictly speaking, among the four maintenance actions, only batch corrosion inhibitor and cleaning pigging are commonly seen in the industry for internal

corrosion mitigation according to the report by The Canadian Association of Petroleum Producers (CAPP) [74]. In this study, we added internal coating because although internal coating is usually applied during the manufacturing process, coating repair is a common maintenance action if it is damaged during the operation [75,76]. In addition, replacement was included to available maintenance actions so that the maintenance scheduler has an option to select when the corrosion is so severe that no other maintenance actions can stop the pipeline failure.

Each of available actions shown in Table 12 has its specific influence on the pipe in terms of corrosion mitigation. In order to quantify the influence of maintenance actions except for "Replacement", a discount factor (df) ranging from 0 to 1 was proposed for each available action. Updated corrosion rate was obtained by multiplying corrosion rate with df. Specifically, $df = 0$ stands for no corrosion propagation condition, whereas $df = 1$ stands for no corrosion mitigation condition. It should be noted that once a maintenance action passes its lifetime, its effect on corrosion disappears and df turns into 1 immediately.

The discount factors and the lifetime of different maintenance actions are listed in Table 13. According to Table 13, "Do nothing" has no effect on corrosion mitigation; therefore, $df_{do\_nothing} = 1$ and no lifetime is specified; "Batch corrosion inhibitior" reduces the corrosion rate once it is added, but the efficiency decays over the lifetime according to $df_{inhibitor}$ shows. In general, the lifetime of corrosion inhibitor is around 1 month according to [47]; "Internal coating" and "Cleaning pigging" turn the corrosion rate into 0 within their lifetimes, meaning $df_{internal\_coating} = 0$ and $df_{cleaning\_pigging} = 0$. However, the lifetime of "Internal coating" is 5

years [28], whereas the lifetime of "Cleaning pigging" is only 2 weeks [47]. The short lifetime of "Cleaning pigging" is due to the fact that water, solids, and debris are likely to show up again during the operation after the application of pigging.

Table 12. Available maintenance actions of the maintenance scheduler.

Actions	Descriptions	Comments
Do nothing	• No mitigation is done	• The corrosion proceeds
Batch corrosion inhibitor	• A chemical that adsorbs onto the metal surface and reacts with it to form a protective film	• Corrosion inhibitor is added from the inlet of the pipeline • Corrosion rate drop is based on the inhibitor efficiency • Effective only within its lifetime
Internal coating	• An artificial coating that isolates the pipe from the corrosive environment and prevents water from reaching the pipe surface	• No corrosion propagation during its lifetime
Cleaning pigging	• A gadget that effectively cleans up liquids and corrosive solids	• No corrosion propagation during its lifetime
Replacement	• Replace the corroded segment with a new one	• Renew corrosive environment • No more corrosion defects

The action space of the maintenance scheduler were discretized into 5 actions, including "Do nothing", "Batch corrosion inhibitor", "Internal coating", "Cleaning pigging", and "Replacement". According to the definition of the environment, the corrosion process inside the pipeline continues on a daily basis; however, the maintenance scheduler updates itself with the latest states of the environment on a monthly basis through monthly inspections. Once the maintenance scheduler

receives the information, it decides which action to take from action spaces and the environment will be affected by that action in accordance with the discount factors defined in Table 13.

Table 13. Discount factors and lifetime of maintenance actions.

Actions	Discount Factors	Lifetime
Do nothing	$df_{do\_nothing} = 1$	-
Batch corrosion inhibitior	$df_{inhibitor} = 1 - 0.9487e^{-0.023 \times inhibitor\_lifetime}$ [77]	1 month [47]
Internal coating	$df_{internal\_coating} = 0$	5 years [28]
Cleaning pigging	$df_{cleaning\_pigging} = 0$	2 weeks [47]

7.4.2.3 *Reward function*

The reward is the feedback from the environment to let the maintenance scheduler understand how good the action it takes is at the certain state. In general, the maintenance scheduler as an agent in typical MDP problem has to strive for the goal toward maximizing the total reward it receives in the long run. Therefore, the reward has to reflect the goal of the maintenance scheduler, specifically, avoid catastrophic corrosion-related failures, namely leakage and burst; extend the lifetime of the pipeline; reduce the maintenance costs in this study. To develop the reward function of the maintenance scheduler, two types of rewards were defined, namely, cost and bonus in which cost type includes “Cost of maintenance” and “Cost of failure”, and bonus type includes “Life extension

reward". To differentiate cost and bonus, cost was defined as negative reward, whereas bonus was defined as positive reward. The total reward that the maintenance scheduler receives is the summation of all the cost and bonus. The descriptions of the whole reward function are summarized in Table 14.

Assigning values to the reward function is always an important but difficult task in MDP as it directly influences the agent's decision on actions. The representative reward function should reflect the generic information of the pipeline maintenance such as the average cost of a specified maintenance practice on real operating gas pipelines. In this study, the values of the reward function were specified with respect to the maintenance costs and pipe failure costs. At this stage, these values are just single numbers as the problem was confined to a small segment and any spatial effect of the pipeline was ignored. The values of the reward function in the unit of $10,000 of the maintenance scheduler is shown in Table 15.

Table 14. Descriptions of the reward function of the maintenance scheduler.

Types		Descriptions
Cost	Cost of maintenance	• The cost is associated with each maintenance action. • The cost is applied to the maintenance scheduler at the end of each month.
	Cost of failure	• The cost is associated with two pipe failures, namely, leak and burst. • The cost is applied to the maintenance scheduler when the environment (i.e. pipeline) is in the failure state. • This cost is considerably larger than the cost of maintenance due to the huge loss of human life and property.
Bonus	Life extension reward	• The bonus is associated with the extension of the pipe lifetime. • The bonus is applied to the maintenance scheduler at the end of each month if the environment is not in one of the two terminal states, namely, failure state and replacement state. • The bonus is relatively small compared to the cost.

Table 15. Values of the reward function of the maintenance scheduler.

Types		Cases	Values
Cost	Cost of maintenance	Do nothing	0
		Batch corrosion inhibitor	-13
		Internal coating	-80
		Cleaning pigging	-3.5
		Replacement	-160
	Cost of failure	Leak	-160 * 3
		Burst	-160 – 160 * 10
Bonus	Life extension reward	Life extension reward per month	+7

For the cost of maintenance, it should be noted that the values were assigned based on the premise that the cost of inspection was neglected. Firstly, "Do nothing" costs $0 as no maintenance action is done after the inspection. Secondly, the cost of "Batch corrosion inhibitor" is based on the cost of corrosion inhibitors and the amount of corrosion inhibitor needed. According to [47], batch-treatment is to add corrosion inhibitors to the inlet in which one-third of the tubing volume is needed for the inhibition efficiency to be over 90%. Based on that, "Batch corrosion inhibitor" was estimated to cost $130000/mile. Thirdly, the cost of "Internal coating" should be understood as the cost of coating repair, which is usually much costlier compared to corrosion inhibitor or pigging because it requires a portion of the pipe system to be shut down for excavation and coating. Therefore, the cost of "Internal coating" was estimated to be $800000/mile according to [78]. Fourthly, the cost "Cleaning pigging" is based on the distance it needs to go through to do cleaning. According to [79], the cost was estimated to be roughly $35000/mile. Finally, the cost of "Replacement" is hard to define because the cost differs from different operators depending on the size and productivity of the pipeline. Overall, "Replacement" is definitely more expensive than other type of maintenance practices. Here, the cost was estimated to be $1600000/mile.

For the cost of failure, both "Leak" and "Burst failures are costlier than the cost of any maintenance actions. Failures involve not only the unplanned interruption of the service but also catastrophic hazards imposed on the surrounding environment and human life. Again, the exact cost of failure is hard to quantify. Here, "Leak" failure was assumed to be three times of the cost of "Replacement". "Burst" failure is a severer failure than "Leak" failure; therefore, the cost was assumed to be the cost of "Leak" failure plus ten times of the cost of "Replacement".

For the life extension reward, the value was set to be $70000 based on the results of the sensitivity analysis that was performed with different values of the life extension reward in the evaluation section, which will be introduced later.

7.4.2.4 *Maintenance scheduler learning algorithm*

There are two main categories of RL algorithms depending on the sizes of state and action spaces, namely, tabular solution method and approximate solution method. Tabular solution method is suitable for small-scale problems, whereas approximate solution method is suitable for large-scale problems [80]. The development of maintenance scheduler in this study adopted tabular solution method as the maintenance scheduler is built to solve a relatively small problem (i.e., to optimize maintenance policy for corroded gas pipelines) with finite sizes of state and action spaces. The applied algorithms are model free in nature because the maintenance scheduler treats the model as a black box that generates the required data for the learning process.

Among many learning methods of model free tabular solution method, temporal difference (TD) learning is one of the most popular methods. The basic idea is to update the current estimate of a value given the acquired information in the current time step. Many algorithms are developed based on the concept of TD learning, including Q-learning and Sarsa (an acronym for state, action, reward, state, action) algorithms. Two algorithms all aim at developing optimal maintenance management policy by learning from the optimal action-value function (or Q-value) but in slightly different ways.

The action-value function $Q^{\pi}(s,a)$ is defined as the expected cumulative discounted future rewards if an agent performs action a at state s under the policy π. In short, it can quantitatively evaluate the value of an agent's decision making at a certain state. The mathematical expression of $Q^{\pi}(s,a)$ is given by:

$$Q^{\pi}(s,a) = E\left[\sum_{k=0}^{terminal} \gamma^{k} R_{t+k+1} | S_t = s, A_t = a\right] \tag{111}$$

where γ is reward decay factor, R_{t+1} is gained reward at state S_{t+1} after action $A_t = a$ is performed at state $S_t = s$ at time step t. It is assumed that the trajectory is finite and ends at a terminal state (i.e., replacement state or failure state in this case).

In general, the optimal policy for an agent is to take the action with the largest Q-values at each state. However, a model free or data-driven RL algorithm has no access to the model and therefore can only estimate the Q-values based on it experiences on the previous interactions with the environment. This leads to a problem that if an agent always makes a decision based on its current knowledge, it is blind to other actions with higher actual value functions if the current estimates of the value functions are inaccurate. Therefore, during the learning process an agent should not only exploit the current knowledge of Q-values but also explore more actions to update the estimates of Q-values. This technique is known as exploration-exploitation trade-off.

Two RL algorithms were introduced and implemented in this study:

(1) Q-learning

Q-learning has gained its popularity because it is simple to formulate and implement with reasonable computation and memory costs. The pseudocode of the implemented Q-learning algorithm is shown in Figure 40. Three model parameters, namely, learning rate (α), reward decay rate (γ), and exploration rate (ε) were defined. The simulation of an episode starts with a fresh pipeline (i.e., no corrosion) as the environment which the agent interacts with by performing maintenance actions to mitigate the internal corrosion until one of the terminal states is met. ε-greedy policy was used to account for the exploration-exploitation trade-off when the agent needs to choose the next action. Specifically, the agent exploits its current knowledge and takes the best action with the highest Q-value ($a' = argmax_a Q(s,a)$) with the probability $(1-\varepsilon)$. ε is the probability (or exploration rate) that the agent explores other suboptimal actions randomly. Here, the decaying ε-greedy policy was applied to optimize its learning behavior. At the beginning, the agent starts with a high ε and tends to do exploration more. As the learning process continues, ε is set to be smaller as the agent becomes mature and it tends to exploit its knowledge more to make decisions [81]. The mathematical expression of the decaying ε-greedy policy is given by.

$$\epsilon = \min(\epsilon) + (\max(\epsilon) - \min(\epsilon))e^{d\epsilon \times iteration} \quad (112)$$

where $d\epsilon$ is exploration decay rate.

Q-learning pseudocode

Parameters: learning rate(α), reward decay($\boldsymbol{\gamma}$), exploration rate($\boldsymbol{\epsilon}$)

(1) Initialize $Q(s,a)$ for $\forall s \in S$ and $\forall a \in A_s$ by zero
(2) Loop for each episode:
(3) Start from a brand new pipe with no corrosion ($s = 0$)
(4) Set the first action as do nothing ($a = 0$)
(5) Loop for each month:
(6) Take action a
(7) Observe the reward (R), and end of the month state (s')
(8) Update Q table by: $Q(s,a) \leftarrow Q(s,a) + \alpha[R + \gamma max_a Q(s',a) - Q(s,a)]$
(9) Choose the next action (a') with $\boldsymbol{\epsilon}$-greedy policy
(10) $a \leftarrow a'$
(11) $s \leftarrow s'$
(12) Until the episode ends by either replacement, failure, or end of the episode

Figure 40. Pseudocode for the Q-learning algorithm.

(2) Sarsa

Sarsa is another popular tabular RL algorithm, which is an acronym for state, action, reward, state, action. Compared to Q-learning algorithm, Sarsa algorithm improves its estimation of $Q^{\pi}(s,a)$ by incorporating the arriving state, the gained reward, and the next action it plans to perform in the next time step based on the Bellman optimality equation [82] given by:

$$Q(s,a) = E[R_{t+1} + \gamma Q(S_{t+1}, A_{t+1}) | S_t = s, A_t = a] \quad (113)$$

The pseudocode of the implemented Sarsa algorithm is shown in Figure 41. Four model parameters, namely, learning rate (α), reward decay rate (γ), exploration rate (ε), and trace decay factor (λ) were defined. The initial settings if Q-value, state and action spaces are the same as Q-learning algorithm. The updating of Q-values for choosing action $A_t = a$ at state $S_t = s$ is given as:

$$Q(S_t, A_t) \leftarrow Q(S_t, A_t) + \alpha\delta \tag{114}$$

where δ is TD error, the difference between the previous and the new estimates of the Q-value.

Episode learning (or n-step learning) technique was added to Sarsa algorithm and became Sarsa(λ) algorithm. The advantage of Sarsa(λ) algorithm is that, the Q-values of all the previous steps that are experienced until the current time step are updated according to the new reward at each time step. In other words, the reward of current step is back-propagated to all previous steps. This was done by considering the eligibility trace of each state-action pair ($E(s, a)$). Specifically, $E(s, a)$ of a state-action pair is set to 1 once it is visited by the agent. However, if this state-action pair is not visited in the following time step, $E(s, a)$ decays by $\gamma\lambda$. on the basis of the decaying $E(s, a)$.

Sarsa(λ) pseudocode

Parameters: learning rate(α), reward decay($\boldsymbol{\gamma}$), exploration rate(ε), lambda (λ)

(1) Initialize $Q(s, a)$ for $\forall s \in S$ and $\forall a \in A_s$ by zero
(2) Loop for each episode:
(3) Initialize $\mathrm{E}(\mathrm{s}, \mathrm{a})$ for $\forall s \in S$ and $\forall a \in A_s$ by zero
(4) Start from a brand new pipe with no corrosion ($s = 0$)
(5) Set the first action as do nothing ($a = 0$)
(6) Loop for each month:
(7) Take action a
(8) Observe the reward (R), and end of the month state (s')
(9) Choose the next action (a') with ε-greedy policy
(10) $\delta = R + \gamma Q(s', a') - Q(s, a)$
(11) $E(s, a) = 1$
(12) Loop for $\forall s \in S$ and $\forall a \in A_s$
(13) $Q(s, a) \leftarrow Q(s, a) + \alpha\delta E(s, a)$
(14) $\mathrm{E}(s, a) \leftarrow \gamma\lambda E(s, a)$
(15) $a \leftarrow a'$
(16) $s \leftarrow s'$
(17) Until the episode ends by either replacement, failure, or end of the episode

Figure 41. Pseudocode for the Sarsa(λ) algorithm.

7.4.3 *Evaluation method*

This section described the methodology to, firstly, compare the performance of the proposed maintenance scheduler by Q-learning and the periodic maintenance policy; secondly, conduct sensitivity analysis of the proposed maintenance scheduler by Q-learning; thirdly, compare model performance of the proposed maintenance scheduler by Q-learning and by Sarsa(λ).

(1) Evaluation of the model performance

Three metrics of performance were defined with respect to the three corresponding goals of the maintenance scheduler. Q-learning maintenance scheduler was trained for 1000 episodes with the simulation time steps set to be 480 months (i.e., 40 years). The minimum and maximum exploration rates were set to be 0.0005 and 0.8, respectively, and the exploration decay rate was set to be 0.002. For model evaluation, 20 episodes of simulation were run with the time steps set to be 288 months (i.e., 24 years) and the averaged metrics of performance were reported to account for the randomness of the environment. The detailed descriptions of the metrics of the performance for model evaluation are shown in Table 16.

Table 16. Descriptions of the metrics of performance for model performance evaluation.

No.	Metrics of performance	Goals of the maintenance scheduler
1	Number of failures in 20 full episode runs	Avoiding catastrophic failures, including leak and burst
2	Average life length in the unit of month over 20 full episode runs	Extending the pipe lifetime
3	Average monthly cost of maintenance and failure over 20 full episode runs	Reducing the maintenance cost

As periodic maintenance policy (i.e., each maintenance actions is applied at its specified and fixed time interval) is the most common maintenance practice in the oil and gas industry, the performance of the periodic maintenance policy was served as the baseline performance and compared with the model performance of the proposed maintenance scheduler. The usage period of each maintenance action in the periodic maintenance policy differs from different pipeline operators; therefore, different scenarios of the periodic maintenance policy were considered and listed in Table 17.

Table 17. Different scenarios of the periodic maintenance policy.

Scenarios	Usage period of each maintenance actions (months)			
	Batch corrosion inhibitor	**Internal coating**	**Cleaning pigging**	**Replacement**
1	1	120	1	288
2	2	120	1	288
3	3	120	1	288
4	1	180	1	288
5	2	180	1	288
6	3	180	1	288
7	1	120	2	288
8	2	120	2	288
9	3	120	2	288
10	1	180	2	288
11	2	180	2	288
12	3	180	2	288

(2) Sensitivity analysis

Sensitivity analysis was done by conducting different simulations with various model parameters, including life extension reward, batch corrosion inhibitor lifetime, internal coating lifetime, and cleaning pigging lifetime. Specifically, for each scenario, 1000 episodes were run with the simulation time steps set to be 480 months (i.e., 40 years) to train Q-learning maintenance scheduler in which each episode ends by either reaching the maximum time steps or one of the terminal states. Then, the same evaluation method of the model performance described before was used and the metrics of performance of each scenario were compared. Different scenarios of the sensitivity analysis of the maintenance scheduler by Q-learning are shown in
Table 18.

Table 18. Different scenarios of the sensitivity analysis of the maintenance scheduler.

Scenarios	Life extension reward ($10,000)	Internal coating lifetime (months)	Cleaning pigging lifetime (months)	Batch corrosion inhibitor lifetime (months)
Baseline	+7	60	0.5	1
1	+1	60	0.5	1
2	+9	60	0.5	1
3	+7	36	0.5	1
4	+7	60	1	1
5	+7	60	0.5	4

(3) Model performance comparison between Q-learning and Sarsa(λ)

In order to compare the model performance of the maintenance scheduler by Q-learning and by Sarsa(λ), both maintenance schedulers were trained with the model parameters listed in Table 19 for 1000 episodes with the simulation time steps set to be 480 months (i.e., 40 years). Then, the same evaluation method of the model performance mentioned above was used but with simulation time steps changing to 480 months (i.e., 40 years).

Table 19. Cost and effective lifetime of maintenance actions, failure costs, and life extension reward.

Type	Value	Lifetime
Pigging maintenance cost	-3.5	1
Inhibitor maintenance cost	-13	1
Coating maintenance cost	-80	5
Replacement maintenance cost	-160	NA
Leakage failure cost	-480	NA
Burst failure cost	-1760	NA
Life extension reward per month	+7	NA

8 Evaluation results of the Smart Condition-Based Maintenance scheduler on dry gas pipeline

This section includes the results and discussion of the model performance evaluation of the proposed maintenance scheduler by Q-learning and the periodic maintenance policy, sensitivity analysis of the proposed maintenance scheduler by Q-learning, and the model performance comparison between Q-learning and Sarsa(λ).

8.1 Evaluation of the model performance

8.1.1 *Periodic maintenance policy*

The results of performance in terms of defined performance metrics by the periodic maintenance policy for different scenarios as described in Table 17 is shown in Table 20.

The results show that no scenario is terminated because of the pipe failure due to burst; however, most of them (around 75%) suffer pipeline failure due to leak at least once in 20 episodes. Among these cases, around 58.3% of them have pipeline failure due to leak in all 20 episodes. In short, the pipeline will fail due to leak under the periodic maintenance policy following scenario 3, 5, 6, 8, 9, 11, and 12 in 25 years. Conversely, no any pipe failure is found under the scenario 1, 4, and 7.

In order to find the dominating factor that increases the reliability of pipeline under the periodic maintenance policy, the effect of usage period of each maintenance action on average lifetime and average monthly cost was studied. Figure 42, Figure 43, and Figure 44 show the effect of usage

period of batch corrosion inhibitor, internal coating, and cleaning pigging on average lifetime and average monthly cost. The results show similar trends that if each maintenance action is applied more frequently (i.e., lower usage period), average lifetime of the pipeline increases. Intuitively, frequent maintenance action corresponds to high cost spent on maintenance. However, according to the results, more frequent maintenance action actually leads to lower average monthly cost because the cost of pipeline failure is much higher than the cost of maintenance. This finding can also explain why scenarios that have not suffered any pipe failure in 20 episodes all have lower usage period of maintenance action, particularly batch corrosion inhibitor compared to other scenarios as shown in Table 20. Therefore, according to the results, it is found that frequent application of batch corrosion inhibition (i.e., every 1 month) is helpful of ensuring the pipeline integrity under the periodic maintenance policy. The best scenario is 7 with batch corrosion inhibitor, internal coating, and cleaning pigging being applied every 1 month, 120 months, and 2 months, respectively, on both lifetime and cost point of views.

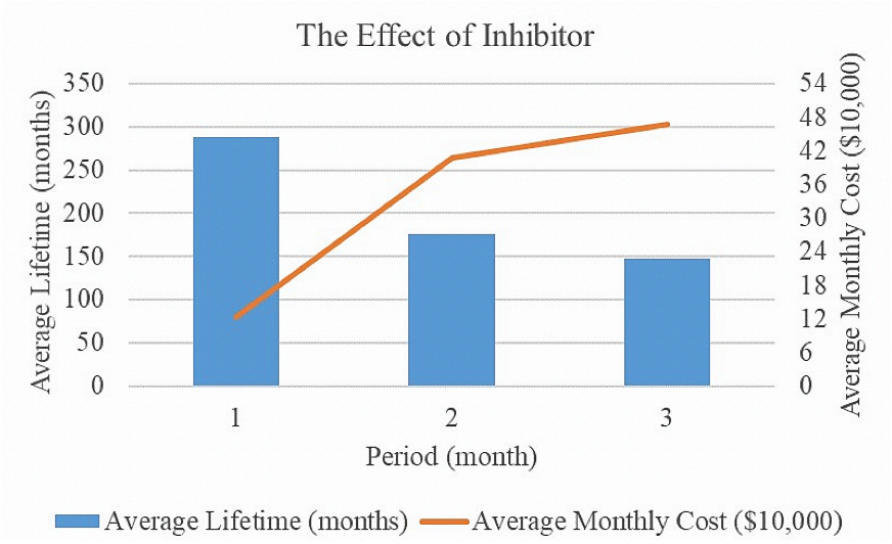

Figure 42. The effect of usage period of batch corrosion inhibitor on average lifetime and average monthly cost.

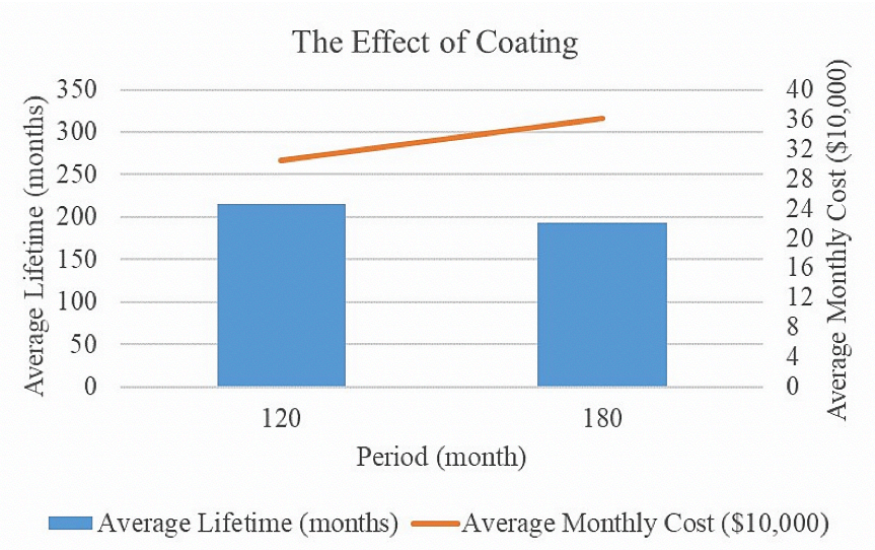

Figure 43. The effect of usage period of internal coating on average lifetime and average monthly cost.

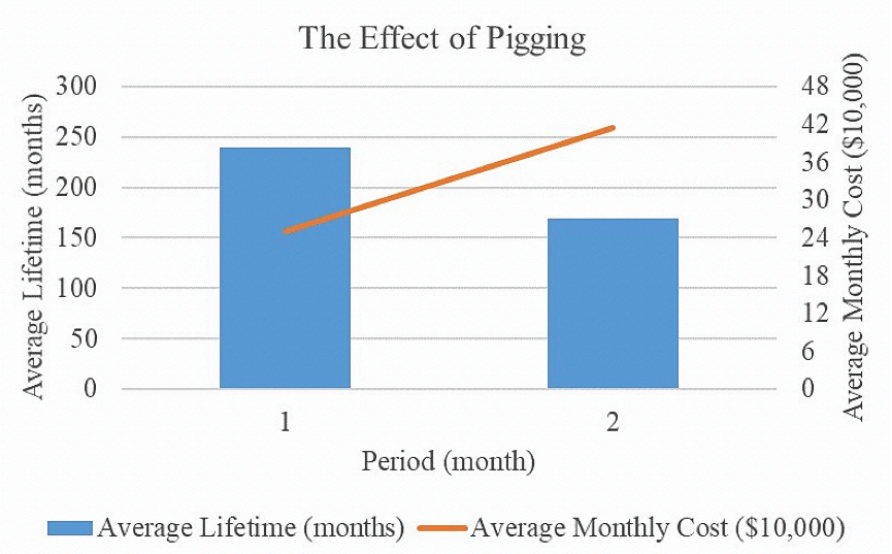

Figure 44. The effect of usage period of cleaning pigging on average lifetime and average monthly cost.

In conclusion, around 75% scenarios of the maintenance policy have at least one pipe failure due to leak. The study shows that frequent applications of maintenance action can not only increase the average lifetime but also the average monthly cost. Among all maintenance actions, the frequent application of batch corrosion inhibitor (i.e., every month) is important to ensure the pipeline integrity.

Table 20. Results of performance by the periodic maintenance policy.

Scenarios	Number of burst failures	Number of leak failures	Average lifetime	Average monthly cost
1	0	0	288.0	13.40
2	0	5	273.0	14.38
3	0	20	216.5	33.28
4	0	0	288.0	12.43
5	0	20	215.6	34.14
6	0	20	154.1	42.45
7	0	0	288.0	11.65
8	0	20	111.9	55.99
9	0	20	113.6	53.91
10	0	1	287.8	11.66
11	0	20	105.3	58.87
12	0	20	106.6	56.87

8.1.2 *Proposed maintenance scheduler by Q-learning*

The results of performance in terms of defined performance metrics by the Q-learning maintenance scheduler is shown in Table 21. It can be seen that no pipe failure happens in 20 episodes. This result was compared to the result of best scenario (i.e., scenario 7) of periodic maintenance policy shown in Table 20. Although both of them reached the full lifetime without any failure within 20 episodes, the Q-learning maintenance scheduler reduces the average monthly cost by more than 58% of the periodic maintenance policy. It leads to a conclusion that the developed maintenance scheduler has superior performance compared to the periodic maintenance policy in ensuring the pipeline integrity but also reducing the maintenance cost at the same time.

Table 21. Results of performance by the Q-learning maintenance scheduler.

Number of burst failures	Number of leak failures	Average lifetime	Average monthly cost
0	0	288.0	4.86

In order to investigate the decisions of maintenance action made by the Q-learning maintenance scheduler, the result of one evaluation in terms of maintenance actions and the corresponding CDP and CLP is plotted and shown in Figure 45. The bottom displays the CDP and CLP over time, while the top displays all the maintenance actions taken over time. The result shows that the maintenance scheduler takes "Do nothing" at the beginning; however, when the corrosion level rises to a certain level that it thinks may pose risk to the pipeline integrity (i.e., $CDP = 0.57$ and $CLP = 0.18$, it chooses to do "Internal coating" in which the corrosion will not propagate within the lifetime of the coating. Then, once the lifetime of the coating is passed, the maintenance scheduler repeatedly chooses to do "Internal coating" until it reaches the time step of simulation. It should be noted that the maintenance scheduler is smart enough to take "Do nothing" during the 5 years effective life of the coating to avoid the unnecessary cost of other maintenance actions that have no influence on corrosion while internal coating is still effective.

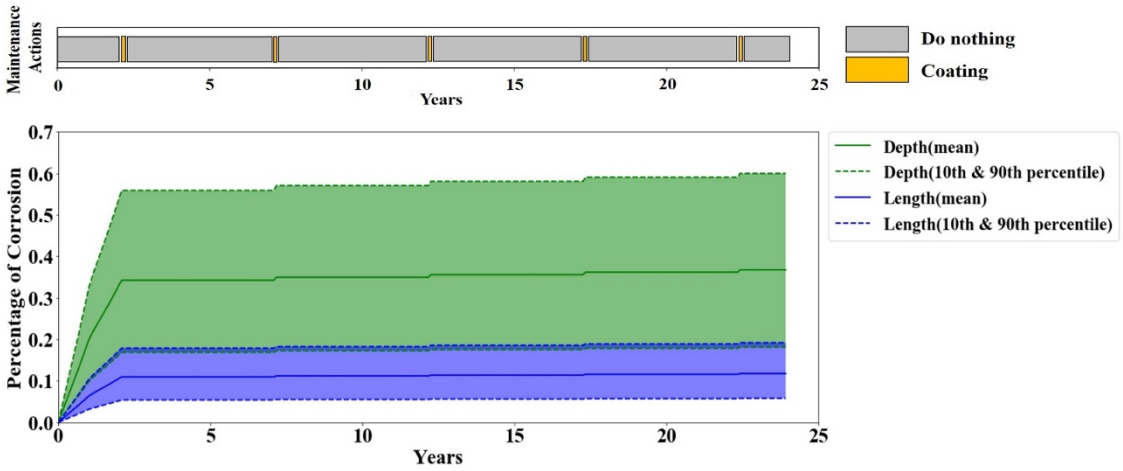

Figure 45. Plotted result of one evaluation episode by the Q-learning maintenance scheduler.

8.2 Sensitivity analysis

The results of the sensitivity analysis of the Q-learning maintenance scheduler in comparison with the baseline scenario as described in

Table 18 are shown in Table 22. It can be seen that none of these scenarios encounters any of the pipeline failure within the time scope of simulation in 20 episodes. In addition to the average lifetime, the average cost of every scenario is also much lower than that of the periodic maintenance policy. This result implies that the Q-learning maintenance scheduler can still come up with optimal maintenance policy even with different model parameters. However, although the average lifetime is equal, the average monthly cost actually differs in each scenario. The effect of usage period of maintenance action on the maintenance scheduler's behavior was discussed in the following paragraphs.

Table 22. Results of sensitivity analysis of the Q-learning maintenance scheduler.

Scenarios	Number of burst failures	Number of leak failures	Average lifetime	Average monthly cost
Baseline	0	0	288	4.86
1	0	0	288	7.03
2	0	0	288	4.86
3	0	0	288	7.62
4	0	0	288	4.34
5	0	0	288	5.03

In scenario one, the only difference from the baseline scenario is that the life extension reward is reduced from 7 to 1. According to the definition, the life extension reward is to motivate the maintenance scheduler to extend the lifetime of the pipeline; therefore, reducing this metric would make the maintenance scheduler intuitively less eager to live longer. However, the result shows that the pipeline survives with no pipeline failure to the end of simulation, which is due to the fact that the cost associated to any pipe failure is much larger than the bonus. Avoiding the catastrophic pipe failure is still an optimal decision on a cost-effect point of view. On the contrary, the reduce of life extension reward indeed has some minor effect on the average monthly cost i.e., the average monthly cost is 1.5 times higher than the baseline scenario. Figure 46, which displays the plotted result of one episode in sensitivity analysis scenario 1, shows that the maintenance scheduler performs “Batch corrosion inhibitor” at the beginning following by a small period of “Cleaning pigging” until the corrosion becomes severe. Then, it repeatedly performs “Internal coating” and

"Do nothing" in between until the end of simulation. The frequent application of "Batch corrosion inhibitor" leads to the higher average monthly cost compared to the baseline scenario.

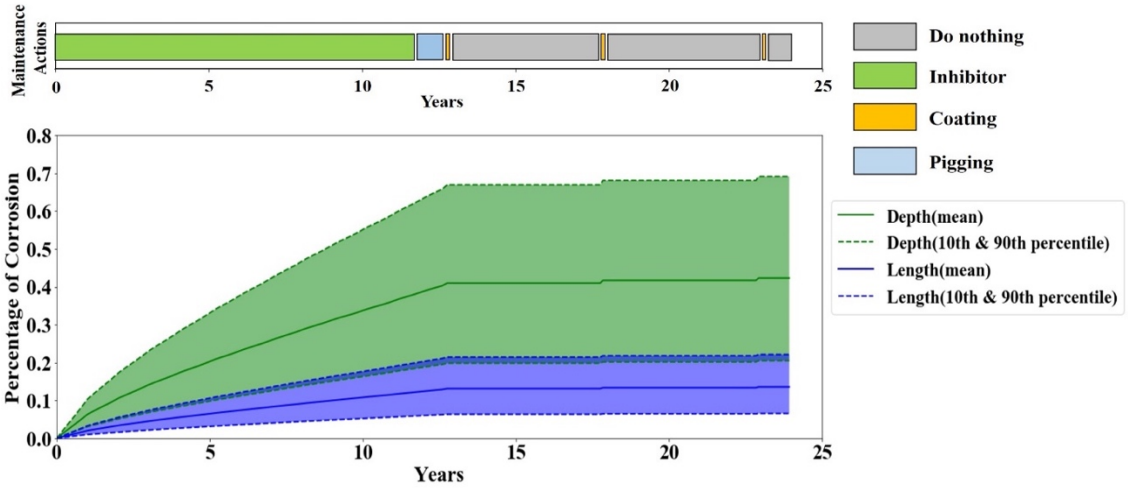

Figure 46. Plotted result of one episode in sensitivity analysis scenario one by the Q-learning maintenance scheduler.

In scenario two, the only difference from the baseline scenario is that the life extension reward is increased from 7 to 9, which means the maintenance scheduler is motivated to extend the lifetime of the pipeline. However, Figure 47 shows that the maintenance scheduler's behavior is the same as the baseline scenario. In addition, their average lifetime and average monthly cost are identical. It implies that small increase of the life extension reward takes no effect on the maintenance scheduler in making decision for short time of simulation.

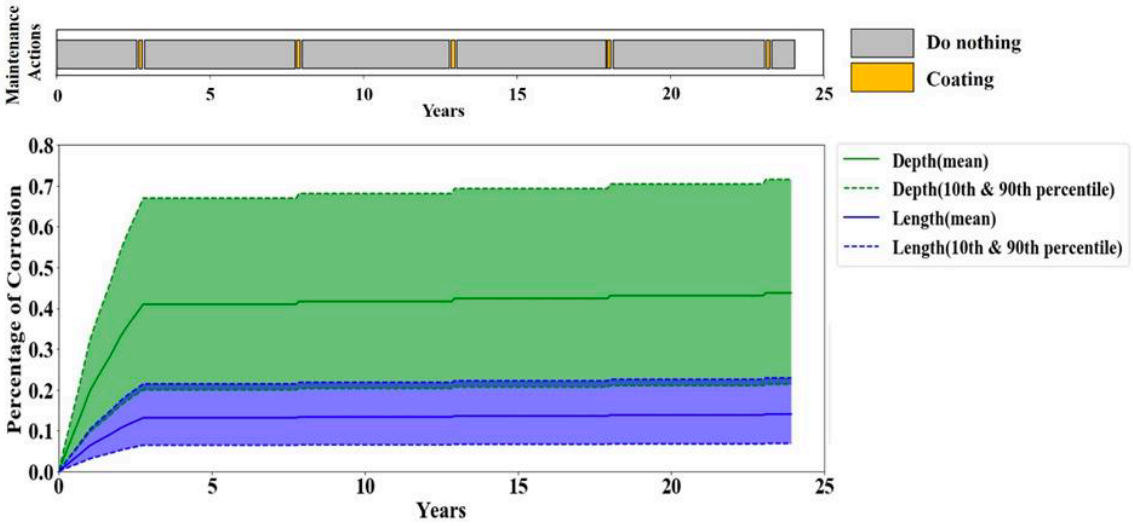

Figure 47. Plotted result of one episode in sensitivity analysis scenario 2 by the Q-learning maintenance scheduler.

Therefore, another sensitivity analysis of scenario 2 was done with simulation scope extended to 60 years and the new result is displayed in Figure 48. According to the figure, the maintenance scheduler decides to perform "Batch corrosion inhibitor" after around 1.5 years until the corrosion damage reaches medium to high. Then, repeated "Internal coating" and "Do nothing" were applied to the end of the simulation. Based on the results, it can be concluded that in order to maintain the pipeline integrity for longer time, the maintenance scheduler adjusts the maintenance policy, otherwise, the pipeline could have failure if the same maintenance policy as shown in Figure 47 is adopted.

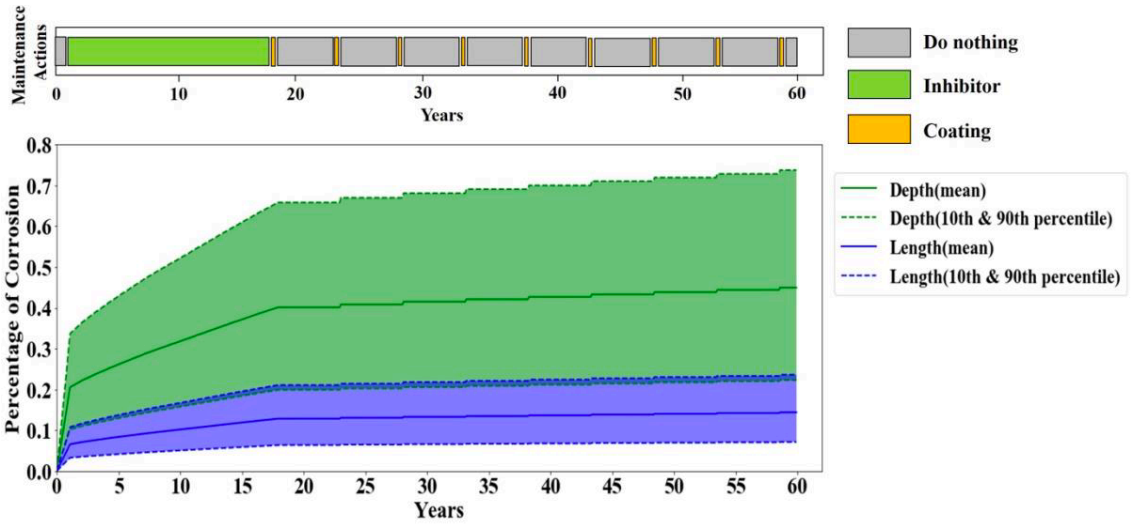

Figure 48. Plotted result of one episode in sensitivity analysis scenario two by the Q-learning maintenance scheduler with extended simulation scope to 60 years.

In scenario three, the difference from the baseline scenario is that the internal coating lifetime is decreased from 60 months (5 years) to 36 months (3 years). This change would make the "Internal coating" become less cost-effective among other available maintenance actions. In react to this change as shown in Figure 49, the maintenance scheduler decides to perform "Batch corrosion inhibitor" following by "Cleaning pigging" until the corrosion damage reaches medium to high. Then, repeated "Internal coating" and "Do nothing" were applied until it comes to the end of the simulation. This result shows that although "Internal coating" is less appealing to the maintenance scheduler intuitively, it still prefers "Internal coating" to other maintenance actions when the corrosion damage is high enough to pose the failure threat to the pipeline. However, the frequent application of "Internal coating" compared to the baseline scenario inevitably results in higher average monthly cost.

In scenario four, the difference from the baseline scenario is that the cleaning pigging lifetime is increased from 0.5 month to 1 month. The purpose is to make "Pigging cleaning" a more attractive option to the maintenance scheduler and observe how it would influence the maintenance policy. According to Figure 50, the maintenance scheduler chooses "Do nothing" at the beginning, but after a short period it switches to "Cleaning pigging" and sticks to it for the next 10 years. Afterward, again it repeatedly performs "Internal coating" and "Do nothing" when the corrosion damage reaches a medium to high level as this is a relatively conservative and safe action pair in face of high risk of pipe failure. In addition, although "Batch corrosion inhibitor" and "Cleaning pigging" have identical lifetime in this scenario, the maintenance scheduler only performs "Cleaning pigging" because it is much cheaper than "Batch corrosion inhibitor". One thing worth mentioning is that scenario four is the only one that has lower average monthly cost than the baseline scenario among five studied scenarios.

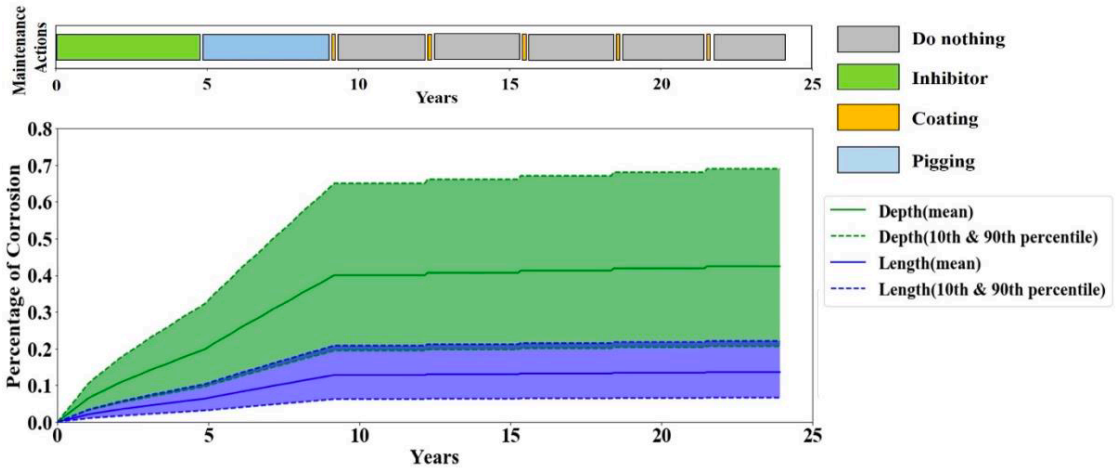

Figure 49. Plotted result of one episode in sensitivity analysis scenario three by the Q-learning maintenance scheduler.

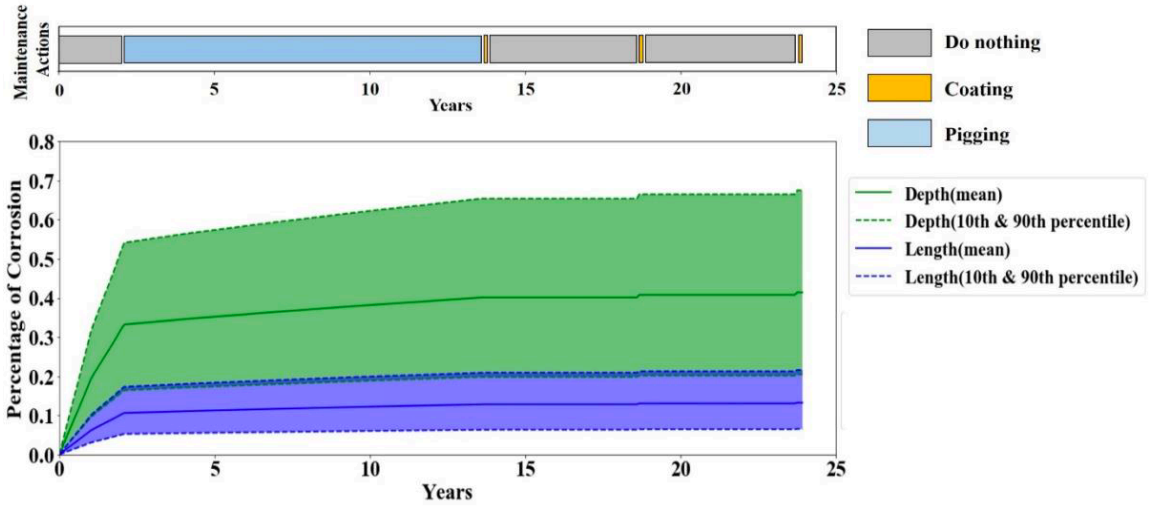

Figure 50. Plotted result of one episode in sensitivity analysis scenario four by the Q-learning maintenance scheduler.

In scenario five, the difference from the baseline scenario is that the corrosion inhibitor lifetime is increased from 1 month to 4 months. The purpose is to study the effect of longer corrosion inhibitor lifetime on the maintenance policy by the maintenance scheduler. Figure 51 shows that this time the maintenance scheduler performs "Batch corrosion inhibitor" more often. Not until the corrosion damage reaches medium to high does it switch to repetitive "Internal coating" and "Do nothing" like other scenarios until the end of the simulation.

In conclusion, the developed Q-learning maintenance scheduler is able to adjusts its maintenance policy with respect to different model parameters and maintenance parameters. All the studied scenarios have no pipe failure in 20 episodes, rendering the maintenance scheduler a reliable tool of pipeline integrity management. Finally, the sensitivity analysis leads to a conclusion that the

maintenance scheduler has a preference on “Internal coating” when the pipeline is exposed to the high risk of pipe failure (i.e., $CDP \cong 0.65$) due to internal corrosion.

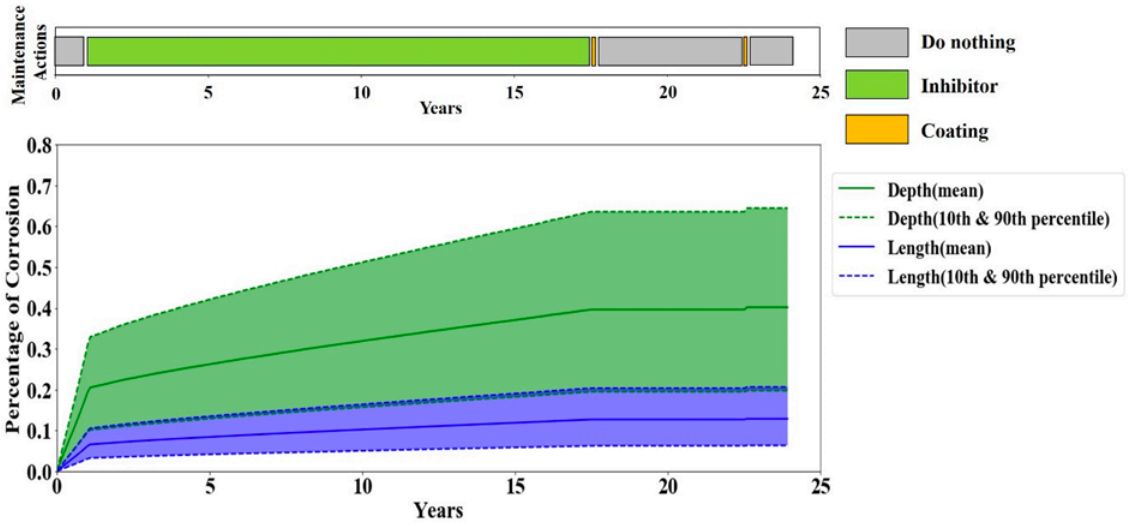

Figure 51. Plotted result of one episode in sensitivity analysis scenario five by the Q-learning maintenance scheduler.

8.2.1 *Model performance comparison between Q-learning and Sarsa(λ)*

The results of model performance of Q-learning and Sarsa(λ) maintenance schedulers are shown in Table 23. It can be seen that Sarsa(λ) maintenance scheduler is as reliable as Q-learning maintenance scheduler as there is no any pipe failure happened over the simulation scope (i.e., 40 years) in 20 episodes. Moreover, the average monthly cost of Sarsa(λ) maintenance scheduler is 10% lower than that of Q-learning maintenance scheduler, rendering it a better model on a cost-effective point of view.

Table 23. Model performances of Q-learning and Sarsa(λ) maintenance schedulers.

Algorithms	Number of burst failures	Number of leak failures	Average lifetime	Average monthly cost
Q-learning	0	0	480.0	4.72
Sarsa(λ)	0	0	480.0	4.24

The plotted results of one episode by Q-learning and Sarsa(λ) maintenance schedulers are shown in Figure 52 to investigate the difference of maintenance policy. Figure 52 (a) shows that Sarsa(λ) maintenance scheduler performs "Cleaning pigging" in early stage and sticks to it for around 4 years. After that, when the corrosion damage increases to a level ($CDP \cong 0.65$), the repetitive "Internal coating" and "Do nothing" are applied until the end of simulation. On the other hand, Figure 52 (b) shows that Q-learning maintenance scheduler has a similar maintenance policy as Sarsa(λ) maintenance scheduler, but it does not perform "Cleaning pigging" until CDP is as high as 0.5. Moreover, the period of "Cleaning pigging" is shorter, and the number of times of "Internal coating" is higher, resulting in higher average monthly cost. It should be noted that none of the maintenance schedulers takes "Batch corrosion inhibitor" along the simulation of corrosion, which indicates the intelligence of maintenance schedulers because they know "Cleaning pigging" is a more cost-effective option than "Batch corrosion inhibitor" according to Table 19.

In conclusion, the optimal maintenance policies of Q-learning and Sarsa(λ) are similar, both of each satisfy the three goals of an ideal maintenance scheduler. However, Sarsa(λ) maintenance scheduler has slightly better performance than Q-learning maintenance scheduler in terms of the average monthly cost i.e., a 10% reduction of the overall maintenance cost in the pipeline lifetime.

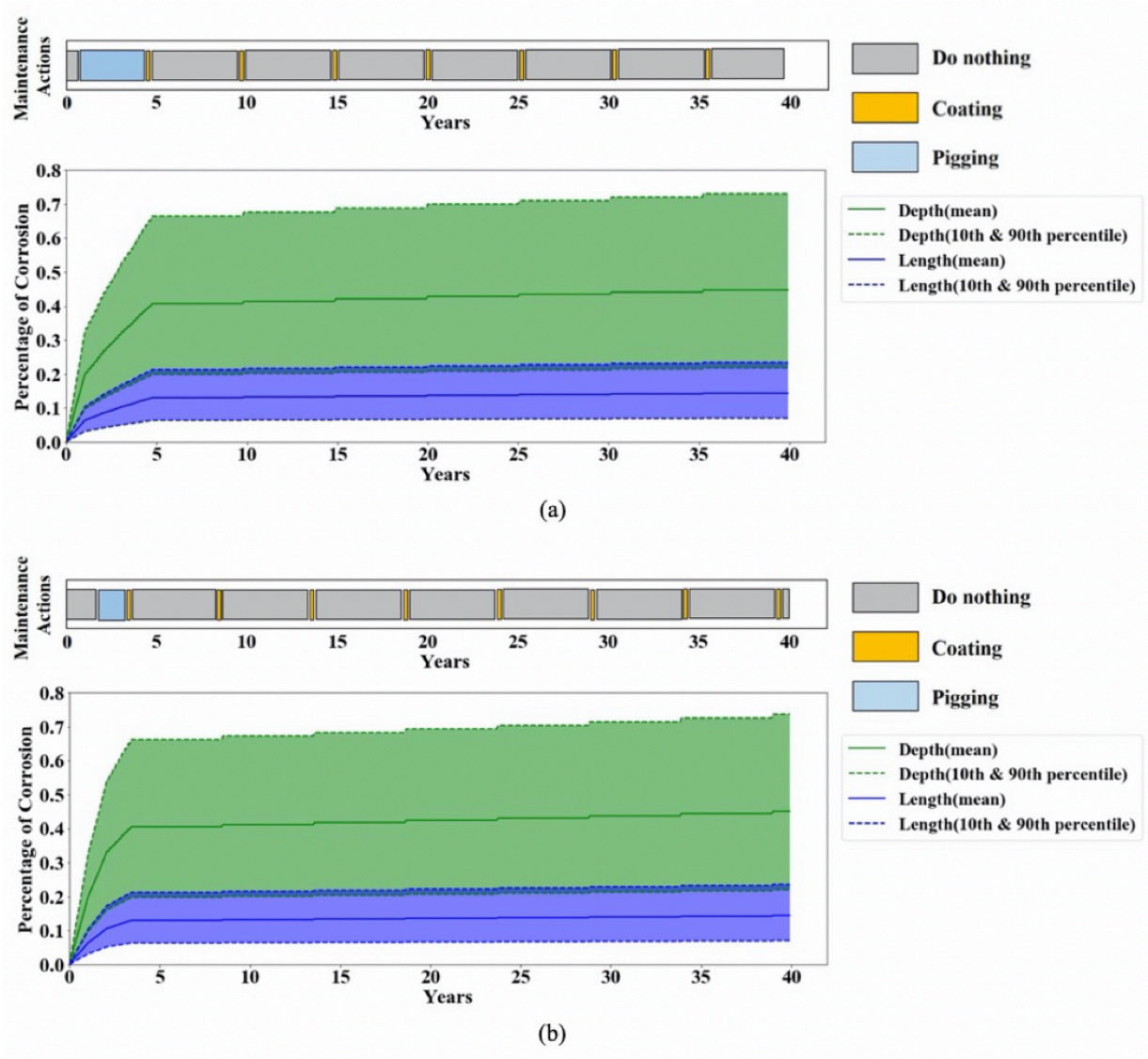

Figure 52. Plotted results of one episode by (a) Sarsa(λ) and (b) Q-learning maintenance schedulers.

8.3 Conclusions

This study proposed a methodology to optimize the maintenance management in gas transmission pipelines by RL decision-making approaches. The methodology includes an environment, which

is simulated by the proposed internal corrosion predictive model, and an agent, which is modeled by model-free RL algorithms, namely, Q-learning and Sarsa(λ). The result of model performance shows that the proposed smart maintenance scheduler reduces 58% of the average monthly maintenance costs and improves the reliability of the pipeline compared to the periodic maintenance policy. The result of sensitivity analysis shows that the maintenance scheduler adjusts itself to develop different optimal maintenance policies with respect to different model and maintenance action parameters. The result of model comparison between Q-learning and Sarsa(λ) shows that both models have similar pattern in decision making; however, Sarsa(λ) maintenance scheduler has lower average monthly cost than Q-learning.

The proposed maintenance scheduler is model-free, and therefore it can be applied to an IoT monitoring data to derive the optimal maintenance policy of a pipeline from its history data. The proposed maintenance scheduler can serve as a bench mark for gas pipeline maintenance optimization subject to internal corrosion because it endorses the usefulness of the condition-based maintenance and encourages its further development in other types of physical assets.

Part C

9 Pipeline health and monitoring management (PSIM) software

This chapter introduced a software framework for pipeline system integrity and management (PSIM). The software features include pipeline system-level integrity modeling, corrosion prognosis, sensor placement optimization, and inspection/maintenance schedule optimization. The focus was on the introduction of the model framework. The work that have been done in this research was integrated to the corrosion prognosis, system-level reliability, and inspection/maintenance schedule optimization features of the software. A case study was provided to demonstrate the software.

9.1 Introduction

Pipeline failures have caused a major impact on human lives and property damage. According to PHMSA [5] regulation §191.3, a "serious" incident is defined as an event where gas is released from a pipeline and caused death and injury, while a "significant" incident is defined when there is a property damage of more than $50,000. Reports by PHMSA have shown that average 12 deaths and 66 injuries happen annually from 2009 to 2018 [83].

From a system point of view, natural gas transmission pipeline systems can fail by many failure mechanisms. The most common ones are equipment failure, corrosion failure, excavation damage, and natural force damage [33]; however, among all of them corrosion failures in the form of leak

and burst are usually disastrous, leading to economic and life loss. Due to harsh operating conditions, natural gas transmission pipelines are exposed to risks of both internal and external corrosion. Internal corrosion often occurs inside the pipe due to corrosive environments caused by aqueous CO_2, H_2S, Cl^-, or solids and bacterial activities. Internal corrosion includes uniform corrosion, erosion corrosion, pitting corrosion, corrosion fatigue, and microbiologically-influenced corrosion depending on operating conditions and design of a pipe. As for external corrosion, it often occurs on the outer surface of the pipe where the pipe materials contact with corrosive soils. External corrosion happens mostly due to the malfunction of mitigation measures such as coatings or cathodic protection. Common external corrosion includes pitting corrosion and stress corrosion cracking [22].

Since long time ago, in-line inspection has long been regarded as the most efficient way of ensuring the integrity of corroded natural gas transmission pipelines. However, it is costly both on an economic and human point of views because a typical gas transmission pipeline is hundreds of miles long. Fortunately, over the past few decades, corrosion predictive models that can predict corrosion levels based on the monitoring data have been developed to prioritize the areas with most risks, and thus engineers can take advantage of the predictions to make decisions and take actions on corrosion mitigation [3]. The PSIM software as a integrity management tool is developed to meet this demand.

The following sections discussed the software features including pipeline system-level integrity modeling, corrosion prognosis, and inspection/maintenance schedule optimization. Moreover, a

demonstration of the software platform was provided via a case study in which a gas transmission pipeline was studied and results of analyzes were discussed.

9.2 Overview of the software platform

The developed PSIM software is a web application designed to do risk-based pipeline integrity management to support pipeline operators in decision-making and planning activities. The developed software consists of 6 main features:

(1) Pipeline Network Building

(2) Live Data Monitoring

(3) Corrosion Simulation

(4) System-Level Failure Analysis

(5) Sensor Placement Optimization

(6) Maintenance and Inspection Schedule Optimization

The **"Pipeline Network Building"** feature enables the user to add customized transmission pipeline systems to study. The **"Live Data Monitoring"** feature displays real-time as well as historic senor data of operating conditions. The **"Corrosion Simulation"** feature quantifies the corrosion degradation as well as pipeline segment failure probability for both internal and external corrosion. The **"System-Level Failure Analysis"** feature enables the development of system-level fault tree which consists of any factors that may influence the system integrity. In addition, the

software will calculate the system failure probability based on the fault tree. The **"Corrosion Simulation"** results are fed into the **"Sensor Placement Optimization"** and **"Maintenance and Inspection Schedule Optimization"** features where **"Sensor Placement Optimization"** feature shows the optimal locations to place sensors in order the maximize the likelihood of defect detection with a minimal cost and the **"Maintenance and Inspection Schedule Optimization"** shows the recommended actions to take to ensure the pipe integrity against corrosion.

9.3 Development of the software features

This section introduced only the **"Corrosion Simulation", "System-Level Failure Analysis",** and **"Maintenance and Inspection Schedule Optimization"** features because they are related to the research work that have been done in this thesis.

9.3.1 *System-Level Failure Analysis*

Transporting fuel from wellheads to consumers is a complex process. Fuel has to be transported through different pipelines as shown in Figure 53. Take natural gas for example, firstly, gathering pipelines are used to transport the gas from the production wells, either from onshore or offshore sites, to a processing and treatment plant. When the gas has been refined to remove impurities including hydrocarbons, water, helium, hydrogen sulfide, sulfur, and carbon dioxide by the oil and water separation process and gas dehydration, transmission pipelines are used to carry the gas across the states to the city gate. Transmission pipelines have the longest length and the highest

pressures (200-1500 psi usually). Due to safety issues, federal regulations suggest that transmission pipelines have to be buried at least 30 inches deep in rural areas and 36 inches in higher population density areas. In the United States, there are more than 300,000 miles of gas transmission pipelines and the number is still increasing. To preserve the level of pressure for transportation, compressor stations are installed along these pipelines along with valves to control the flow. Once the gas reaches the city gate, an odorant (i.e., mercaptans) is added to the gas by gas companies in order to make it identifiable when leakage happens. Then, the gas is delivered to customers by distribution pipelines at a lower pressure (up to 200 psi for gas mains and up to 10 psi for residential service lines). Unlike gathering pipelines and transmission pipelines, most of which are made of steels, distribution pipelines could be made of steels and plastics.

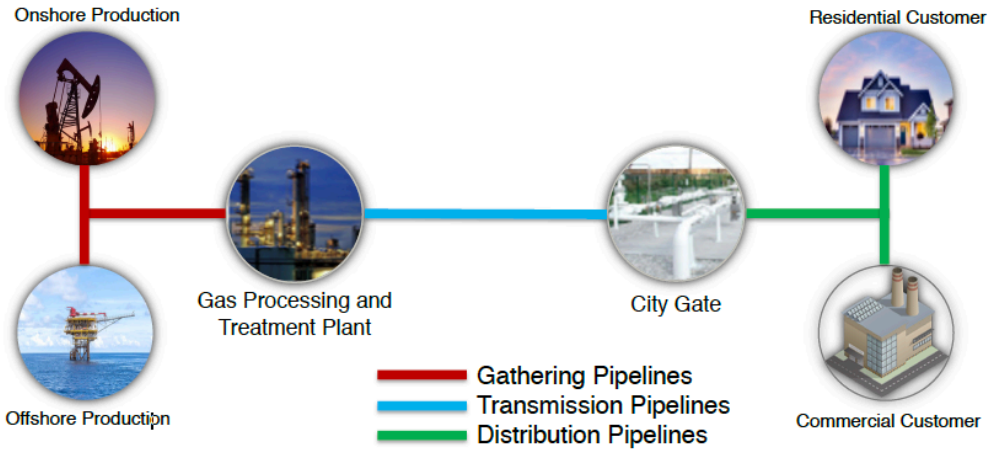

Figure 53. Networks of natural gas from production to customers.

Here we focus on transmission pipelines; therefore, in order to study the pipeline system integrity, the pipeline system has to be defined in the first place. In this study, the pipeline system was defined as the set of equipment that will transport the natural gas from the gas processing and treatment plant to the city gate after which the gas is distributed to customers. The system consists of transmission pipeline segments and compressor stations. Compressor stations are usually powered by natural gas engines or electric motors which are built every 50 to 100 miles [5] along the pipeline. The pipeline system was divided into multiple sub-systems referred to as transmission phases as shown in Figure 54. We define each transmission phase as a sub-system consisting of a compressor station and a pipeline segment. Therefore, a complete pipeline system may be composed of several transmission phases between the gas processing and treatment plant and the city gate, in which they are connected in series.

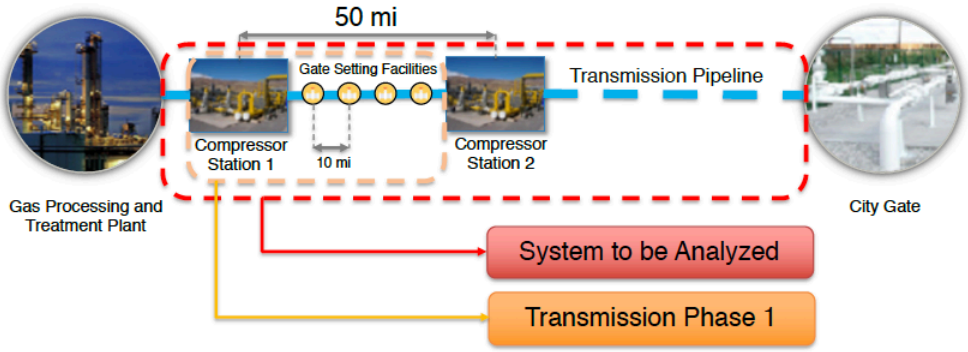

Figure 54. Gas transmission pipeline system consisting of different transmission phases.

System-level integrity modeling starts from developing a fault tree consisting of all possible factors that influence the integrity of the pipeline system in order to systematically quantify the failure

probability of the system. An example of the fault tree analysis of a gas transmission pipeline is shown in Figure 55. As different transmission phases are connected in series, which means failure of any of them fails the pipeline system, an "or" gate is used. Within each transmission phase, both the compressor station and the pipe segment failures will lead to a system failure in which the compressor station fails due to the failure of the lubrication system, power system, shaft seal system, or compressor unit [84]. Many factors may lead to pipe segment failures. They can be categorized into external and internal factors. Specifically, external factors include natural force (e.g., flooding, earthquake, and severe weather/subsidence), corrosion (i.e., external or internal), and third-party damage, while internal factors include material and welding defect.

It is worth mentioning that failure probability due to corrosion is calculated by the "**Corrosion Simulation**" feature embedded in the PSIM software, which will be described in the next subsection. In short, a dynamic corrosion simulation will be executed to estimate the corrosion degradation and the failure probability based on the operating conditions. Overall, the fault tree provides a top down decomposition of the projected pipeline system in terms of failure probability based on the likelihood (i.e., failure rate, probability) of failure of the different system components.

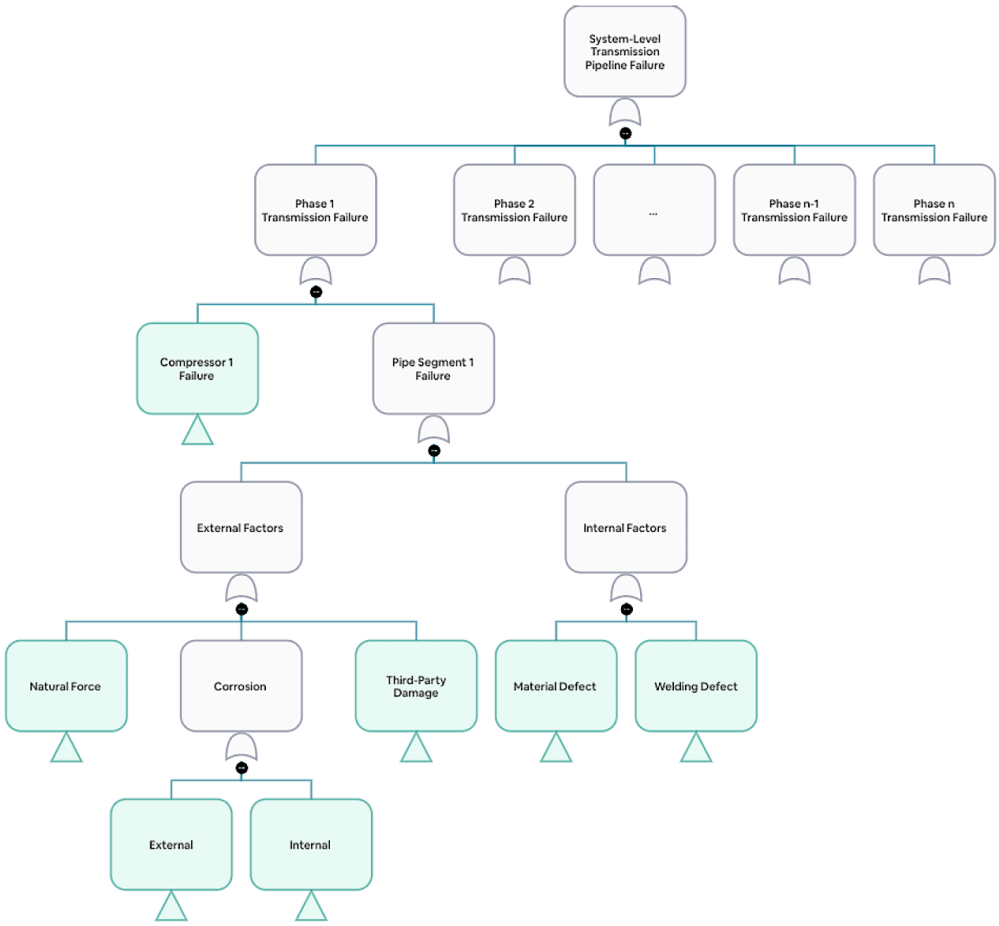

Figure 55. Fault tree of the system-level gas transmission pipeline.

9.3.2 *Corrosion Simulation*

The "**Corrosion Simulation**" feature is fulfilled by corrosion predictive models. This section introduced the methodology to develop two Bayesian Network (BN)-based corrosion predictive models for natural gas transmission pipelines subject to internal and external corrosion, respectively. The construction of a BN model requires several steps. Firstly, build a graphical representation of the chain of events in a cause-consequence relationship leading to corrosion

failure. Secondly, develop the conditional probability tables (CPTs) based on available data such as physics-based models, field data, and expert knowledge among which the physics-based models are the most reliable one with solid science background [35]. In this study, the development of conditional probability tables was mainly based on physics-based or semi-empirical models, whereas a few of them are based on empirical models or expert judgement. In the BN-based corrosion predictive models, denotation (*node name*) represent the name of a node.

9.3.2.1 *BN internal corrosion model*

Figure 56 shows the proposed BN-based internal corrosion model that consists of three parts, namely, corrosion model, mechanical model, and reliability model. The model considers five types of corrosion that may take place inside the pipe and predicts instantaneous corrosion rate given operating conditions. Considered corrosion types include uniform corrosion, pitting corrosion, microbiologically influenced corrosion (MIC), erosion corrosion, and corrosion fatigue. It should be mentioned that as the presence of water is an essential factor for the corrosion for corrosion process to take place and proceed, a wetting factor (*Wetting Factor*) was applied to each corrosion model for corrosion predictions. Mechanical model calculates the burst pressure (or remaining strength) based on the accumulated corrosion damage and pipeline design parameters. Reliability model calculates the probability of failure caused by corrosion failure based on the limit state function of load and resistance. The details of discretized nodes of the BN-based internal corrosion models are listed in ANNEX A. The descriptions of each type of corrosion were discussed as follows.

9.3.2.1.1 Uniform corrosion

In oil and gas pipelines, if the corrosion leads to the uniform reduction of pipe walls following by the formation of corrosion products, it is called uniform corrosion. It is caused by the presence of carbon dioxide (CO_2) and hydrogen sulfide (H_2S) in an aqueous environment because CO_2 and H_2S become acidic when dissolved in water and corrosion reactions take place at steel surfaces. Uniform corrosion has been studied over the past 20 years, and a number of predictive models have been developed including mechanistic [14,41], semi-empirical [10,85], and empirical models [23,58].

In this study, the uniform corrosion was modelled by the proposed physics-of-failure (POF)-based model described in "**Chapter 5.1 Internal corrosion model**", which can predict time-dependent corrosion rate given pipeline operating parameters. These parameters are temperature (*Temperature*), partial pressure of CO_2 (pCO_2), partial pressure of H_2S (pH_2S), pH level (pH), and the flow velocity of gas (*Flow Velocity*).

9.3.2.1.2 Pitting corrosion

Most of the time, corrosion in oil and gas pipelines is not uniform, instead, it happens locally and leads to localized pits, which is often referred to pitting corrosion. Pitting corrosion is reported to be the most serious corrosion problem in the oil and gas industry because it is hard to detect without comprehensive and frequent in-line inspection [86].

In general, pitting corrosion is likely to happen at the area where protective layers are destroyed and fresh steels are exposed to the corrosive environment. In this study, the Papavinasam model described in "**Chapter 5.1 Internal corrosion model**" was adopted to model pitting corrosion. This model is developed through numerous experiments considering a variety of pipeline operating or environmental parameters including wall shear stress (*Wall Shear Stress*), total operating pressure (*P*), solids (R_{solids}), partial pressure of H_2S (pH_2S), partial pressure of CO_2 (pCO_2), temperature (Temperature), sulfate ions concentration ($[SO_4^{2-}]$), bicarbonate ions concentration ($[HCO_3^-]$), and chloride ions concentration ($[Cl^-]$). Stochastic nature of pitting corrosion is considered by a distributed function consisting of corrosion rate predictions by each operating and environmental parameter.

9.3.2.1.3 Erosion corrosion

Erosion corrosion is defined as a degradation mechanism of pipe materials by the synergistic effect of mechanical action for erosion and electrochemical action for corrosion. Erosion corrosion is not as common as pitting or uniform corrosion, but it still poses threat to the oil and gas industry as it accounts for 9% among corrosion-related pipeline failure [87]. This study used Nesic model [88] to simulate erosion corrosion behaviors in which the presence of solids as well as the flow inside the pipes play an important role. The model inputs include operating parameters such as flow velocity (*Flow Velocity*) and particle mass (*Particle Mass*) and pipe design parameters such as pipe yield strength (*Yield Strength*) and impact angle (*Impact Angle*). One assumption is made that a particle must have a normal impact velocity greater than the critical velocity constant (0.668 m/s)

for erosion corrosion to happen. For detailed descriptions of this model, the readers are referred to the original papers [88].

9.3.2.1.4 Microbiologically influenced corrosion (MIC)

Bacterial activity by microbes tends to form biofilms which become acidic when they trap electrolytes and acids inside the pipe. Then, corrosive environments are developed that are prone to the occurrence of MIC [89]. The presence of biofilms on the steel surface forms a galvanic cell, promoting galvanic corrosion locally. Therefore, MIC is likely to take place in the form of pitting corrosion. In this study, MIC behavior was simulated by the Pots model [45], which takes operating parameters, environmental parameters, and mitigation parameters into account that are related to the formation of biofilms by microbes. The model inputs include concentration of carbon from fatty acid (*[C]*), use of biocide (*Biocide*), concentration of oxygen (*[O]*), frequency of pigging (*Pigging*), concentration of nitrogen (*[N]*), ratio between concentration of carbon and, nitrogen (*C:N ratio*), concentration of dissolved solids (*[Solids]*), flow velocity (*FVMIC*), presence of debris (*Debris*), and temperature (*TMIC*), each of which corresponds to a value that is used to calculate corrosion rate. For detailed descriptions of this model, the readers are referred to the original paper [45].

9.3.2.1.5 Corrosion fatigue

The presence of corrosive environments and cyclic loads inside the pipe may lead to corrosion fatigue, the synergistic effect of corrosion and fatigue. The sources of cyclic loads in gas transmission pipelines include mechanical vibrations caused by compressor stations and thermal stresses due to significant changes in operating temperatures caused by shutdowns or seasonal variances. This process starts with pitting nucleation by pitting corrosion and then propagates with fatigue cracks that finally leads to fracture [90]. This study adopted the Paris law-based model [91,92] to predict the corrosion fatigue behavior assuming a corrosion damage already exists as the nucleation point for fatigue cracks. The model inputs include coefficient (*Coefficient*), which represents material characteristics; exponent (*Exponent*), which reflects mechanistic dependencies; alternating stress intensity (K), which is influenced by alternating stress (*Stress Range*) and initial pit length (*Defect Length*); frequency of change in cyclic load (*Frequency*).

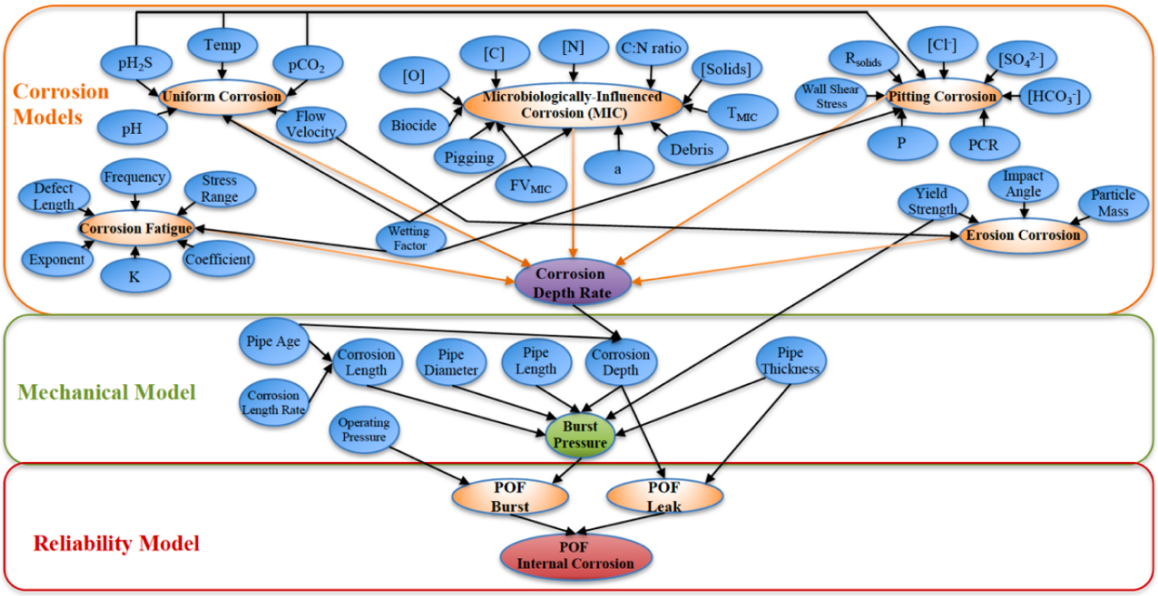

Figure 56. BN model for internal corrosion assessment.

9.3.2.2 *BN external corrosion model*

Figure 57 shows the proposed BN-based external corrosion model that also consists of a corrosion model, a mechanical model, and a reliability model as the proposed BN-based internal corrosion model. Two common types of external corrosion, namely pitting corrosion and stress corrosion cracking (SCC) were considered. The details of discretized nodes of the BN external corrosion model were listed in ANNEX B. The descriptions of each type of corrosion were discussed as follows.

9.3.2.2.1 Pitting corrosion

Underground oil and gas pipelines can suffer pitting corrosion results from inadequate cathodic protection or coating disbandment [93]. In this study, Velazquez et al. model [94] was used to predict the maximum pit depth caused by pitting corrosion. As the pit growth rate is significantly influenced by characteristics of soil, operating parameters, and mitigation operations. This model relates the pit growth rate to soil and pipe characteristics by a multivariate regression method, which is calibrated with field data. Pit growth rate is described by a power law function with its pitting proportionality (*Coefficient*) and exponent factors (*Exponent*) determined by a variety of parameters including resistivity (*Resistivity*), sulphate ions concentration ($[SO_4^{2-}]$), bicarbonate ions concentration ($[HCO_3^-]$), chloride ions concentration ($[Cl^-]$), water content of the soil (*Water Content*), pH level of the soil (*pH*), pipe/soil potential (*Pipe Soil Potential*), bulk density of the soil (*Bulk Density*), and redox potential (*Redox Potential*). Mitigation operation parameter included in this model is lifetime of a coating (*Coating Lifetime*) above which the corrosion may take place.

9.3.2.2.2 Stress corrosion cracking

SCC occurs when oil and gas pipelines are subjected to corrosive soil environments and small loading cycles where mechanical-electrochemical interaction happens. The source of external loading usually results from longitudinal strain caused by soil movement. Two types of SCC have been identified, namely, high pH SCC (pH > 9.0) and near-neutral pH SCC (pH ≈ 6.5) [95].

However, although SCC has been studied over past decades, few equation-based predictive models are developed. This study adopted a finite element model firstly developed via COMSOL Multiphysics [96] and later modified by authors' previous work [34] to simulate SCC behaviors. This model studies the changes of corrosion potential and corrosion current density on an already existing corrosion defect on the outer pipe wall subjected to a tensile strain under near-neutral condition. Model inputs include anodic current density (*Anodic* i_0) and cathodic current density (*Cathodic* i_0) for electrochemical reactions, strain (*Strain (Displacement)*) for elastoplastic stress modeling, and defect depth (*Defect Depth*) and defect length (*Defect Length*) for a corrosion defect geometry. For details of this model, the readers are referred to the original paper [34].

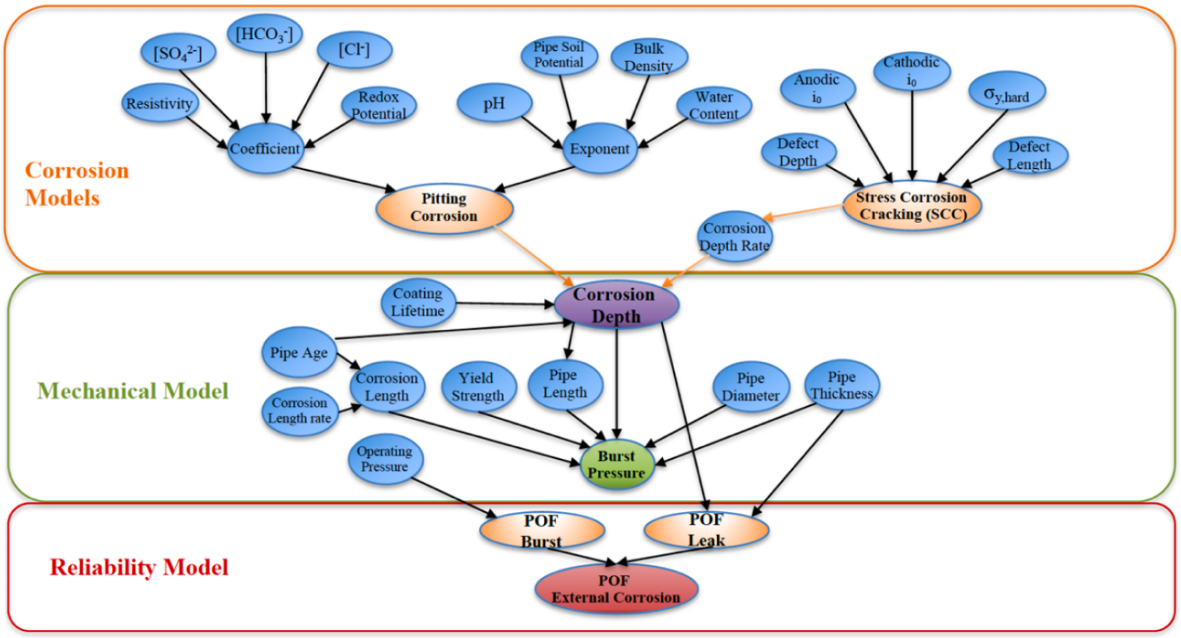

Figure 57. BN model for external corrosion assessment.

9.3.2.3 *Mechanical and reliability model*

All of the above-mentioned corrosion models, namely, uniform corrosion, pitting corrosion, microbiologically-influenced corrosion, erosion corrosion, and corrosion fatigue affect the corrosion depth rate (*Corrosion Depth Rate*). Here, corrosion rate in length (*Corrosion Length Rate*) is modeled as an independent variable of Corrosion Depth Rate because there is no direct evidence that the growths of corrosion length and depth are correlated. A linear growth model is used to obtain the total corrosion length (*Corrosion Length*) after a certain time of operation (*Pipe Age*). On the other hand, for the total corrosion depth (*Corrosion Depth*) calculation, MIC, erosion corrosion, and corrosion fatigue are assumed to follow a linear growth in which the corrosion rate of each constituent is a constant, while that of uniform and pitting corrosion are time dependent.

Not only the thickness of the pipe wall will reduce due to the corrosion damage, but also the strength of the pipe deteriorates with increasing age. Although a number of burst pressure models have been developed to calculate the remaining strength of a corroded pipeline, this study chooses ASME B31G [69] and DNV-RP-F101 [70] because they are convenient to implement with decent accuracy. However, ASME B31G is only suitable for low toughness steels while DNV-RP-F101 is suitable for medium to high toughness steels. The burst pressure is controlled by the geometry of corrosion defects including defect depth (*Corrosion Depth*) and defect length (*Corrosion Length*) as well as the characteristics of pipe materials including pipe length (*Pipe Length*), pipe diameter (*Pipe Diameter*), pipe thickness (*Pipe Thickness*), and yield stress or flow stress (*Yield Strength*).

The burst pressure equations of ASME B31G mechanical model were already introduced in **"Chapter 8.4.1.3 Pipeline mechanical and reliability model"**, whereas the burst pressure equations for DNV-RP-F101 mechanical model are shown as follows:

$$P_b^{F101} = (\sigma_h)\left[\frac{1-\left(\frac{d}{w}\right)}{1-\left(\frac{d}{Mw}\right)}\right]\left(\frac{2w}{D-w}\right) \quad where \quad M = \sqrt{1+0.31\left(\frac{l}{\sqrt{Dw}}\right)^2} \qquad (115)$$

where P_b^{F101} is burst pressure by DNV-RP-F101; σ_h is hoop stress; w is pipe wall thickness; D is pipe outer diameter; M is Folias factor.

As for the reliability model, two common failure modes that happen in gas pipelines due to corrosion, namely, leak and burst were considered in this study. Since the mechanical models used for calculating the burst pressure are deterministic in nature, it cannot be directly used to obtain failure probability. Instead, a probabilistic approach involving the formulation of limit state functions of leak and burst needs to be developed. Afterwards, the probability of failure given leak (*POF Leak*) or burst (*POF Burst*) was obtained by using the Monte Carlo technique to account for the uncertainties of the defined loads and strengths in the limit state functions. Specifically, the same equations described in **"Chapter 8.4.1.3 Pipeline mechanical and reliability model"** were used. Finally, since either of these two failure modes takes place, the pipe will fail. The one that has higher probability will be regarded as the probability of failure by internal corrosion (*POF Internal Corrosion*). The calculation of probability of failure by external corrosion (*POF Internal Corrosion*) was obtained followed the same process.

9.3.3 *Inspection/Maintenance Optimization*

At this stage, **"Inspection/Maintenance Optimization"** feature provides two predictions with respect to risks caused by corrosion-related pipe failures. Firstly, it gives recommended actions, namely, do nothing, inspection, and repair based on the corrosion prediction results in terms of probability of failure. Specifically, the recommendation is based on the DNV-RP-F101 criteria [70] that takes into consideration the failure probability values in terms of leak and burst. Whenever POF leak or POF burst is between 10^{-3} and 10^{-5}, inspection is required; whenever they are larger than 10^{-3}, repair is required; otherwise, no action is needed. Secondly, it provides the optimal schedule and types of maintenance practices to be performed that can maintain the pipeline integrity while minimizing the maintenance costs by the proposed RL-based maintenance scheduler described in **"Chapter 8: Smart Condition-Based Maintenance with Reinforcement Learning for Dry Gas Pipeline Subject to Internal Corrosion"**. The considered maintenance practices include "Batch corrosion inhibitor", "Internal coating", "Cleaning pigging", and "Repair" as well "Do nothing".

10 Case study – Kinder Morgan's North Texas Pipeline

This section demonstrated the PSIM software by a case study. Only corrosion-related analyzes were done and discussed in the following sub-sections.

10.1 System specification

The case study is a section of the Kern River Gas Transmission Pipeline was chosen. This 36-inch-diameter steel pipe has 2 transmission phases (denoted as Phase 1 and Phase 2), each of which is composed of one compressor and one pipeline segment. The pipeline is built into the software by specifying the coordinates of the pipeline segments as shown in Figure 58. The user interface of the software shows different modules located on the top of the window. Firstly, pipe information in the form of shapefile was inserted into the **"Pipeline Network Building"** feature in order to create a new pipeline to be studied. **"Live Data Monitoring"** feature displays the monitoring operating parameters e.g., operating temperature, operating pressure, flow velocity, etc. This case study specifically utilized **"Corrosion simulation"**, **"System-Level Failure Analysis"**, and **"Inspection/Maintenance Schedule Optimization"** features to study the pipeline integrity of a corroded pipeline as a demonstration.

The basic design variables of two phases are demonstrated in Table 24, which are provided by the users. Firstly, a system-level fault tree of the pipeline system was developed. Secondly, corrosion prognosis was done in which the outputs of it would be inserted back to the fault tree in calculation of system failure probability. Finally, inspection and maintenance schedule optimizations were

performed based on the corrosion results to aid decision makings in sensor placement and inspections.

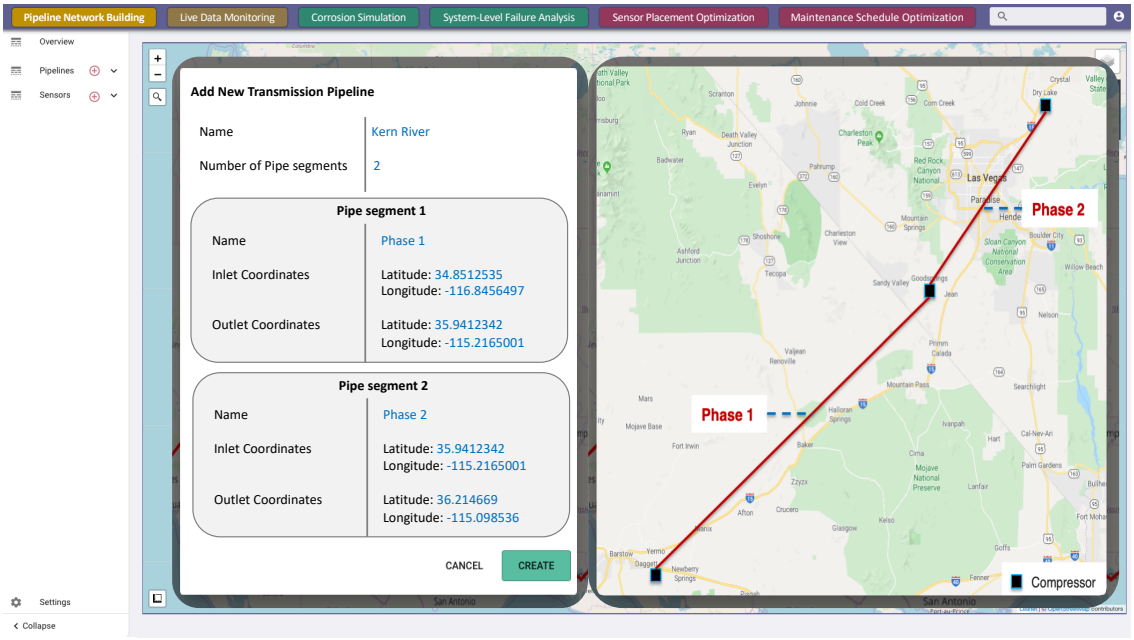

Figure 58. Kern River gas transmission pipeline network developed in the PSIM software.

Table 24. Basic design variables of Phase 1 and Phase 2 of the demonstrated transmission pipeline.

Parameters	Phase 1	Phase 2
Inner Diameter, ID (in)	36	36
Outer Diameter, OD (in)	38	38
Wall Thickness, W (in)	1	1
Length, L (miles)	103.917	86.658
Yield Strength, YS (MPa)	448	448

The **"Live Data Monitoring"** module shows the real-time monitoring data that is continuously generated by the sensors. The monitoring data of this case study is shown in Figure 59.

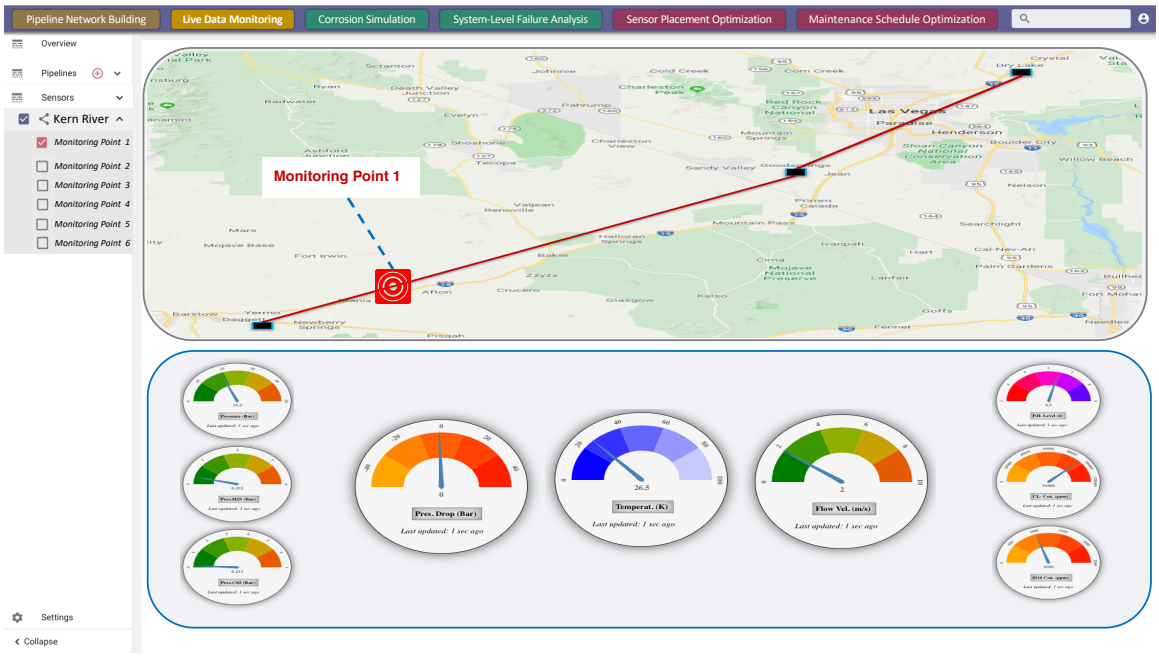

Figure 59. Live data monitoring feature of the software platform.

10.2 System Analysis and Modeling

In this case study, the system consists of 2 transmission phases. The first phase transmits natural gas from the Daggett compressor station to the Goodsprings compressor station through 102.56 miles (165.05 kilometers) pipeline segment. The seconds phase transmits the gas from the Goodsprings compressor station to the Dry Lake compressor station through 86.66 miles (139.47 kilometers) pipeline segment. Figure 60 shows the fault tree of this pipe system where all failure causes are taken into account.

Except for corrosion node, the probability of each node was determined based on literature data. The compressor reliability is extracted from the literature [84] and is shown in Figure 61. The pipeline failure probabilities due to natural force, third-party damage, material defect, and welding defect are taken from the research work presented in the literature [97] and are presented in

Table 25. The probability of corrosion node was determined by the **"Corrosion Simulation"** feature described in the next sub-section.

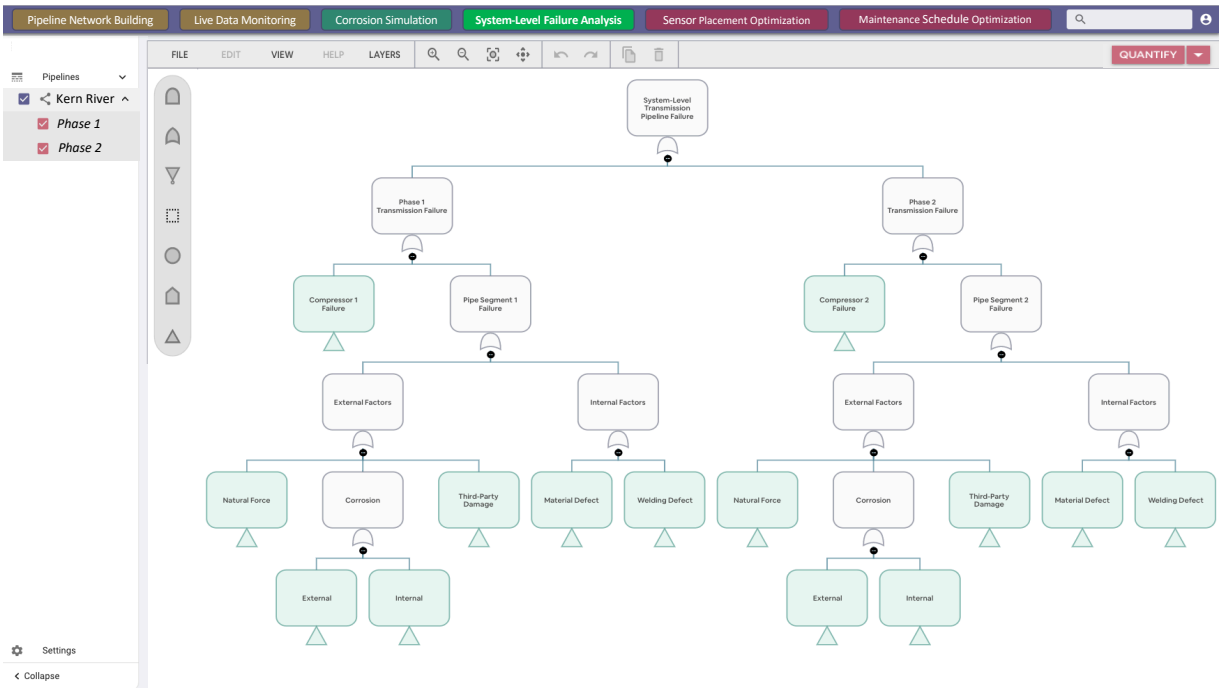

Figure 60. Fault tree of the studied section of the Kern River Gas Transmission Pipeline.

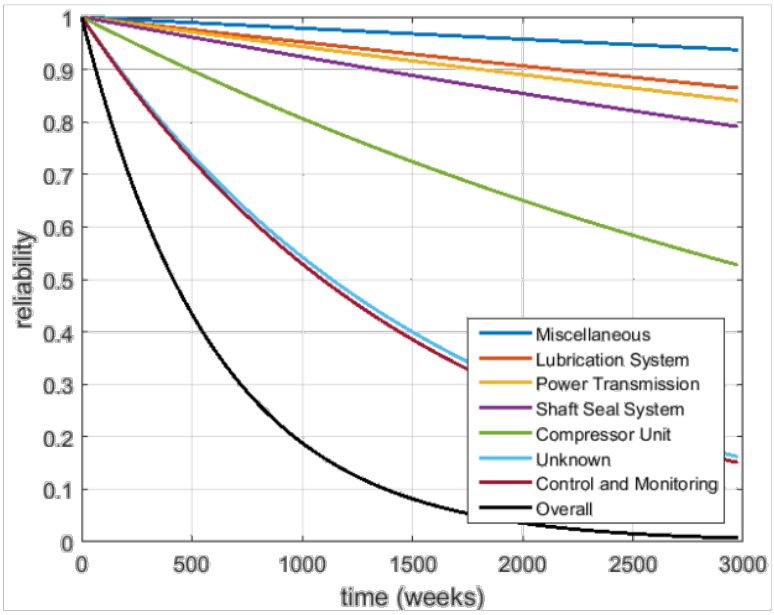

Figure 61. Reliability of a gas compressor over time [84].

Table 25. Failure probabilities of basic events for the fault tree analysis.

Basic Event	Description	Probability
Natural Force	Risk of natural disaster due to earthquake, flooding, or subsidence	0.00026266
Third-Party Damage	Risk of interference from the third party due to parties ignore signage, implicit signage, sabotage, or overload	0.0075406
Material Defect	Risk of material defect due to design defect of material or construction defect of material	0.0005688
Welding Defect	Risk of weld-seam defect due to design defect of weld-seam or construction defect of weld-seam	0.000523

10.3 Results of corrosion simulation

Both the results of internal corrosion modeling and external corrosion modeling by **"Corrosion Simulation"** feature were discussed as follows.

10.3.1 *Internal corrosion modeling*

Due to the lack of live monitoring data at this time, the live monitoring operating data was simulated by a proposed methodology described in **"4.2.1 Temporal variability"** in consideration of temporal variability with assumed operating parameters. For internal corrosion, the operating parameters at near inlet of the demonstrated transmission pipeline are presented in Table 26. A portion of the simulated operating parameters results are shown in Table 27, which shows the time-dependency in daily variation because the corrosion modeling was conducted on a daily granuarity. According to the system definition, each transmission phase consists of a compressor at the inlet to maintain the transmission force for gas transportation, and this force may decrease over the

length of the pipe. Moreover, operating temperature is also found to decrease over the length of the pipe [24], rendering us to make an assumption in this study that spatial variability of operating parameters was only considered for temperature, pressure, partial pressure of H_2S, and partial pressure of CO_2. In other words, other operating parameters were only modeled to be time-dependent but not location-independent.

Table 26. Operating parameters at near inlet of the demonstrated transmission pipeline.

Variables	Type	COV	Mean	
			Phase 1	**Phase 2**
Temperature, T (℃)	Lognormal	0.03	26	25
Soil temperature, T_amb (℃)	Lognormal	0.02	15	17
Pressure, P (bar)	Lognormal	0.10	62	50
CO_2 percentage in Gas, %_ CO_2 (%)	Lognormal	0.10	0.56	0.46
H_2S percentage in Gas, %_H_2S (%)	Lognormal	0.10	0.61	0.30
pH	Lognormal	0.10	6.5	6.7
Flow velocity, V (m/s)	Lognormal	0.05	3	3.5
Chloride ion concentration, Cl (ppm)	Lognormal	0.15	2000	1000
Sulphate ion concentration, Cl (ppm)	Lognormal	0.15	1000	1500
		Lower limit	**Upper limit**	
Probability of solids presence, S (%)	Uniform	50	100	

*Partial pressure of H_2S (=P × % H_2S/100); partial pressure of CO_2 (=P × % CO_2/100).

Table 27. A portion of the simulated results of time-dependent operating parameters.

Time (day)	Temperature (K)	Soil Temperature (K)	Operating Pressure (bar)	H_2S Partial Pressure (bar)	CO_2 Partial Pressure (bar)	pH	Flow Velocity (m/s)	Chloride Ions (ppm)	Sulphate Ions (ppm)	Solids (%)
0	305.5063	292.4915	53.9361	0.3856	0.3321	6.578	3.0774	2053.86	891.887	68.2
1	303.1870	281.5281	64.0112	0.4285	0.3207	7.498	3.3490	1948.22	993.140	21.9
2	300.8724	283.5577	57.6863	0.3711	0.3122	6.329	2.9389	2169.53	1100.70	4.27
3	307.9069	287.4584	58.9141	0.3760	0.3829	6.937	2.9319	2495.63	852.038	17.1
…										
357	287.9477	286.6430	43.9673	0.4186	0.3480	6.430	3.0055	2022.50	997.775	44.9
358	317.9171	286.9760	68.0592	0.3671	0.3137	6.395	2.9017	1786.11	919.773	99.8
359	302.5259	283.5387	58.6378	0.4217	0.4121	8.526	2.9617	2162.85	1229.63	62.3

Time-evolution schematic of predicted internal corrosion depths for Phase 1 transmission pipe is shown in the right side of Figure 62. It can be seen that corrosion depths increase with increasing time; however, the increase rate actually drops as corrosion rates decrease over time, which is one of the characteristics of internal corrosion [4]. Time-evolution schematics of probability of leak and burst due to internal corrosion for Phase 1 transmission pipe at near inlet are shown in the right side of Figure 62. As expected, both POF-leak and POF-burst show increasing trends over time.

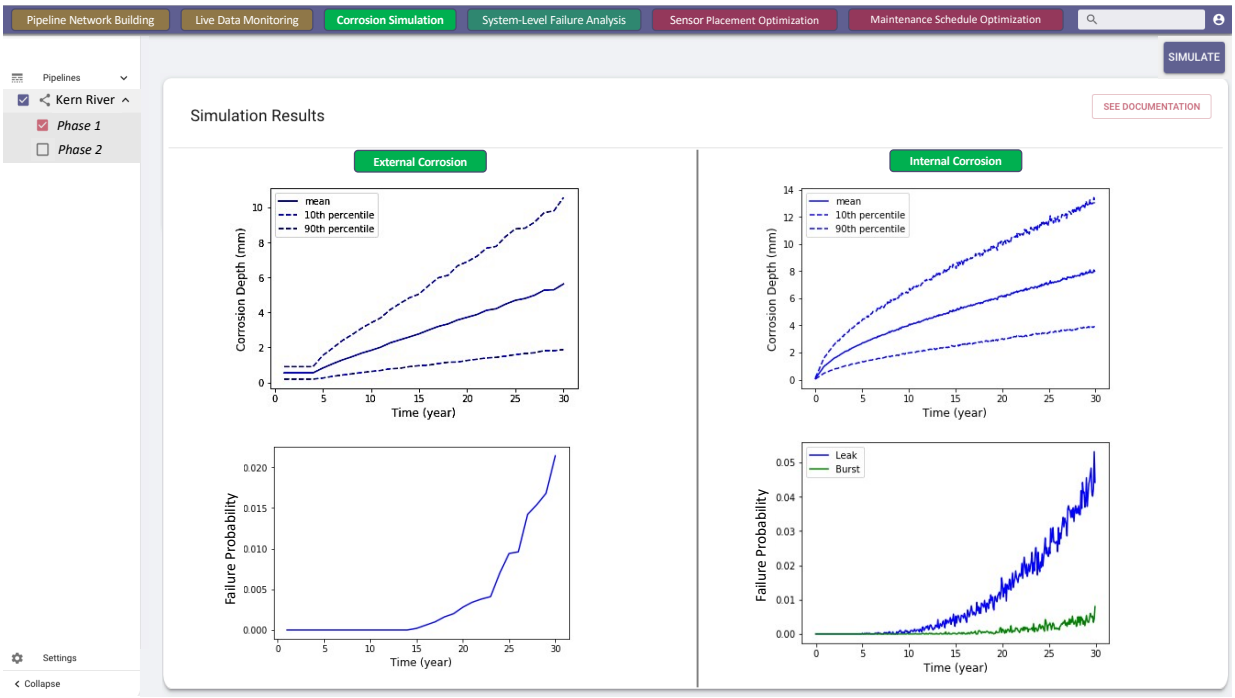

Figure 62. Time-evolution schematics of predicted external and internal corrosion depths and failure probability for Phase 1 transmission pipeline segment

The same analyzes were performed for Phase 2 transmission pipe in the **"Corrosion Simulation"** feature in calculation of POF-leak and POF-burst for internal corrosion. In addition, the highest ones among POF-leak and-POF burst (i.e., max(POF-leak, POF-burst)) of Phase 1 and Phase 2, respectively, was regarded as the segment failure probabilities for internal corrosion nodes in the fault tree analysis for Phase I and Phase 2, respectively.

10.3.2 *External corrosion modeling*

External corrosion failures depend on the availability and the efficiency of mitigation measures such as cathodic protections and coatings [35]. Besides mitigation measures, soil and pipe conditions are also key factors of external corrosion for an underground transmission pipeline. Due to lack of field data, the soil and pipe data for external corrosion modeling was taken from other literature [28,96,98]. Table 28 shows the soil and pipe data of the demonstrated pipeline in which some of the variables are probabilistic while some of them are deterministic.

Corrosion simulation of Phase 1 transmission pipe for external corrosion were conducted in consideration of time-dependency. Time-evolution schematic of predicted external corrosion depths for Phase 1 transmission pipe is shown in the left side of Figure 62. It can be seen that due to the application of coating, the corrosion does not propagate until the lifetime of the coating is reached. The parts of the pipe where the coating is broken suffers external corrosion, which is contributed by pitting corrosion and SCC. Time-evolution schematics of probability of leak due to external corrosion for Phase 1 transmission pipe is also shown in the left side of Figure 62. The result shows that POF-leak, as the main external corrosion failure, increases over time after the coating has broken for several years.

Table 28. Soil and pipe data of the demonstrated transmission pipeline for external corrosion modeling.

Variable, symbol (units)	Probability function
Resistivity, re (Ω-m)	Lognormal (50, 2931)
Sulphate, sc (ppm)	Lognormal (154, 25328)
Bicarbonate, bc (ppm)	Lognormal (19, 436)
Chloride, cc (ppm)	Lognormal (41, 3135)
Water content, wc(%)	Normal (24, 38)
pH, ph	Gumbel (6.13, 0.84)
Pipe/soil potential, pp (V)[1]	Normal (-0.86, 0.04)
Bulk density, bd (g/ml)	Normal (1.30, 0.007)
Redox potential, rp (mV)[2]	Uniform (2.14, 348)
[1]Cathodic i_0, i_{0_c} (A/m^2)	Normal (0.015, 0.1)
[1]Anodic i_0, i_{0_a} (A/m^2)	Normal (0.0024, 0.01)
[2]Defect depth, dd (mm)	Uniform (0.1, 5)
[2]Defect length, dl (mm)	Uniform (0.5, 10)
[3]Displacement, disp (mm)	Uniform (0.1, 1.5)
	Deterministic function
Coating type, ct	Constant (0.7651)
Coating lifetime, cl	Constant (5)

The same analyzes were performed for Phase 2 transmission pipe in **"Corrosion simulation"** feature in calculation of POF-leak for external corrosion. A recommended action was also given based on the corrosion simulation results. Finally, the POF-leak of Phase 1 and Phase 2,

respectively, was used as segment failure probabilities for external corrosion nodes in the fault tree analysis for Phase I and Phase 2, respectively

10.3.3 *Results of system-level failure analysis*

All possible failure causes that could fail the pipeline segments were added to the fault tree as shown in Figure 60. One of the novelties of this software is that the quantification is dynamic as the corrosion failure probabilities are changing over time with changing operating parameters received from the sensors. The result of the system-level failure analysis of the studied Kern River Gas Transmission Pipeline is displayed in Figure 63 which shows the system failure probability over time. The predicted failure probability increases over time because although failure probabilities of many basic events were assumed time-independent, corrosion actually propagates over time and break the pipe segment if no mitigation is done, leading to the failure of the pipe system.

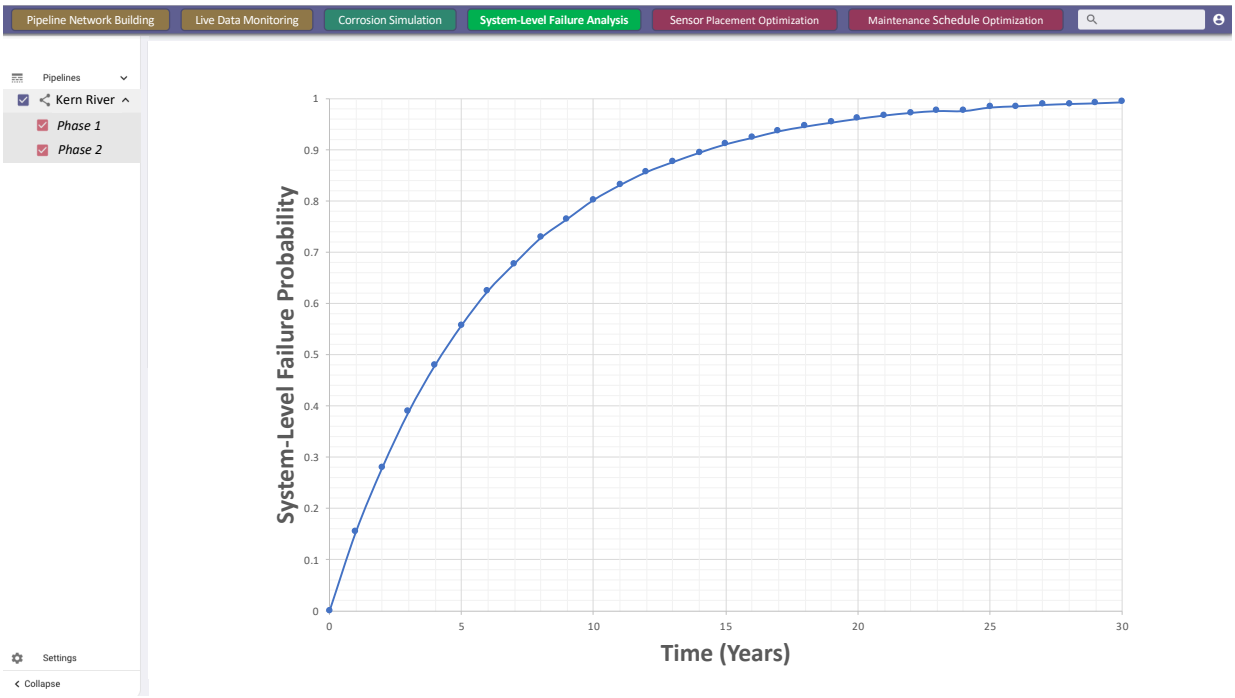

Figure 63. Failure probability of the studied section of Kern River transmission pipeline over time.

10.3.4 *Results of Inspection/Maintenance Schedule Optimization*

The **"Inspection/Maintenance Schedule Optimization"** feature gives a recommended action based on the corrosion results along the pipeline segments and also provides optimal maintenance schedule suggestions over the lifetime of the pipe in a goal of reducing the maintenance cost while maintaining the pipe integrity with the aid of a RL-based maintenance scheduler. The results for this case study are displayed in the left side of Figure 64. Analysis results show that repair along the transmission pipeline is required after 10 years of operation if no maintenance is performed during the operation. Moreover, the corrosion depth and length over time of the pipe following the recommended maintenance actions by the maintenance scheduler is also shown in the right side of

Figure 64. This figure shows that if the cleaning pigging, which removes bacteria, solids, and corrosive elements, is applied in the recommended time intervals, the pipe integrity can be assured as corrosion depth percentage (CDP) is still below 0.4, which is lower than the well-accepted leak criterion 0.8. In addition, the results by the maintenance scheduler shows that it more cost-effective to do maintenance actions based on the condition-based maintenance (CBM) strategy than doing repairs when the pipe fails. The results show that the optimal maintenance schedule is to perform cleaning pigging every month between 33 months (2.75 years) and 94 months (7.83 years), and 247 months (20.58 years) and 360 months (30 years).

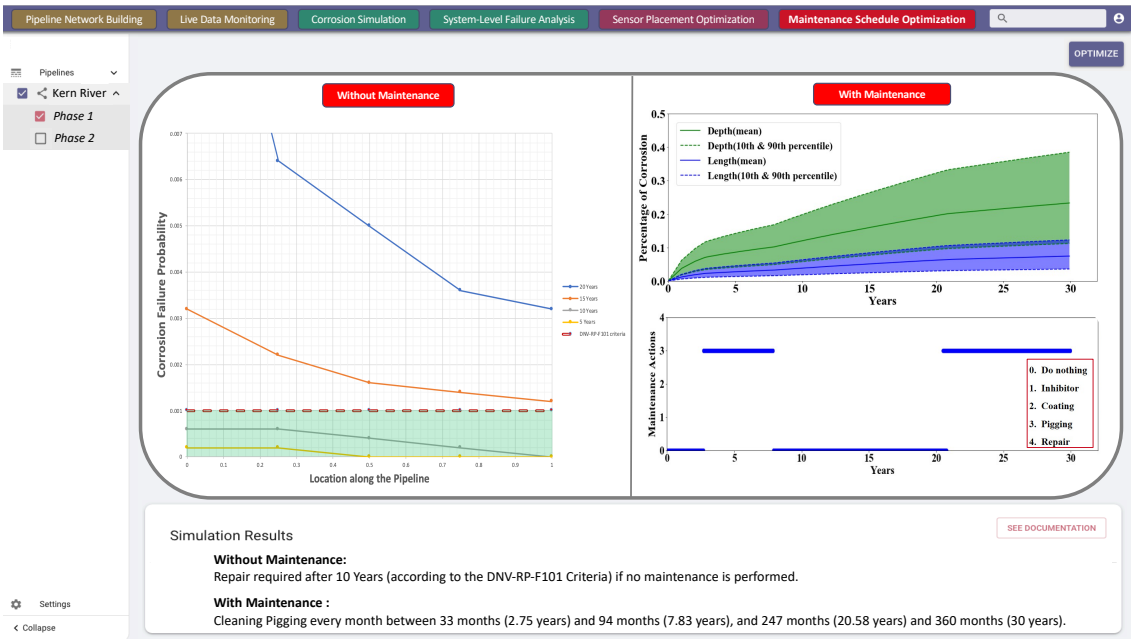

Figure 64. Recommended maintenance actions over time based on predicted corrosion failure probability and corrosion depth and length along the pipeline.

10.4 Conclusions

In conclusion, the developed pipeline health monitoring and management models showed the ability to quantify the health state of the pipeline over time and help the operators make risk-informed decisions. The platform design is supported by a multidisciplinary science and engineering approach for a comprehensive, state-of-the-art solution. The software platform integrates the data, methods, and technologies into a dynamic pipeline health monitoring system supported by multiple probabilistic predictive models which analyzed all causal factors that could fail the pipeline. In addition, this total system health management support tool provided dynamic mitigation suggestions to the user based on the simulation results such as the need of an additional sensor at a given location for a better structural health monitoring of the pipeline or the optimal timing of an inspection/ repair of a given pipeline. Finally, the PSIM software platform could be deployed in a control room as a dynamic health monitoring dashboard or in a mobile version for field inspection and maintenance purposes.

11 Summary and Conclusions

Transporting natural gas from production to consumers is a critical and complex process. First of all, gas have to be extracted from the wellhead and transported through different kinds of pipelines. There are gathering pipelines, transmission pipelines, and distribution pipelines. The research interest of this dissertation is on the transmission pipeline because during the transportation the transmission pipeline is subject to corrosive environment. That means they are exposed to pipeline failure caused by corrosion. Although there are several causes of pipeline failure, "corrosion failure" is the second highest (20%). Moreover, corrosion failure tends to occur in old pipes (average 46 years old). This implies that corrosion is a continuous degradation and it will propagate until the pipe breaks if no mitigation is ever performed during the operation.

Fortunately, pipeline system integrity management can be used to assess and mitigate pipeline risks in an effort to reduce both the likelihood and consequences of pipeline incidents. The general PSIM tool includes four steps. In order to develop a PSIM tool, this dissertation has accomplished three objectives:

1. Developed a corrosion predictive model that can take both temporal and spatial variabilities of operating parameters into account for corrosion predictions. The corrosion model consists of a modified uniform corrosion model and a selected pitting corrosion model. The proposed modified uniform corrosion model was validated with experimental data. Moreover, the proposed corrosion predictive model has verified its model application of

field-operating gas pipelines as most deviations between model predictions and measured corrosion rate of field data are smaller than a factor of 2.

2. On top of the corrosion predictive model, we further developed a smart condition-based maintenance algorithm which is designed to do cost-optimized maintenance management for natural gas pipelines. The proposed methodology consists of a data-driven RL-based agent (i.e., Q-learning or SARSA) and a test bench (i.e., natural gas pipeline segment), which is simulated by a pipe model. The maintenance scheduler successfully avoids any failures within the simulation time step and reduces 58% of the average monthly maintenance costs compared to the best selected periodic maintenance policy.

3. Finally, the abovementioned two research works were integrated into the PSIM software, specifically contributing to **"Corrosion Simulation"**, **"System-level Failure Analysis"**, and **"Inspection/Maintenance Schedule Optimization"** features. This software is a dynamic pipeline health monitoring and management tool that can fulfil the pipeline integrity management purpose and aid pipeline operators in decision makings. The corrosion-related features of the software were demonstrated via a case study.

12 Recommendations and Future Work

At this stage, the proposed corrosion predictive model for internal corrosion is designed for natural gas pipelines subject to aqueous CO_2/H_2S corrosive environment, which are made of mild steels. The model has been calibrated with some experimental data and validated with some field data in this dissertation; however, as the model is semi-empirical in nature, it is possible to further adjust the model to support natural gas pipelines with different operating parameters and different materials once more data is available.

The proposed maintenance scheduler is developed to serve as a bench mark for maintenance optimization of natural gas pipelines. According to the results of sensitivity analysis, the decision makings made by the maintenance scheduler are significantly influence by the model parameters; therefore, although the test bench of the model is based on a simulated environment (i.e., simulated pipeline segment by a pipe model), further improvement by real data is doable by transfer learning (TL), which is a machine learning technique that is able to store the gained knowledge from one problem and apply it to a different but related problem.

Currently, the PSIM software supports pipeline integrity management analysis of natural gas pipelines. That is to say, most of corrosion-related features "**"Corrosion Simulation"**, **"System-level Failure Analysis"**, **"Sensor Placement Optimization"**, and **"Inspection/Maintenance Schedule Optimization"** are developed based on the corrosion predictive models of natural gas pipelines subject to aqueous CO_2/H_2S corrosive environment buried underground. However, these

features will be extended to support oil pipelines in the future with available data; therefore, users can have more options in choosing the types of pipelines they are interested in.

13 References

[1] Kiefner, J. F., and Rosenfeld, M. J., 2012, "The Role of Pipeline Age in Pipeline Safety," INGAA, Oct.

[2] Koch, G. H., Brongers, M. P., Thompson, N. G., Virmani, Y. P., and Payer, J. H., 2002, *Corrosion Cost and Preventive Strategies in the United States*, United States. Federal Highway Administration.

[3] Nešić, S., 2007, "Key Issues Related to Modelling of Internal Corrosion of Oil and Gas Pipelines–A Review," Corrosion science, **49**(12), pp. 4308–4338.

[4] Heidary, R., Gabriel, S. A., Modarres, M., Groth, K. M., and Vahdati, N., 2018, "A Review of Data-Driven Oil and Gas Pipeline Pitting Corrosion Growth Models Applicable for Prognostic and Health Management," Int. J. Progn. Health Manag, **9**(1).

[5] "PHMSA | Pipeline and Hazardous Materials Safety Administration" [Online]. Available: https://www.phmsa.dot.gov/. [Accessed: 09-Jan-2020].

[6] Elgaddafi, R., Naidu, A., Ahmed, R., Shah, S., Hassani, S., Osisanya, S. O., and Saasen, A., 2015, "Modeling and Experimental Study of CO2 Corrosion on Carbon Steel at Elevated Pressure and Temperature," Journal of Natural Gas Science and Engineering, **27**, pp. 1620–1629.

[7] Revie, R. W., 2011, *Uhlig's Corrosion Handbook*, John Wiley & Sons.

[8] Zheng, Y., Ning, J., Brown, B., and Nešić, S., 2014, "Electrochemical Model of Mild Steel Corrosion in a Mixed H2S/CO2 Aqueous Environment in the Absence of Protective Corrosion Product Layers," Corrosion, **71**(3), pp. 316–325.

[9] De Waard, C., and Milliams, D. E., 1975, "Carbonic Acid Corrosion of Steel," Corrosion, **31**(5), pp. 177–181.

[10] de Waard, C., Lotz, U., and Milliams, D. E., 1991, "Predictive Model for CO2 Corrosion Engineering in Wet Natural Gas Pipelines," CORROSION, **47**(12), pp. 976–985.

[11] Nordsveen, M., Nešic, S., Nyborg, R., and Stangeland, A., 2003, "A Mechanistic Model for Carbon Dioxide Corrosion of Mild Steel in the Presence of Protective Iron Carbonate Films—Part 1: Theory and Verification," Corrosion, **59**(5), pp. 443–456.

[12] Nešic, S., Nordsveen, M., Nyborg, R., and Stangeland, A., 2003, "A Mechanistic Model for Carbon Dioxide Corrosion of Mild Steel in the Presence of Protective Iron Carbonate Films—Part 2: A Numerical Experiment," Corrosion, **59**(6), pp. 489–497.

[13] Nešic, S., and Lee, K.-L., 2003, "A Mechanistic Model for Carbon Dioxide Corrosion of Mild Steel in the Presence of Protective Iron Carbonate Films—Part 3: Film Growth Model," Corrosion, **59**(7), pp. 616–628.

[14] Sun, W., and Nešić, S., 2009, "A Mechanistic Model of Uniform Hydrogen Sulfide/Carbon Dioxide Corrosion of Mild Steel," CORROSION, **65**(5), pp. 291–307.

[15] G46-94, A., 2005, "Standard Guide for Examination and Evaluation of Pitting Corrosion."

[16] Ossai, C. I., Boswell, B., and Davies, I. J., 2015, "Predictive Modelling of Internal Pitting Corrosion of Aged Non-Piggable Pipelines," Journal of The Electrochemical Society, **162**(6), pp. C251–C259.

[17] Nuhi, M., Seer, T. A., Al Tamimi, A. M., Modarres, M., and Seibi, A., 2011, "Reliability Analysis for Degradation Effects of Pitting Corrosion in Carbon Steel Pipes," Procedia Engineering, **10**, pp. 1930–1935.

[18] Bazán, F. A. V., and Beck, A. T., 2013, "Stochastic Process Corrosion Growth Models for Pipeline Reliability," Corrosion Science, **74**, pp. 50–58.

[19] Bhattacharya, R. N., and Waymire, E. C., 2009, *Stochastic Processes with Applications*, Siam.

[20] Provan, J. W., and Rodriguez III, E. S., 1989, "Part I: Development of a Markov Description of Pitting Corrosion," Corrosion, **45**(3), pp. 178–192.

[21] Zhang, S., and Zhou, W., 2013, "System Reliability of Corroding Pipelines Considering Stochastic Process-Based Models for Defect Growth and Internal Pressure," International Journal of Pressure Vessels and Piping, **111**, pp. 120–130.

[22] Papavinasam, S., 2013, *Corrosion Control in the Oil and Gas Industry*, Elsevier.

[23] Papavinasam, S., Doiron, A., and Revie, R. W., 2010, "Model to Predict Internal Pitting Corrosion of Oil and Gas Pipelines," CORROSION, **66**(3), pp. 035006-035006–11.

[24] Lawson, K., 2005, "Pipeline Corrosion Risk Analysis–an Assessment of Deterministic and Probabilistic Methods," Anti-Corrosion Methods and Materials, **52**(1), pp. 3–10.

[25] Hasan, S., Khan, F., and Kenny, S., 2012, "Probability Assessment of Burst Limit State Due to Internal Corrosion," International Journal of pressure vessels and piping, **89**, pp. 48–58.

[26] Kale, A., Thacker, B. H., Sridhar, N., and Waldhart, C. J., 2004, "A Probabilistic Model for Internal Corrosion of Gas Pipelines," *Proceedings of the 5th Biennial International Pipeline Conference (IPC'04)*, Citeseer, pp. 2437–2445.

[27] Seghier, M. E. A. B., Keshtegar, B., Correia, J. A., Lesiuk, G., and De Jesus, A. M., 2019, "Reliability Analysis Based on Hybrid Algorithm of M5 Model Tree and Monte Carlo Simulation for Corroded Pipelines: Case of Study X60 Steel Grade Pipes," Engineering Failure Analysis, **97**, pp. 793–803.

[28] Modiri, B., Pourgol Mohammad, M., Yazdani, M., Nasirpouri, F., and Salehpour, F., 2014, "Piping Anti–Corrosion Coating Life Assessment," *ASME 2014 International Mechanical Engineering Congress and Exposition*, American Society of Mechanical Engineers Digital Collection.

[29] Wu, K.-Y., and Mosleh, A., 2019, "Effect of Temporal Variability of Operating Parameters in Corrosion Modelling for Natural Gas Pipelines Subject to Uniform Corrosion," Journal of Natural Gas Science and Engineering, **69**, p. 102930.

[30] Mahmoodzadeh, Z., Wu, K.-Y., Droguett, E. L., and Mosleh, A., 2020, "Condition-Based Maintenance with Reinforcement Learning for Dry Gas Pipeline Subject to Internal Corrosion," ResearchGate [Online]. Available: https://www.researchgate.net/publication/338719373_Condition-Based_Maintenance_with_Reinforcement_Learning_for_Dry_Gas_Pipeline_Subject_to_Internal_Corrosion?channel=doi&linkId=5e27437892851c3aadccfaca&showFulltext=true. [Accessed: 22-Jan-2020].

[31] Wu, K. Y., and Mosleh, A., 2018, "Probabilistic Model for Internal Uniform/Pitting Corrosion of Gas Pipelines," Probabilistic Safety Assessment and Management PSAM, **14**, p. 13.

[32] Wu, K. Y., Diaconeasa, M. A., and Mosleh, A., 2018, "The Impact of Time-Varying Operating Parameters on the Corrosion Rate and Depth of Gas Pipelines," Probabilistic Safety Assessment and Management PSAM, **2014**, p. 10.

[33] Chalgham, W., Diaconeasa, M., Wu, K.-Y., and Mosleh, A., "A DYNAMIC PIPELINE NETWORK HEALTH ASSESSMENT SOFTWARE PLATFORM FOR OPTIMAL RISK-BASED PRIORITIZATION OF INSPECTION, STRUCTURAL HEALTH MONITORING, AND PROACTIVE MANAGEMENT."

[34] Chalgham, W., Wu, K.-Y., and Mosleh, A., 2019, "External Corrosion Modeling for an Underground Natural Gas Pipeline Using COMSOL Multiphysics," p. 15.

[35] Ayello, F., Jain, S., Sridhar, N., and Koch, G. h., 2014, "Quantitive Assessment of Corrosion Probability—A Bayesian Network Approach," CORROSION, **70**(11), pp. 1128–1147.

[36] Pankow, J. F., and Morgan, J. J., 1979, "Dissolution of Tetragonal Ferrous Sulfide (Mackinawite) in Anoxic Aqueous Systems. 1. Dissolution Rate as a Function of PH, Temperature, and Ionic Strength," Environmental Science & Technology, **13**(10), pp. 1248–1255.

[37] Tewari, P. H., and Campbell, A. B., 1979, "Dissolution of Iron during the Initial Corrosion of Carbon Steel in Aqueous H2S Solutions," Canadian journal of Chemistry, **57**(2), pp. 188–196.

[38] Pankow, J. F., and Morgan, J. J., 1980, "Dissolution of Tetragonal Ferrous Sulfide (Mackinawite) in Anoxic Aqueous Systems. 2. Implications for the Cycling of Iron, Sulfur, and Trace Metals," Environmental Science & Technology, **14**(2), pp. 183–186.

[39] Droguett, E. L., Groen, F., and Mosleh, A., 2004, "The Combined Use of Data and Expert Estimates in Population Variability Analysis," Reliability Engineering & System Safety, **83**(3), pp. 311–321.

[40] "R-DAT --- Prediction Technologies Inc" [Online]. Available: http://www.prediction-technologies.com/rdat.html. [Accessed: 09-Jan-2020].

[41] Zheng, Y., Ning, J., Brown, B., and Nešić, S., 2016, "Advancement in Predictive Modeling of Mild Steel Corrosion in CO2- and H2S-Containing Environments," CORROSION, **72**(5), pp. 679–691.

[42] Farelas, F., Brown, B., and Nesic, S., 2013, "Iron Carbide and Its Influence on the Formation of Protective Iron Carbonate in CO2 Corrosion of Mild Steel," CORROSION/2013, paper, **2291**.

[43] Singer, M., Brown, B., Camacho, A., and Nesic, S., 2007, "Combined Effect of CO2, H2S and Acetic Acid on Bottom of the Line Corrosion," CORROSION 2007.

[44] Liao, K., Yao, Q., Wu, X., and Jia, W., 2012, "A Numerical Corrosion Rate Prediction Method for Direct Assessment of Wet Gas Gathering Pipelines Internal Corrosion," Energies, **5**(10), pp. 3892–3907.

[45] Pots, B. F., Kapusta, S. D., John, R. C., Thomas, M. J. J., Rippon, I. J., Whitham, T. S., and Girgis, M., 2002, "Improvements on de Waard-Milliams Corrosion Prediction and Applications to Corrosion Management," *CORROSION 2002*, Nace International.

[46] Ahammed, M., and Melchers, R. E., 1995, "Probabilistic Analysis of Pipelines Subjected to Pitting Corrosion Leaks," Engineering Structures, **17**(2), pp. 74–80.

[47] Burt, V., 2015, *Corrosion in the Petrochemical Industry*, ASM International.

[48] Kadhim, A., Al-Okbi, A. K., Jamil, D. M., Qussay, A., Al-Amiery, A. A., Gaaz, T. S., Kadhum, A. A. H., Mohamad, A. B., and Nassir, M. H., 2017, "Experimental and Theoretical Studies of Benzoxazines Corrosion Inhibitors," Results in physics, **7**, pp. 4013–4019.

[49] Straub, D., and Faber, M. H., 2007, "Temporal Variability in Corrosion Modeling and Reliability Updating," Journal of Offshore Mechanics and Arctic Engineering, **129**(4), pp. 265–272.

[50] Khan, F., and Howard, R., 2007, "Statistical Approach to Inspection Planning and Integrity Assessment," Insight-Non-Destructive Testing and Condition Monitoring, **49**(1), pp. 26–36.

[51] Shibata, T., 2011, "Corrosion Probability and Statistical Evaluation of Corrosion Data," Uhlig's Corrosion Handbook, **51**, p. 365.

[52] "EasyFit - Distribution Fitting Software" [Online]. Available: http://www.mathwave.com/. [Accessed: 27-Jan-2020].

[53] Kasai, N., Maeda, T., Tamura, K., Kitsukawa, S., and Sekine, K., 2016, "Application of Risk Curve for Statistical Analysis of Backside Corrosion in the Bottom Floors of Oil Storage Tanks," International Journal of Pressure Vessels and Piping, **141**, pp. 19–25.

[54] Sato, N., 1971, "A Theory for Breakdown of Anodic Oxide Films on Metals," Electrochimica Acta, **16**(10), pp. 1683–1692.

[55] SP0110, N. S., 2010, "Wet Gas Internal Corrosion Direct Assessment Methodology for Pipelines," Houston, TX: NACE.

[56] Anderko, A., 2000, "SIMULATION OF FeCO~ 3/FeS SCALE FORMATION USING THERMODYNAMIC AND ELECTROCHEMICAL MODELS," *CORROSION-NATIONAL ASSOCIATION OF CORROSION ENGINEERS ANNUAL CONFERENCE-*, NACE.

[57] Crolet, J. L., Thevenot, N., and Dugstad, A., 1999, "Role of Free Acetic Acid on the CO2 Corrosion of Steels," *CORROSION 99*, NACE International.

[58] Sridhar, N., Dunn, D. S., Anderko, A. M., Lencka, M. M., and Schutt, H. U., 2001, "Effects of Water and Gas Compositions on the Internal Corrosion of Gas Pipelines—Modeling and Experimental Studies," CORROSION, **57**(3), pp. 221–235.

[59] Bogdan, P., and Pedram, M., 2018, "Toward Enabling Automated Cognition and Decision-Making in Complex Cyber-Physical Systems," *2018 IEEE International Symposium on Circuits and Systems (ISCAS)*, pp. 1–4.

[60] Brous, P., Janssen, M., and Herder, P., 2019, "Next Generation Data Infrastructures: Towards an Extendable Model of the Asset Management Data Infrastructure as Complex Adaptive System," Complexity, **2019**.

[61] Xanthopoulos, A. S., Kiatipis, A., Koulouriotis, D. E., and Stieger, S., 2017, "Reinforcement Learning-Based and Parametric Production-Maintenance Control Policies for a Deteriorating Manufacturing System," IEEE Access, **6**, pp. 576–588.

[62] Wei, M., and Qi, C., 2012, "Reinforcement Learning Based Maintenance Scheduling for a Two-Machine Flow Line with Deteriorating Quality States," *2012 Third Global Congress on Intelligent Systems*, IEEE, pp. 176–179.

[63] Aissani, N., Beldjilali, B., and Trentesaux, D., 2009, "Dynamic Scheduling of Maintenance Tasks in the Petroleum Industry: A Reinforcement Approach," Engineering Applications of Artificial Intelligence, **22**(7), pp. 1089–1103.

[64] Compare, M., Bellani, L., Cobelli, E., and Zio, E., 2018, "Reinforcement Learning-Based Flow Management of Gas Turbine Parts under Stochastic Failures," The International Journal of Advanced Manufacturing Technology, **99**(9–12), pp. 2981–2992.

[65] Alaswad, S., and Xiang, Y., 2017, "A Review on Condition-Based Maintenance Optimization Models for Stochastically Deteriorating System," Reliability Engineering & System Safety, **157**, pp. 54–63.

[66] Ahmad, R., and Kamaruddin, S., 2012, "An Overview of Time-Based and Condition-Based Maintenance in Industrial Application," Computers & industrial engineering, **63**(1), pp. 135–149.

[67] Jiang, M., Deng, C., Pan, Z., Wang, L., and Sun, X., 2018, "Multiobject Tracking in Videos Based on LSTM and Deep Reinforcement Learning," Complexity, **2018**.

[68] Zhou, W., 2010, "System Reliability of Corroding Pipelines," International Journal of Pressure Vessels and Piping, **87**(10), pp. 587–595.

[69] Committee, A. B., 2009, "ASME B31G-2009: Manual for Determining the Remaining Strength of Corroded Pipelines," American Society of Mechanical Engineers.

[70] Veritas, D. N., 2004, "Recommended Practice DNV-RP-F101 Corroded Pipelines," Hovik, Norway, **11**, pp. 135–138.

[71] Association, C. S., 2007, "CSA Z662-07, Oil and Gas Pipeline Systems," Ontario, Canada.

[72] Bea, R., and Xu, T., 1999, "Corrosion Effects on Burst Pressures RAM PIPE REQUAL," University of California at Berkeley, p. 103e104.

[73] Timashev, S., and Bushinskaya, A., 2016, *Diagnostics and Reliability of Pipeline Systems*, Springer.

[74] "CAPP | A Unified Voice for Canada's Upstream Oil and Gas Industry," CAPP [Online]. Available: https://www.capp.ca/. [Accessed: 03-Feb-2020].

[75] "(20) (PDF) Internal Coating-A Must in Gas Pipelines," ResearchGate [Online]. Available: https://www.researchgate.net/publication/315099108_Internal_Coating-A_must_in_Gas_Pipelines. [Accessed: 03-Feb-2020].

[76] Palmer-Jones, R., and Paisley, D., 2000, "Repairing Internal Corrosion Defects in Pipelines-a Case Study," *INTERNATIONAL PIPELINES REHABILITATION AND MAINTENANCE CONFERENCE, 4º*.

[77] Yadav, M., Sinha, R. R., Kumar, S., and Sarkar, T. K., 2015, "Corrosion Inhibition Effect of Spiropyrimidinethiones on Mild Steel in 15% HCl Solution: Insight from Electrochemical and Quantum Studies," RSC Advances, **5**(87), pp. 70832–70848.

[78] "Protecting a Pipeline When Its Coating Has Aged" [Online]. Available: http://www.materialsperformance.com/articles/coating-linings/2017/03/protecting-a-pipeline-when-its-coating-has-aged. [Accessed: 04-Feb-2020].

[79] "'WOOO – PIG – SOOIE!' - The Business of Pipeline Integrity II | RBN Energy" [Online]. Available: https://rbnenergy.com/wooo-pig-sooie-the-business-of-pipeline-integrity-ii. [Accessed: 04-Feb-2020].

[80] Sutton, R. S., and Barto, A. G., 1998, *Introduction to Reinforcement Learning*, MIT press Cambridge.

[81] Leibo, J. Z., Zambaldi, V., Lanctot, M., Marecki, J., and Graepel, T., 2017, "Multi-Agent Reinforcement Learning in Sequential Social Dilemmas," arXiv preprint arXiv:1702.03037.

[82] Szepesvári, C., 2010, "Algorithms for Reinforcement Learning," Synthesis lectures on artificial intelligence and machine learning, **4**(1), pp. 1–103.

[83] "Pipeline Incident 20 Year Trends | PHMSA" [Online]. Available: https://www.phmsa.dot.gov/data-and-statistics/pipeline/pipeline-incident-20-year-trends. [Accessed: 06-Apr-2020].

[84] Spüntrup, F. S., Londono, J., Skourup, C., Thornhill, N., and Imsland, L., 2018, "Reliability Improvement of Compressors Based on Asset Fleet Reliability Data," IFAC-PapersOnLine, **51**(8), pp. 217–224.

[85] Wu, K.-Y., and Mosleh, A., 2019, "Effect of Temporal Variability of Operating Parameters in Corrosion Modelling for Natural Gas Pipelines Subject to Uniform Corrosion," Journal of Natural Gas Science and Engineering, **69**, p. 102930.

[86] Papavinasam, S., Revie, R. W., I.Friesen, W., Doiron, A., and Panneerselvan, T., 2011, "Review of Models to Predict Internal Pitting Corrosion Of Oil and Gas Pipelines," Corrosion Reviews, **24**(3–4), pp. 173–230.

[87] Shirazi, S. A., Mclaury, B. S., Shadley, J. R., Roberts, K. P., Rybicki, E. F., Rincon, H. E., Hassani, S., Al-Mutahar, F. M., and Al-Aithan, G. H., 2015, "Erosion–Corrosion in Oil and Gas Pipelines," *Oil and Gas Pipelines*, John Wiley & Sons, Ltd, pp. 399–422.

[88] Nešić, S., and Postlethwaite, J., 1991, "A Predictive Model for Localized Erosion—Corrosion," CORROSION, **47**(8), pp. 582–589.

[89] Jia, R., Unsal, T., Xu, D., Lekbach, Y., and Gu, T., 2019, "Microbiologically Influenced Corrosion and Current Mitigation Strategies: A State of the Art Review," International Biodeterioration & Biodegradation, **137**, pp. 42–58.

[90] Arzaghi, E., Abbassi, R., Garaniya, V., Binns, J., Chin, C., Khakzad, N., and Reniers, G., 2018, "Developing a Dynamic Model for Pitting and Corrosion-Fatigue Damage of Subsea Pipelines," Ocean Engineering, **150**, pp. 391–396.

[91] Ritchie, R. O., 1979, "Near-Threshold Fatigue-Crack Propagation in Steels," International Metals Reviews, **24**(1), pp. 205–230.

[92] Harlow, D. G., and Wei, R. P., 1994, "Probability Approach for Prediction of Corrosion and Corrosion Fatigue Life," AIAA Journal, **32**(10), pp. 2073–2079.

[93] Peabody, A. W., 2001, "Peabody's Control of Pipeline Corrosion: Second Edition.," Peabody's control of pipeline corrosion: second edition., (Ed.2).

[94] Velázquez, J. C., Caleyo, F., Valor, A., and Hallen, J. M., 2009, "Predictive Model for Pitting Corrosion in Buried Oil and Gas Pipelines," CORROSION, **65**(5), pp. 332–342.

[95] Liu, Z. Y., Wang, X. Z., Du, C. W., Li, J. K., and Li, X. G., 2016, "Effect of Hydrogen-Induced Plasticity on the Stress Corrosion Cracking of X70 Pipeline Steel in Simulated Soil Environments," Materials Science and Engineering: A, **658**, pp. 348–354.

[96] Xu, L. Y., and Cheng, Y. F., 2013, "Development of a Finite Element Model for Simulation and Prediction of Mechanoelectrochemical Effect of Pipeline Corrosion," Corrosion Science, **73**, pp. 150–160.

[97] Shan, X., Liu, K., and Sun, P.-L., 2017, "Risk Analysis on Leakage Failure of Natural Gas Pipelines by Fuzzy Bayesian Network with a Bow-Tie Model," Scientific Programming, **2017**.

[98] Caleyo, F., Velázquez, J. C., Valor, A., and Hallen, J. M., 2009, "Probability Distribution of Pitting Corrosion Depth and Rate in Underground Pipelines: A Monte Carlo Study," Corrosion Science, **51**(9), pp. 1925–1934.

Annex A

DISCRETIZED NODES OF THE BBN INTERNAL CORROSION MODEL

Variables	Description	Causes	States	Unit
Wetting Factor	Wetted Not Wetted	—	1 0.1	
pH2S	Partial pressure of hydrogen sulfide	—	0-10 10-100 100-1000 1000-10000	mbar
pCO2	Partial pressure of carbon dioxide	—	0-10 10-100 100-1000 1000-10000	mbar
Flow Velocity	Flow velocity of gas	—	0-1 1-2 2-3 3-4.5	m/s
Temp	Temperature	—	0-25 25-50 50-75 75-100	℃
pH	pH level	—	4-5 5-6 6-7 7-8	
Uniform Corrosion	Uniform corrosion rate	Wetting Factor pH2S pCO2 Flow Velocity Temp pH	0-0.01 0.01-0.1 0.1-1 1-5 5-10	mm/y
P	Total pressure	—	1-10 10-50 50-100 100-150	bar
Wall Shear Stress	Wall shear stress due to the flow of gas	—	0-10 10-20 20-30	Pa

R_{solids}	W/ solid W/O solid	—	0 1	
$[Cl^-]$	Concentration of chloride ions	—	0-100 100-1000 1000-10000 10000-100000	ppm
$[SO_4^{2-}]$	Concentration of sulphate ions	—	0-10 10-100 100-1000 1000-2500	ppm
$[HCO_3^-]$	Concentration of bicarbonate ions	—	0-10 10-100 100-1000 1000-4000	ppm
PCR	Average pit growth rates due to every individual effects	—	0-0.01 0.01-0.1 0.1-1 1-5 5-10	mm/y
Pitting Corrosion	Pitting corrosion rate	Wetting Factor P Wall Shear Stress R_{solids} $[Cl^-]$ $[SO_4^{2-}]$ $[HCO_3^-]$ PCR	0-0.01 0.01-0.1 0.1-1 1-5 5-10	mm/y
[C]	Concentration of carbon from fatty acid ≥ 20 mg/L Concentration of carbon from fatty acid < 20 mg/L	—	1 0.2	
Biocide	Routinely used Not routinely used	—	0.2 1	
[O]	Oxygen ingress ≥ 50 ppb Oxygen ingress < 50 ppb	—	5 1	
Pigging	Never Once 13 weeks	—	1 0.3	

	Once 4 weeks Once 1 week		0.001 0.0001	
C:N ratio	< 10 ≥ 10	—	1 0.4	
[N]	≥ 5 mg/L < 5 mg/L	—	1 0.2	
[Solids]	Dissolved_solid < 60 g/L Dissolved_solid ≥ 60 g/L and SRB grows Dissolved_solid ≥ 60 g/L and SRB doesn't grow	—	1 0.2 0.0001	
FV_{MIC}	Flow velocity < 1 m/s Flow velocity = 2 m/s Flow velocity = 2.5 m/s Flow velocity = 3 m/s	—	1 0.6 0.1 0.01	
Debris	Yes No	—	2 1	
T_{MIC}	10℃ ≤ Temperature ≤ 45℃ Temperature < 10℃ or Temperature > 45℃	—	1 0.2	
Microbiologically-Influenced Corrosion (MIC)	Microbiologically-influenced corrosion rate	Wetting Factor [C] Biocide [O] Pigging C:N ratio [N] [Solids] FV_{MIC} Debris T_{MIC}	 0-0.01 0.01-0.1 0.1-1 1-5 5-10	mm/y
Yield strength	Yield strength of the pipe	—	10-250 250-500 500-750 750-1000	MPa
Impact Angle		—	0-15 15-30	degree

	Impact angle between the solid and the pipe surface		30-45 45-60	
Particle Mass	Mass of the particle	—	0.1-1 1-10 10-100 100-200	g
Erosion Corrosion	Erosion corrosion rate	Particle Density Impact Angle Particle Mass	0-0.01 0.01-0.1 0.1-1 1-5 5-10	mm/y
Exponent	Exponent of the Paris equation	—	0-1 1-2 2-3	
Stress Range	The range between maximum and minimum stress	—	0-100 100-200 200-300	MPa
K	Stress concentration factor	—	0-1 1-2 2-3	
Defect Length	Initial radius of the pit	—	0-0.01 0.01-0.1 0.1-1 0.1-10	mm
Coefficient	Coefficient of the Paris equation	—	$10^{-12} – 10^{-11}$ $10^{-11} – 10^{-10}$ $10^{-10} – 10^{-9}$	
Frequency	The frequency of the stress change	—	1-2 2-3 3-4	/day
Corrosion Fatigue	Corrosion fatigue corrosion rate	Exponent Stress Range K Defect Length Coefficient Frequency	0-0.01 0.01-0.1 0.1-1 1-5 5-10	mm/y

Pipe Age	Age of the pipe	—	0-10 10-20 20-30 30-40 40-50	year
Corrosion Depth Rate	Total corrosion rate in term of depth	Uniform Corrosion Pitting Corrosion Microbiologically-Influenced Corrosion (MIC) Corrosion Fatigue	0-0.01 0.01-0.1 0.1-1 1-5 5-10	mm/y
Corrosion Length Rate	Total corrosion rate in term of length	—	0-0.01 0.01-0.1 0.1-1 1-5 5-10	mm/y
Corrosion Depth	Total depth of corrosion	Corrosion Depth Rate Pipe Age	0-5 5-10 10-100 100-500	mm
Corrosion Length	Total length of corrosion	Corrosion Length Rate Pipe Age	0-5 5-10 10-100 100-500	mm
Pipe Length	Length of the pipe	—	10-160 160-320 320-480 480-640	km
Pipe Diameter	Diameter of the pipe	—	10-150 150-300 300-450 450-600	mm
Pipe Thickness	Thickness of the pipe	—	1-10 10-20 20-30	mm

Operating Pressure	Operating pressure (like “P” node)	—	1-10 10-50 50-100 100-150	bar
Burst Pressure	Remaining strength of the pipe	Corrosion Length Yield Strength Pipe Length Pipe Diameter Pipe Thickness Corrosion Depth	0-250 250-500 500-750 750-1000	MPa
POF Leak	Failure probability of leak	Pipe Thickness Corrosion Depth	0-25 25-50 50-75 75-100	%
POF Burst	Failure probability of burst	Burst Pressure Operating Pressure	0-25 25-50 50-75 75-100	%
POF Internal Corrosion	Total failure probability of internal corrosion	POF Leak POF Burst	0-25 25-50 50-75 75-100	%

Annex B

DISCRETIZED NODES OF THE BBN EXTERNAL CORROSION MODEL

Nodes	Description	Causes	States	Unit
Resistivity	Resistivity of the soil	—	1-250 250-500 500-750 750-1000	Ω-m
$[SO_4^{2-}]$	Sulphate ions concentration of the soil	—	0-10 10-100 100-1000 1000-2500	ppm
$[HCO_3^-]$	Bicarbonate ions concentration of the soil	—	0-10 10-100 100-1000 1000-4000	ppm
$[Cl^-]$	Chloride ions concentration of the soil	—	0-100 100-1000 1000-10000 10000-100000	ppm
Redox Potential	Oxidation / reduction potential (Relative to the standard hydrogen electrode)	—	1-100 100-200 200-300 300-400	mV
Coefficient	Coefficient of the external corrosion model	Resistivity $[SO_4^{2-}]$ $[HCO_3^-]$ $[Cl^-]$ Redox Potential	0-0.25 0.25-0.5 0.5-0.75 0.75-1	
pH	pH level of the soil	—	4-5 5-6 6-7 7-8	
Pipe Soil Potential	Pipe/soil potential (Relative to a $Cu/CuSO_4$ reference electrode)	—	(-2) – (-1.5) (-1.5) – (-1.0) (-1.0) – (-0.5) (-0.5) – 0	V
Bulk Density	Bulk density of the soil	—	0-0.5 0.5-1	g/cm^3

			1-1.5 1.5-2	
Water Content	Water content of the soil	—	0-25 25-50 50-75 75-100	%
Exponent	Coefficient of the external corrosion model	pH Pipe Soil Potential Bulk Density Water Content	0-0.25 0.25-0.5 0.5-0.75 0.75-1	
Coating Lifetime	Lifetime of the external coating	—	0-5 5-10 10-15 15-20	year
Pipe Age	Age of the pipe	—	0-10 10-20 20-30 30-40 40-50	year
Pitting Corrosion	Pitting corrosion rate	Coefficient Exponent Coating Lifetime Pipe Age	0-0.01 0.01-0.1 0.1-1 1-5 5-10	mm/y
Cathodic i_0	Cathodic current density by electrochemical model	—	$10^{-3} – 10^{-2}$ $10^{-2} – 10^{-1}$ 10^{-1} - 1	A/m^2
Anodic i_0	Anodic current density by electrochemical model	—	$10^{-3} – 10^{-2}$ $10^{-2} – 10^{-1}$ 10^{-1} - 1	A/m^2
Defect Depth	Initial corrosion defect depth	—	0-0.01 0.01-0.1 0.1-1 1-10	mm
Defect Length	Initial corrosion defect length	—	0-0.01 0.01-0.1 0.1-1	mm

			1-10	
Strain (Displacement)	Displacement of the pipe by the soil movements	—	0-1 1-2 2-5	mm
SCC	Stress corrosion cracking rate	Cathodic i_0	0-0.01	mm/y
		Anodic i_0	0.01-0.1	
		Strain(Displacement)	0.1-1	
		Defect Depth	1-5	
		Defect Length	5-10	
Corrosion Length Rate	Total corrosion rate in term of length	—	0-0.01 0.01-0.1 0.1-1 1-5 5-10	mm/y
Corrosion Depth	Total depth of corrosion	Corrosion Length Rate	0-5	mm
		Pipe Age	5-10 10-100 100-500	
Corrosion Length	Total length of corrosion	Corrosion Length Rate	0-5	mm
		Pipe Age	5-10 10-100 100-500	
Yield Strength	Yield strength of the pipe material	—	10-250 250-500 500-750 750-1000	MPa
Pipe Length	Length of the pipe	—	10-160 160-320 320-480 480-640	km
Pipe Diameter	Diameter of the pipe	—	10-150 150-300 300-450 450-600	mm
Pipe Thickness	Thickness of the pipe	—	1-10 10-20 20-30	mm

Operating Pressure	Operating pressure	—	1-10 10-50 50-100 100-150	bar
Burst Pressure	Remaining strength of the pipe	Corrosion Length Yield Strength Pipe Length Pipe Diameter Pipe Thickness Corrosion Depth	0-250 250-500 500-750 750-1000	MPa
POF Leak	Failure probability of leak	Pipe Thickness Corrosion Depth	0-25 25-50 50-75 75-100	%
POF Burst	Failure probability of burst	Burst Pressure Operating Pressure	0-25 25-50 50-75 75-100	%
POF External Corrosion	Total failure probability of internal corrosion	POF Leak POF Burst	0-25 25-50 50-75 75-100	%